REACTOR POWER HISTORY FROM FISSION PRODUCT SIGNATURES

A Thesis

by

DAVID J. SWEENEY

Submitted to the Office of Graduate Studies of
Texas A&M University
in partial fulfillment of the requirements for the degree of

MASTER OF SCIENCE

December 2008

Major Subject: Nuclear Engineering

REACTOR POWER HISTORY FROM FISSION PRODUCT SIGNATURES

A Thesis

by

DAVID J. SWEENEY

Submitted to the Office of Graduate Studies of
Texas A&M University
in partial fulfillment of the requirements for the degree of

MASTER OF SCIENCE

Approved by:

Chair of Committee,	William S. Charlton
Committee Members,	Kenneth L. Peddicord
	James Olson
Head of Department,	Raymond Juzaitis

December 2008

Major Subject: Nuclear Engineering

ABSTRACT

Reactor Power History from Fission Product Signatures.

(December 2008)

David J. Sweeney, B.S., Northwestern University

Chair of Advisory Committee: Dr. William S. Charlton

The purpose of this research was to identify fission product signatures that could be used to uniquely identify a specific spent fuel assembly in order to improve international safeguards. This capability would help prevent and deter potential diversion of spent fuel for a nuclear weapons program. The power history experienced by a fuel assembly is distinct and could serve as the basis of a method for unique identification. Using fission product concentrations to characterize the assembly power history would limit the ability of a proliferator to deceive the identification method. As part of the work completed, the TransLat lattice physics code was successfully benchmarked for fuel depletion. By developing analytical models for potential monitor isotopes an understanding was built of how specific isotope characteristics affect the production and destruction mechanisms that determine fission product concentration. With this knowledge potential monitor isotopes were selected and tested for concentration differences as a result of power history variations. Signature ratios were found to have significant concentration differences as a result of power history variations while

maintaining a constant final burnup. A conceptual method for implementation of a fission product identification system was proposed in conclusion.

ACKNOWLEDGEMENTS

I thank my committee chair, Dr. Charlton, and my committee members, Dr. Peddicord, Professor Olson, and also Dr. Boyle for their guidance, support, and above all patience throughout the course of this research.

Thanks also go to my friends and colleagues, especially Gene, Vijay, Grant, David Ames, Corey, and Angie, and the department faculty and staff for making my time at Texas A&M University a great experience.

TABLE OF CONTENTS

CHAPTER Page

LIST OF FIGURES

Page

Page

Page

Page

Page

Page

Page

Page

Page

Page

Page

LIST OF TABLES

CHAPTER I

INTRODUCTION: THE NEED FOR REACTOR POWER HISTORY IDENTIFICATION

A. Initial Motivation

Nuclear Proliferation is a significant issue for today's world with countries like North Korea and Iran providing a seemingly daily reminder of the current danger.[1] Currently the IAEA employs various safeguards at nuclear facilities around the world to prevent a diversion of nuclear materials for nefarious purposes. However, the ability of countries to avert safeguards is evidenced by Iraq and North Korea.[1] New methods to strengthen existing safeguards are needed to detect and deter any attempts to circumvent the safeguards system.

Diversion of spent nuclear fuel in order to obtain plutonium is one method for weapons production.[2] Assuming that it is difficult to defeat IAEA fuel assembly accountancy safeguards in place either at a nuclear reactor, spent fuel pool, or reprocessing plant, a potential proliferator would have to substitute a less attractive fuel assembly for the diverted fuel assembly.

This thesis follows the style of *Nuclear Technology*.

There are several factors upon which a proliferator could preferentially choose some fuel assemblies over other ones for use in a weapons program. Possible characteristics could include a larger concentration of plutonium in the fuel, a higher concentration of Pu-239 in the plutonium, or a lower concentration of Pu-240 in the plutonium.[3] These and other factors are dependent on the power history of the fuel assembly and allow for greater optimization of the final plutonium weapon.

Thus, it would be useful for inspectors to have the ability to uniquely and independently verify the identity of a specific fuel assembly. Current safeguards are in place that can determine a spent fuel assembly's burnup, age, and other parameters. But, a method by which a fuel assembly's full operational or power history is known is necessary for a completely unique identification. Such a method based on the concentration of specific fission products in the spent fuel would be very difficult to deceive through forgery. To forge the desired signal one would have to reprocess the signature isotopes from another fuel assembly and insert them in the exact proportions necessary to the dissolution sample taken by the inspectors or perhaps replace the diverted assembly with an assembly with the exact same operational history (though that may be redundant). The method could be applied at a reprocessing facility by taking a spent fuel sample from the input accountability tank. The sample could then be analyzed and the estimated power history compared against the reactor operator's declaration for the specific fuel assembly. It is the goal of this research to develop a basis for such a fuel assembly identification method to assist in international safeguards.

B. The Safeguards System

The primary vehicle for modern non-proliferation efforts is the Nuclear Nonproliferation Treaty (NPT). First ratified in 1970, the NPT codified the aspects of nonproliferation initiative into an international treaty to which all but four countries in the world have ratified. All non-nuclear weapons state signatories are required to accept safeguards of their nuclear efforts as negotiated and regulated by the IAEA.[4] In 1997 INFCIRC/540, known as the Additional Protocol, came into effect.[5]

The IAEA was established in 1957 by the United Nations as a result of President Eisenhower's Atoms for Peace initiative.[6] With the advent of the NPT the primary role of the IAEA is to serve as the international nuclear watchdog and verify NPT compliance of the member states. The three focuses of the IAEA are verification, safety, and technology. The specific function of the IAEA that applies to this research is defined in the Statute of the IAEA:

> Article III: Functions, A. The Agency is authorized:
> …
> 5. To establish and administer safeguards designed to ensure that special fissionable and other materials, services, equipment, facilities, and information made available by the Agency or at its request or under its supervision or control are not used in such a way as to further any military purpose; and to apply safeguards, at the request of the parties, to any bilateral or multilateral arrangement, or at the request of a State, to any of that State's activities in the field of atomic energy;[7]

This gives the IAEA the mandate to safeguard the nuclear material and facilities of all non-nuclear weapons states with which it has agreements. The Additional Protocol

provided for implementation of stricter verifications and safeguards with the intention of strengthening the IAEA's ability to detect a diversion or use of nuclear material for weapons purposes.

The IAEA uses several methods to prevent proliferation. These methods can be broadly categorized as nuclear material accountancy, containment and surveillance, design verification, reports, inspections, and sampling. Material accountancy involves keeping track of nuclear material through designating areas known as material balance areas (MBAs). Any new material or material missing within an MBA warrants further investigation by the IAEA. Containment and surveillance methods include the placement of IAEA seals and video monitoring systems. Design verification refers to review by IAEA of the design of nuclear facilities to ensure that no modifications to the facility have been made that might facilitate diversion. Reports are made by the facility operators and checked by the IAEA for accuracy. Discrepancies between reports could lead to increased scrutiny. The IAEA has the power, which is increased under the Additional Protocol, to request an inspection of a country's facilities. During these inspections the IAEA may independently verify the material accountancy, containment, surveillance systems, facility design, declaration reports, or take samples from inside or outside the facility to be analyzed. Such analysis may reveal the presence of an undeclared material in violation of a country's safeguards agreements. The proposed method of this research would require samples from a reprocessing facility.

It is necessary to define certain terms frequently used in the safeguards arena. The *objective of safeguards* is defined as,

> the timely detection of diversion of significant quantities of nuclear material from peaceful nuclear activities to the manufacture of nuclear weapons or of other nuclear explosive devices or for purposes unknown, and the deterrence of such diversion by the risk of early detection.[8]

Additionally safeguards are intended to detect undeclared nuclear material and activities. "Nuclear material" refers to any "source material" or "special fissionable material". "Source material" is uranium of natural or less enrichment of the U-235 and thorium in any form. "Special fissionable material" is Pu-239, U-233, or uranium enriched in U-235 or U-233 above natural levels in any form.[7] A "significant quantity" (SQ) is the approximate amount of nuclear material needed to make a nuclear explosive device.[9] With a basic understanding of the legal framework for international safeguards it is now necessary to review prior efforts pertinent to the focus of this research.

C. Previous Work

The purpose of this research is to assist in the safeguards process by developing a technique to identify a spent fuel assembly based on fission product concentrations or signatures. Various methods for identifying specific characteristics of spent fuel assemblies based on fission products concentrations exist and are currently in use. Burnup, fuel age, reactor type, fuel type, and initial fuel enrichment can be identified in several ways.

Methods for determining some of these parameters are well known, specifically uranium concentration, plutonium concentration, minor actinide concentration, burnup, fuel age, and enrichment. Early research developed isotope correlations from isotopic ratios of xenon, krypton, cesium, neodymium, and the overall elemental ratio of uranium to plutonium to determine uranium and plutonium isotopic concentrations.[10,11] These correlations were dependent on fission products with large absorption cross-sections and invariant fission yields (characteristics present in some isotopes of those elements mentioned) in order to reflect changes in the thermal flux for an accurate correlation of uranium and plutonium isotopes.[12] Later studies developed correlations for the concentrations of the higher actinides Np-237, Am-241, and Am-243 from the Pu-240/Pu-239 ratio and the Cs-137 activity. These correlations were found to be accurate within 4, 6, and 15% for Np-237, Am-241, and Am-243, respectively.[13]

An initial survey determined the capability of the following potential burnup monitor isotopes to identify burnup in different fissioning systems: Sr-88, Sr-90, Zr-92, Zr-93, Zr-94, Zr-96, Mo-95, Mo-97, Mo-98, Mo-100, Ru-101, Ru-102, Ru-104, Cs-133, Cs-137, Ce-140, Ce-142, and Nd-148.[14] The results showed that Nd-148 had the most capability to determine burnup in a mixed Pu-239 and U-235 fission source and it has been shown elsewhere that Nd-148 can be used to determine burnup to within 5% accuracy.[15] This study also proposed the use of noble gases for burnup determination. This idea was later refined allowing for burnup determination accuracy within 3.9% from measurements of xenon and krypton isotopic ratios.[16,17] The capability of ruthenium isotopic ratios to determine burnup was also advanced.[18]

Fuel age is the amount of time between spent fuel discharge from the reactor and the time of any subsequent measurement. It has been demonstrated that isotopic ratios of xenon and krypton are capable of accurately distinguishing age within 8%.[19] A distinguishing capability to within 10% has also been demonstrated using the non-gaseous fission products Sr-90, Nb-93, Ru-106, Rh-101, Rh-102, Sb-125, Cs-134, Cs-137, Pm-146, Pm-147.[15]

With the assumption that the only fissioning isotopes are U-235, U-238, Pu-239, Pu-240, and Pu-241 initial enrichment can be determined accurately within 2% using uranium and plutonium isotopic ratios.[15] This assumption neglects the fission of higher actinides such as americium and curium. For most reactor systems today, this is a valid assumption.

Determining the reactor type and fuel type based on spent fuel analysis has been examined but is less developed. It has been suggested that a comparison of low fission yield isotopes such as Sn-126 to high fission yield isotopes such as Zr-93 may reveal information about the neutron energy spectrum and the composition of the fissionable material.[20] Isotopic ratios of the noble gases xenon and krypton have been shown to vary between different reactor types.[16] However, the proposed system has difficulty distinguishing between light water reactors. Ruthenium isotopic ratios have shown similar capabilities and failures.[18] Such information could be used to determine the type of fuel and reactor type.

The focus of this study, methods for determination of reactor power history, remains relatively unexplored. A possible physical mechanism that may exist in the production of certain fission products suggesting a dependence on the total length of shutdowns in a spent fuel assembly's power history has been identified in previous literature and is shown in Figure 1.[15] Fission products that may exhibit this feature were suggested but not investigated. Further no attempt has been made to propose a system by which this or other undiscovered mechanisms may be used to identify a spent fuel assembly. The research presented here proposes such a method with a full investigation of potentially useful fission products.

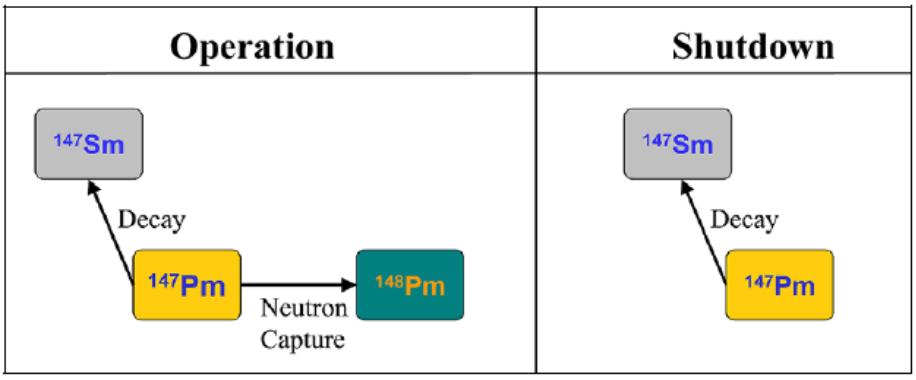

Figure 1. Mechanism by which Sm-147 Concentration is Increased Proportional to the Total Duration of Shutdowns during Reactor Operation. Figure taken from Reference 15.

CHAPTER II

TRANSLAT LATTICE PHYSICS CODE

All reactor simulations for this study are conducted with the lattice physics software TransLat. TransLat is part of the modular software system Transfx produced by TransWare Enterprises Inc. TransLat couples the advanced particle transport theory methods described above with arbitrary geometry modeling techniques. The cross-section set used is based on ENDF/B-VI with over 300 nuclides and 97 energy groups over the 0-10 MeV range for neutron cross-sections. Over 200 nuclides are included in the fuel depletion chains used by TransLat. Before making use of TransLat it is necessary to understand the physics of fission product buildup during reactor operation.

A. Theory of Fission Product Production in Reactors

A method for determining reactor power history based on fission product concentration requires understanding of the basic physics of fission product production and destruction mechanisms within a fissioning system. The general differential equation for the atomic number density of a stable fission product is

$$\frac{dN_j}{dt} = \overline{Y}_f^j \overline{\Sigma}_f \overline{\phi} + \sum_i \lambda_{i\to j} N_{i\to j} - (\lambda_j + \overline{\sigma}_{a,j}\overline{\phi})\overline{N}_j \qquad (1)$$

where $\overline{Y}_f^x$ is the appropriately averaged fission yield of isotope *x* from all fissions, $\overline{\Sigma}_f$ is the appropriately averaged macroscopic fission cross-section of all fissioning isotopes for the system, N_x is the number density of isotope *x*, ϕ is the appropriately averaged

neutron scalar flux, λ_x is the decay constant for isotope *x*, and $\overline{\sigma}_{a,x}$ is the appropriately averaged neutron absorption cross-section of isotope *x*.[21] For the purposes of this research, it was assumed that all fissions are from U-235 and Pu-239. This is a reasonable assumption for most power reactors in the world and allows Equation 1 to be written more explicitly as

$$\frac{dN_j}{dt} = \overline{Y}^{j}_{f,U235}\overline{\sigma}_{f,U235}N_{U235}\overline{\phi} + \overline{Y}^{j}_{f,Pu239}\overline{\sigma}_{f,Pu239}N_{Pu239}\overline{\phi} + \sum_i \lambda_{i\to j}N_{i\to j} - (\lambda_j + \overline{\sigma}_{a,j}\overline{\phi})N_j \qquad (2)$$

where $\overline{Y}^{j}_{f,x}$ is the appropriately averaged fission yield of isotope *j* from the fission of isotope *x* and $\overline{\sigma}_{f,x}$ is the appropriately averaged microscopic fission cross-section for isotope *i*.

Thus the fission yields, fission cross-sections, the concentrations of U-235 and Pu-239, and the neutron flux are the parameters which determine the production of fission products. The neutron flux or neutron population in a reactor is related to the power level during operation. This provides a link between fission product concentration and power history. This link will be further developed in Chapter III.

These fission product equations are a subset of the general reactor physics calculations that are used to model a nuclear reactor. To place them in context and as background for the discussions to be presented, it is worthwhile to review the broader scope of reactor physics calculations.

B. Theory of Reactor Physics Calculations

The fundamental concern of reactor physics is knowledge of the reaction rate of neutron interactions with the atoms of a nuclear system, which requires knowledge of the neutron scalar flux in the system.

The neutron scalar flux is calculated using the general of the Neutron Transport Equation:

$$\frac{1}{v(E)}\frac{\partial}{\partial t}[\psi(\underline{r},E,\underline{\Omega},t)]+\underline{\Omega}\bullet\underline{\nabla}\psi(\underline{r},E,\underline{\Omega},t)+\Sigma_t(\underline{r},E,t)\psi(\underline{r},E,\underline{\Omega},t)$$
$$=S_{ext}(\underline{r},E,\underline{\Omega},t)+\frac{\chi_p(E)}{4\pi}\int_0^\infty dE'\phi(\underline{r},E',t)\upsilon_p\Sigma_f(\underline{r},E',t) \qquad (3)$$
$$+\int_{4\pi}d\Omega'\int_0^\infty dE'\psi(\underline{r},E',\underline{\Omega}',t)\Sigma_s(\underline{r},E'\to E,\underline{\Omega}'\to\underline{\Omega},t)$$

where $v(E)$ is the energy dependent neutron velocity, $\psi(\underline{r},E,\underline{\Omega},t)$ is the angular neutron flux at position $\underline{r}$ having energy E and direction $\underline{\Omega}$ at time t, $S_{ext}(\underline{r},E,\underline{\Omega},t)$ is the external source of neutrons at position $\underline{r}$ having energy E and direction $\underline{\Omega}$ at time t, $\chi_i(E)$ is the energy dependent fission neutron spectrum of delayed neutron precursor i, $C_i(\underline{r},t)$ is the concentration of delayed neutron precursor i at position $\underline{r}$ at time t, $\chi_p(E)$ is the energy dependent prompt fission neutron spectrum, and υ_p is the average number of prompt neutrons released per fission.[22] The neutron scalar flux is then

$$\phi(\underline{r},E,t)=\int_{4\pi}\psi(\underline{r},E,\underline{\Omega},t)d\underline{\Omega} \qquad (4)$$

One final aspect of reactor physics necessary for this discussion is the parameter burnup. Typically fresh fuel in a reactor has a greater amount of fissile material available to produce fission energy than similar fuel that is at the end of its operational life. Burnup describes this fuel usage in the core and is a measure of the fission energy extracted from the fuel. Indirectly burnup relates the amount of fissile material left in the fuel. Thus over the life of the fuel in a reactor core, burnup affects the reaction rates, criticality, and the neutron flux in the reactor. Burnup is expressed as fission energy released per unit mass of fuel, and the most common units used for burnup are megawatt-days per metric ton uranium (MWD/MTU).

TransLat computational theory is built on the integral form of the neutron transport equation. The steady state, multi-energy group integral transport equation is expressed as

$$\psi_g(\underline{r},\underline{\Omega}) = \psi_g(\underline{r} - R\underline{\Omega},\underline{\Omega}) \exp\left[-\int_0^R \Sigma_{t,g}(\underline{r} - R'\underline{\Omega})dR'\right] + \int_0^R Q_g(\underline{r}) \exp\left[-\int_0^{R'} \Sigma_{t,g}(\underline{r} - R''\underline{\Omega})dR''\right]dR' \quad (5)$$

where $\psi_g(\underline{r},\underline{\Omega})$ is the angular neutron flux of neutron energy group g at position $\underline{r}$ with direction $\underline{\Omega}$, $\Sigma_{t,g}(\underline{r} - R'\underline{\Omega})$ is the total macroscopic neutron cross-section for neutrons in energy group g at position $\underline{r} - R'\underline{\Omega}$, and $Q_g(\underline{r})$ is the source of neutrons in neutron energy group g at position $\underline{r}$. Equation 5 can be derived by integrating the transport

equation, given as Equation 3. The integral form describes the amount of neutrons that arrive at some point $\underline{r}'$ from all sources at $\underline{r}'$ and all neutrons from all other points along the path *u* moving in direction $\underline{\Omega}$ as illustrated in Figure 2. It should be noted that in the derivation of Equation 5, *u* as shown in Figure 2 has been substituted by –*R*. The integral form of the neutron transport equation is used to solve for the scalar flux and reaction rates throughout the system by TransLat with the user's choice of one of two possible deterministic techniques. The techniques available to the user are the Method of Collision Probabilities and the Method of Characteristics.[23,24]

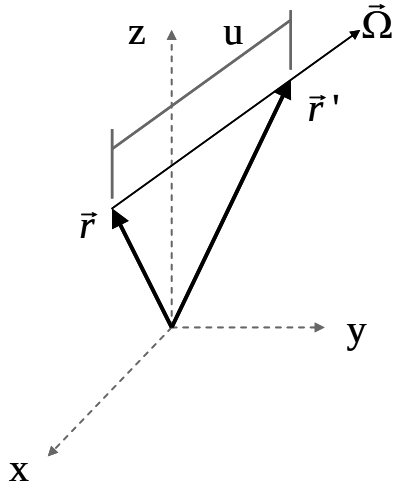

Figure 2. Geometry of Integral Transport Equation.

C. Method of Collision Probabilities

The Method of Collision Probabilities relates a determinable probability of a neutron in one region causing a neutron collision (of any neutron reaction type) in a second region to the neutron collision rate (reaction rate) in the second region. Thus with knowledge

of the cross-sections in the second region and reaction rate of the second region, the flux of the second region can be determined.

The derivation of the Method of Collision Probabilities begins with the definition of an optical path length, $\tau_g(\vec{r}, \vec{r} - R'\vec{\Omega}) = \int_0^{R'} \Sigma_{t,g}(\vec{r} - R"\vec{\Omega}) dR"$. This path length is the effective path length, based on the neutron cross-section of the medium, a neutron must travel to reach a certain point. When the optical path length is substituted the integral transport equation can be written as

$$\psi_g(\underline{r}, \underline{\Omega}) = \psi_g(\underline{r} - R\underline{\Omega}, \underline{\Omega}) \exp\left[-\tau_g(\underline{r}, \underline{r} - R\underline{\Omega})\right] + \int_0^R Q_g(\underline{r} - R'\underline{\Omega}) \exp\left[-\tau_g(\underline{r}, \underline{r} - R'\underline{\Omega})\right] dR' . \quad (6)$$

Assuming an infinite media and integrating over all angles yields the integral form of the scalar flux

$$\phi_g(\underline{r}) = \int_{4\pi} \int_0^{\infty} Q_g(\underline{r} - R'\underline{\Omega}) \exp\left[-\tau_g(\underline{r}, \underline{r} - R'\underline{\Omega})\right] dR' d\underline{\Omega} . \quad (7)$$

Referring back to Figure 2, it is observed that $\vec{r}' = \vec{r} - R'\vec{\Omega}$ and $R' = \left|\vec{r} - \vec{r}'\right|$. This observation combined with the substitution of $dV' = 4\pi R'^2 \, dR' d\vec{\Omega}$ allows Equation 7 to be rewritten as

$$\phi_g(\underline{r}) = \int \frac{Q_g(\underline{r}') e^{-\tau_g(\underline{r}, \underline{r}')}}{4\pi \left|\underline{r} - \underline{r}'\right|^2} dV' . \quad (8)$$

At this point a collision probability may be defined as $P_g(\underline{r},\underline{r}') = \frac{e^{-\tau_g(\underline{r},\underline{r}')}}{4\pi|\underline{r}-\underline{r}'|^2}$. Now the scalar flux may be written as a function of the collision probability such that

$$\phi_g(\underline{r}) = \int Q_g(\underline{r}')P(\underline{r},\underline{r}')dV'. \quad (9)$$

In this manner fluxes are generated for each region in the system typically using power iterations.[25] Computation of the integrals involved in the Method of Collision Probabilities is simplified by use of Ray Tracing methods.[26] Ray Tracing involves following neutron movement along discrete directional paths throughout the system involved. By making use of relations apparent with Ray Tracing, it is possible to evaluate collision probabilities parallel to the neutron path analytically. The ability to obtain such collision probabilities without numerical integration greatly simplifies the problem. Implicit in the derivation of the Method of Collision Probabilities is an assumption that the neutron sources are uniformly distributed in the cell. As cell size grows this assumption is less realistic.

D. Method of Characteristics

The Method of Characteristics discretizes the integral transport equation so that it may be integrated and solved for average angular fluxes. These average angular fluxes are then summed in quadrature in order to obtain scalar fluxes for each region. The initial discretization occurs in two domains: spatial and angle (in this discussion the integral transport equation has already been discretized in the energy domain). The spatial domain is divided into *I* regions where the flux is assumed constant, and the angle

domain is divided into *M* directions. This allows the integral transport equation to be written as

$$\psi_{g,m,i,k}(s_{m,i,k}) = \psi_{g,m,i,k}(0)\, e^{-\Sigma_{t,g,i} s_{m,i,k}} + \frac{Q_{g,i}}{\Sigma_{t,g,i}}\left[1 - e^{-\Sigma_{t,g,i} s_{m,i,k}}\right] \tag{10}$$

where $s_{m,i,k}$ is the distance or path length along segment *k* in direction *m* and in cell *i*. The angular flux is then averaged over the path length $s_{m,i,k}$ and averaged again over all segments *k* as shown in Equations 11 and 12

$$\bar{\psi}_{g,m,i,k} = \frac{Q_{g,i}}{\Sigma_{t,g,i}} + \frac{\psi_{g,m,i,k}(0) - \psi_{g,m,i,k}(s_{m,i,k})}{\Sigma_{t,g,i} s_{m,i,k}} \tag{11}$$

$$\bar{\psi}_{g,m,i} = \frac{\sum_{k=1}^{K} \bar{\psi}_{g,m,i,k} s_{m,i,k} \delta A_i}{\sum_{k=1}^{K} s_{m,i,k} \delta A_i} \quad . \tag{12}$$

The scalar flux of energy group *g* and region *i* is the quadrature sum of the average angular flux of Equation 8 such that

$$\bar{\phi}_{g,i} = \sum_{m=1}^{M} w_m \bar{\psi}_{g,m,i} \quad . \tag{13}$$

The Method of Characteristics is also solved using Ray Tracing and power iterations. In general the Method of Characteristics is superior to the Method of Collision Probabilities in computation time and accuracy. The Method of Collision Probabilities has been in use longer and can be useful for comparisons. For the simulations done in this research the Method of Characteristics was used.[27]

E. TransLat Benchmarking

Prior to making use of TransLat, it is necessary validate its capabilities. TransLat has been benchmarked to MCNP and HELIOS calculations for k-eigenvalues, fission rates, and neutron capture rates in several reactor configurations with very good results.[28,29,30] For the purposes of this research it is necessary to benchmark TransLat's fission product production and depletion capabilities. Doing so will validate the use of TransLat and provide an estimate of the error to be expected from values calculated by TransLat.

In order to evaluate TransLat's fuel depletion capabilities, TransLat was benchmarked against data from analysis of spent nuclear reactor fuel. To do this a fuel pin cell was modeled in TransLat. The fuel pin cell is a representation of a single fuel rod and is illustrated in Figure 3.

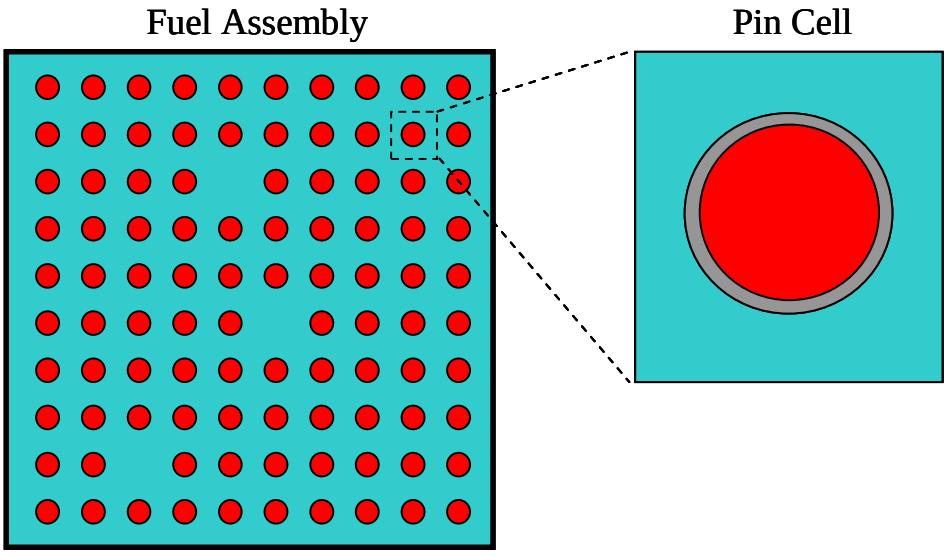

Figure 3. A Pin Cell as Part of a Reactor Fuel Assembly.

Contained in the square pin cell are the fuel rod, fuel and cladding, and surrounding moderator. Though modeling a full reactor fuel assembly may produce more accurate results, the pin cell is chosen for its simplicity to test TransLat's capabilities. In order to increase the accuracy of the simple pin cell, the model is modified from the actual dimensions found in the nuclear reactor simulated. Specifically, the ratio of fuel to moderator in a pin cell is larger than the fuel to moderator ratio in the fuel assembly. This is because not all the fuel rod positions in a fuel assembly are filled with a fuel rod. Thus the dimensions of the pin cell are recalculated to be consistent with the fuel to moderator ratio of the fuel assembly. Table I shows the modified pin cell dimension calculation for H.B. Robinson Unit 2, one of the reactors modeled. Similar tables for the other reactors modeled are shown in Appendix A.

Table I

Modified Pin Cell Calculations for H.B. Robinson Unit 2 Pin Cell

	Actual Assembly Parameters	Modified Pin Cell Parameters
Rods per Assembly	204	--
Rod array	15*15	--
Rod Positions	225	--
Rod O.D. [cm]	1.070	1.070
Rod Area [cm^2]	0.899	0.899
Total Rod Area [cm^2]	183.437	--
Pin Pitch [cm]	1.430	1.502
Pin Cell Area [cm^2]	2.045	2.255
Assembly area [cm^2]	460.103	--
Total Moderator Area [cm^2]	276.665	--
Fuel to Moderator Ratio	0.663	0.663

Three reactors, Calvert Cliffs No.1, H.B. Robinson Unit 2, and Mihama Unit 3, were modeled as pin cells for this study. Values for various isotopic ratios and concentrations measured in the spent fuel samples at different burnup levels for each reactor are reported in available literature.[31,32,33] The measured samples for Calvert Cliffs No. 1 used were from assembly D047 rod MKP109 (ATM-104) with burnup values of 27.35 GWD/MTU, 37.12 GWD/MTU, and 44.34 GWD/MTU. The measured samples for H.B. Robinson Unit 2 used were from assembly BO-5 rod N9 (ATM-101) with burnup values of 16.02 GWD/MTU, 23.81 GWD/MTU, 28.47 GWD/MTU, and 31.66 GWD/MTU. The measured samples for Mihama Unit 3 used were 87C03, 87C04, 87C07, and 87C08 with burnup values of 29.44 GWD/MTU, 32.30 GWD/MTU, 33.70 GWD/MTU, and 34.10 GWD/MTU respectively. The percent difference of the measured values with those corresponding values calculated by TransLat were determined by

$$\%\ \text{Difference} = \frac{(measured - TransLat)}{measured} * 100. \qquad (14)$$

Figure 4 illustrates the results of the benchmarking study graphically.

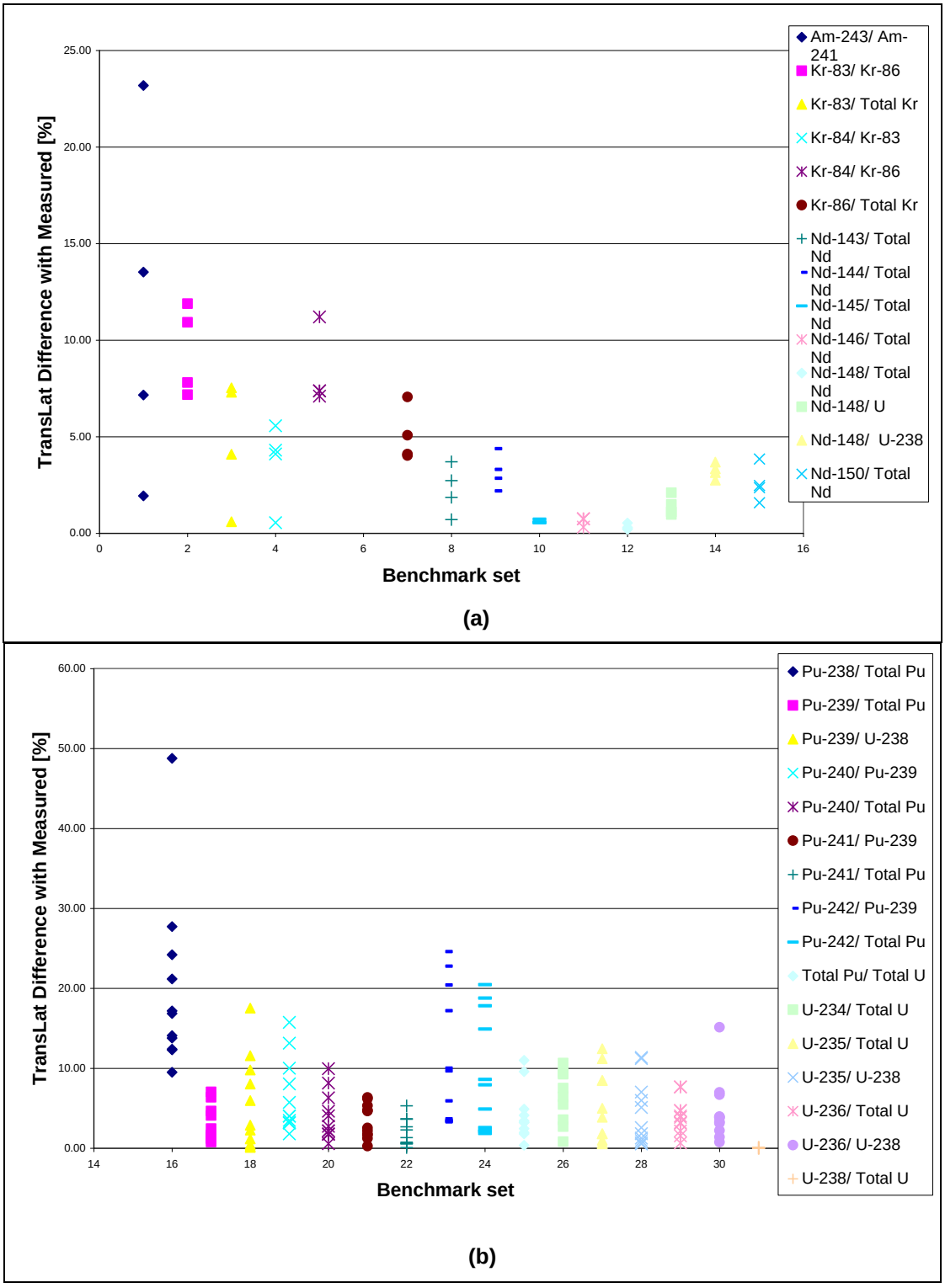

Figure 4. Percent Difference of TransLat Values with All Measured Values of Isotopic Ratio or Concentration for Benchmark Isotope Sets (a)1-15, (b)16-31, (c)32-47,(d)48-65.

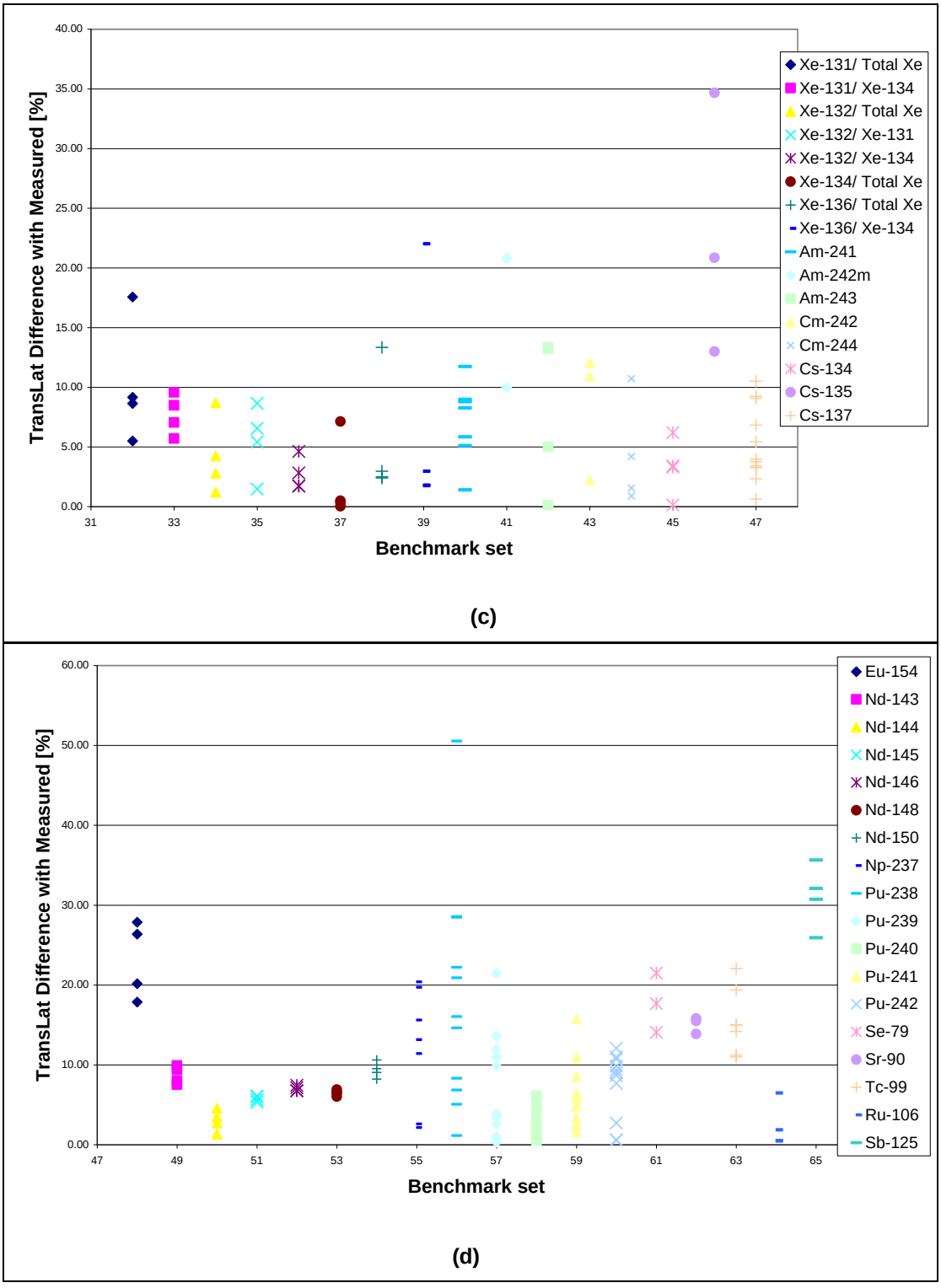

Figure 4. Continued.

As is illustrated in Figure 4, in general TransLat isotopic values are of reasonable accuracy. The overall average percent difference for all ratios and concentration was 7.02 %. Table II summarizes the results of the TransLat benchmarking study for the 489 values of isotopic ratio or concentration compared.

Table II

Overall Results of Benchmarking Study

% Difference of TransLat with Measured	5	10	15	20
Number of TransLat values within Difference	270	388	437	458
% of TransLat values within Difference	55	79	89	94

The table shows that for almost 100 % of values given for fission products and actinides TransLat was within 20 % of the measured values. Approximately 80 % of the values given were calculated by TransLat to within 10 % accuracy. As such a 10 % difference found between TransLat calculated values was taken as a minimum for measurable differences in reality.

The results of this benchmarking study are clear and prove the validity of TransLat for use in this study. Existing reactors were modeled as simple modified pin cells in TransLat. The results of these models had excellent agreement with measured values to within 20 % accuracy and reasonable agreement with measured results to within 10 % accuracy. A 10 % minimum will be required for isotopic concentration differences as a result of power history variations to be considered detectable. It is the goal of this study to identify isotopes that display such detectable differences from variations in power history.

CHAPTER III

PHYSICAL CHARACTERISTICS OF POTENTIAL POWER HISTORY MONITOR ISOTOPES

In order to guide the search for potential power history monitor isotopes, it is necessary to understand the mechanisms by which certain isotopes are produced and the physical characteristics responsible for these mechanisms. A mathematical model was developed that can be manipulated to assess isotope concentrations versus power history parameters.

In this work, the power history is defined as the specific power of a fuel assembly as a function of time denoted $P_s(t)$. The specific power is the amount of energy released per unit mass of fuel at a given time *t* and is commonly described in units of watts per gram of fuel. The neutron flux is proportional to the specific power by the relation

$$\phi(t) = \frac{\rho_U P_s(t)}{\overline{E_R}\,\overline{\Sigma_f}(t)} \tag{15}$$

where ρ_U is the density of uranium in the fuel, $\overline{E_R}$ is the average energy released per fission, and $\overline{\Sigma_f}(t)$ is the average macroscopic fission cross-section at time t.

Substituting Equation 15 into Equation 2 and maintaining the assumption that all fissions are from U-235 and Pu-239 only yields

$$\frac{dN_j}{dt} = Y^j_{f,U235}\sigma_{f,U235}N_{U235}(t)\frac{\rho_U P_s(t)}{\overline{E}_R\overline{\Sigma}_f(t)} + Y^j_{f,Pu239}\sigma_{f,Pu239}N_{Pu239}(t)\frac{\rho_U P_s(t)}{\overline{E}_R\overline{\Sigma}_f(t)} + \sum_i \lambda_{i\to j}N_{i\to j}(t) - (\lambda_j + \sigma_{a,j}\frac{\rho_U P_s(t)}{\overline{E}_R\overline{\Sigma}_f(t)})N_j(t) \quad (16)$$

To further simplify Equation 16 assumptions must be made about the isotope under investigation. Both radioactive and stable isotopes were investigated for their distinguishing capabilities

A. Radioactive Isotope Monitor Model

The radioactive isotope monitor considered for this model is assumed to have no significant parent isotopes and is produced directly from fission only. Figure 5 shows the mass chain decay scheme for the proposed radioactive monitor.

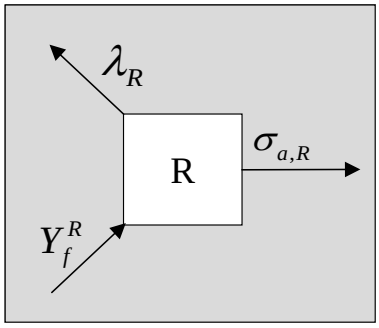

Figure 5. Radioactive Monitor Model Mass Chain Decay Scheme.

For this case, Equation 16 simplifies to

$$\frac{dN_R(t)}{dt} + \left[\lambda_R + \sigma_{a,R}\frac{\rho_U P_s(t)}{\overline{E}_R\overline{\Sigma}_f(t)}\right]N_R(t) = \frac{\rho_U}{\overline{E}_R}\left[\frac{Y^R_{f,U235}}{1+R(t)^{-1}} + \frac{Y^R_{f,Pu239}}{1+R(t)}\right]P_s(t) \quad (17)$$

where $R(t) \equiv \frac{\sigma_{f,U235} N_{U235}(t)}{\sigma_{f,Pu239} N_{Pu239}(t)}$. It should be noted that the concentrations of U-235 and Pu-239 are also dependent on time and the specific power. To avoid a complex integration, the concentrations of U-235 and Pu-239 were approximated by functions of burnup and averaged. Use of average values for the U-235 and Pu-239 concentrations also removes the time dependence of *R*. Figure 6 illustrates the burnup correlations for eight different power history cases run in TransLat. The power history cases are described in section III.E below.

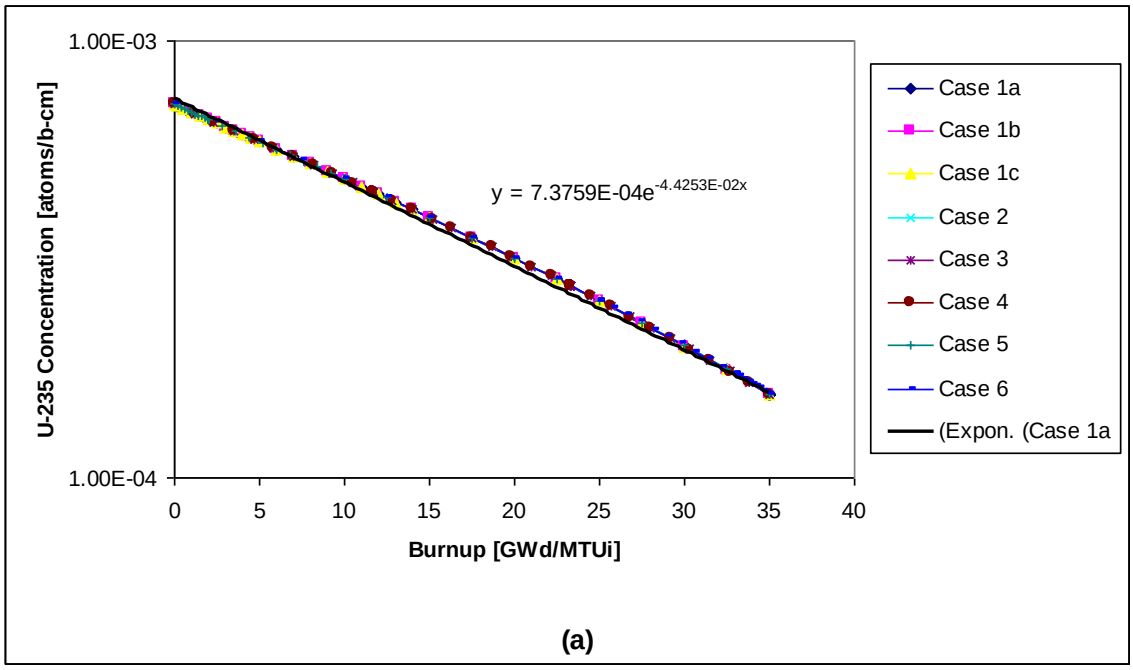

Figure 6. Burnup Correlation for (a) U-235 Concentration and (b) Pu-239 Concentration.

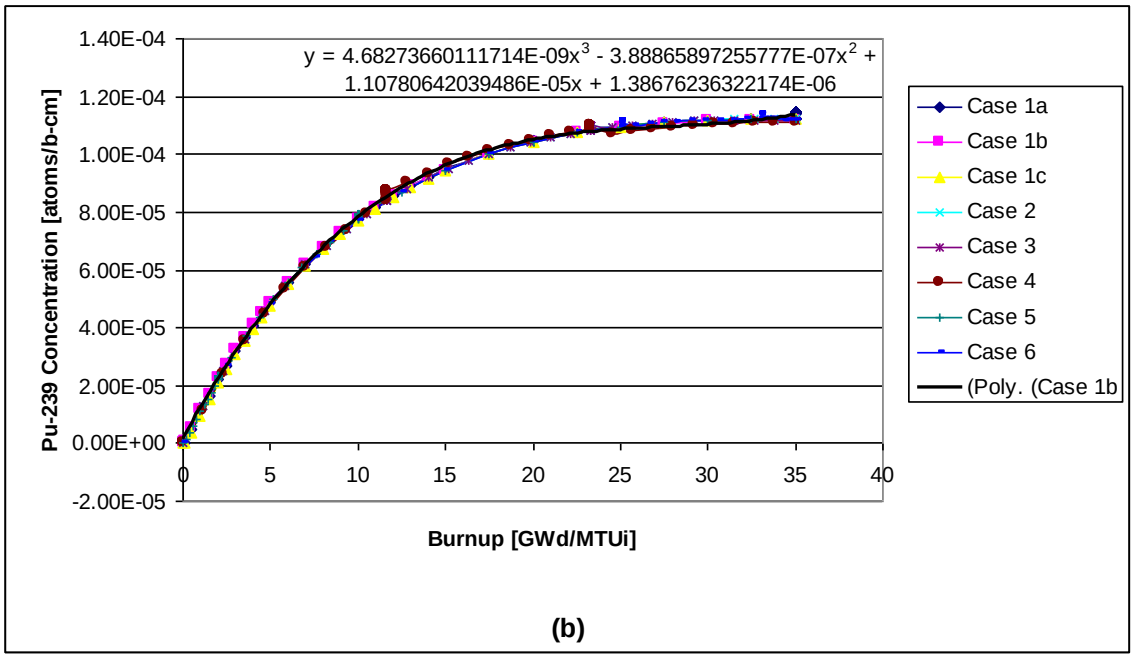

Figure 6. Continued.

B. Average Specific Power Solution for the Radioactive Monitor Model

With Equation 16 sufficiently simplified for the proposed radioactive monitor it may now be solved for the concentration. Equation 17 is not straightforward to integrate though, as the specific power is an unknown function of time. Further, for analytical purposes it would be useful to have a single, isolatable value for specific power with a direct relationship to the monitor concentration. With this in mind, Equation 17 can be integrated to

$$N_R(t) = \frac{\rho_U \overline{P_{s2,R}}}{\overline{E_R}\lambda_{R,eff}}\left[\frac{Y^R_{f,U235}}{1+R^{-1}} + \frac{Y^R_{f,Pu239}}{1+R}\right](1-e^{-\lambda_{R,eff}t}) \tag{18}$$

if an average specific power is assumed as $\overline{P_{s2,R}} \equiv \frac{\int_0^t dt' P_s(t') e^{-\lambda_{R,eff} t'}}{\int_0^t dt' e^{-\lambda_{R,eff} t'}}$ where

$\lambda_{R,eff} \equiv \lambda_R + \sigma_{a,R} \frac{\rho_U \overline{P_{s1}}}{\overline{E}_R \overline{\Sigma}_f}$ and an additional average specific power is defined as

$\overline{P_{s1}} \equiv \frac{\int_0^t dt' P_s(t')}{\int_0^t dt'}$. This model is applied over the lifetime of the fuel with total time including any reactor shutdowns. This model assumes the weighted average specific powers, denoted $\overline{P_{s1}}$ and $\overline{P_{s2,X}}$, are valid for the system. These values are easily determinable from the reactor operator's report for verification with values determined from monitor concentration samples. With enough usable monitors it may also be possible to determine an unknown power history with an iterative scheme based on a Fredholm solution. However, it should be noted that Equation 18 is not valid for isotopes with large neutron absorption cross-sections and experiencing power histories with lengthy shutdowns or large variations in specific power.

C. Piecewise Solution for the Radioactive Monitor Model

An alternative approach to the solution of Equation 17 can be formulated by assuming that the power history can be divided into a piecewise functional of the form $P_s(t) = P_s^i,$ for $t_i < t < t_{i+1},$ for $i = 0,1,...,I$. This is a reasonable assumption as most

reactors are operated at essentially constant power over long time periods. With this assumption the atom concentration for radioactive monitor during step *i* is given by

$$N_R^i(t) = \frac{\rho_U P_s^i}{\overline{E_R}\lambda_{R,eff}}\left[\frac{Y_{f,U235}^R}{1+R^{-1}} + \frac{Y_{f,Pu239}^R}{1+R}\right] *$$
$$\left[1 + \left(\frac{N_R^{i-1}(t_{i-1})\overline{E_R}\lambda_{R,eff}}{\rho_U P_s^i}\left[\frac{Y_{f,U235}^R}{1+R^{-1}} + \frac{Y_{f,Pu239}^R}{1+R}\right]^{-1} - 1\right)e^{-\lambda_{R,eff}(t-t_{i-1})}\right], \text{ for } t_{i-1} < t < t_i \qquad (19)$$

where $\lambda_{R,eff} \equiv \lambda_R + \sigma_{a,R}\frac{\rho_U P_s^i}{\overline{E_R}\overline{\Sigma_f}}$ and $N_R^{i-1}(t_{i-1})$ is the concentration of the radioactive monitor from step *i*-1 at time t_{i-1}. During reactor shutdowns, when the specific power is zero, Equation 19 simplifies to

$$N_R^i(t) = N_R^{i-1}(t_{i-1})e^{-\lambda_R(t-t_{i-1})}. \qquad (20)$$

D. Stable Isotope Monitor Model

A similar development from Equation 16 may be followed to obtain a model for a stable isotope monitor. In this case it was assumed that the stable isotope has a mass chain decay scheme as illustrated in Figure 7. Here the stable daughter isotope is produced from fission and from the decay of its radioactive parent. The radioactive parent is produced only from fission and there are no other radioactive isotopes of significance in the assumed mass chain decay scheme.

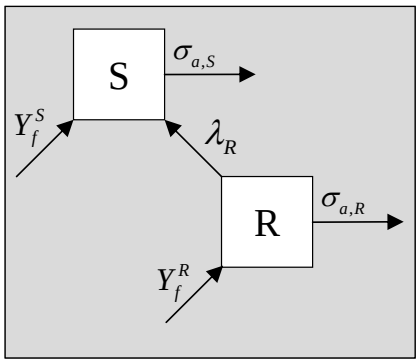

Figure 7. Stable Monitor Model Mass Chain Decay Scheme.

With the assumed decay scheme Equation 16 is simplified to

$$\frac{dN_S(t)}{dt} - (\sigma_{a,S}\frac{\rho_U P_s(t)}{\overline{E}_R \overline{\Sigma}_f})N_S(t) = \frac{\rho_U}{\overline{E}_R}\left[\frac{Y_{f,U235}^S}{1+R^{-1}} + \frac{Y_{f,Pu239}^S}{1+R}\right]P_s(t) + \lambda N_R(t) \tag{21}$$

Equation (21) can be integrated with average specific powers as was done for the radioactive monitor isotope to the solution

$$N_S(t) = \frac{\rho_U}{E_R}\left\{\begin{array}{l}\dfrac{\overline{P_{s2,S}}}{\sigma_{a,S,eff}}\left[\dfrac{Y_{f,U235}^S}{1+R^{-1}} + \dfrac{Y_{f,Pu239}^S}{1+R}\right](1-e^{-\sigma_{a,S,eff}t}) \\ + \dfrac{\lambda_R \overline{P_{s2,R}}}{\lambda_{R,eff}}\left[\dfrac{Y_{f,U235}^R}{1+R^{-1}} + \dfrac{Y_{f,Pu239}^R}{1+R}\right]* \\ \left[\dfrac{1-e^{-\sigma_{a,S,eff}t}}{\sigma_{a,S,eff}} - \dfrac{e^{-\lambda_{R,eff}t} - e^{-\sigma_{a,S,eff}t}}{\sigma_{a,S,eff} - \lambda_{R,eff}}\right]\end{array}\right\}. \tag{22}$$

The average specific power is assumed as $\overline{P_{s2,S}} \equiv \frac{\int_0^t dt' P_s(t') e^{-\sigma_{a,S,eff} t'}}{\int_0^t dt' e^{-\sigma_{a,S,eff} t'}}$ and

$\sigma_{a,S,eff} \equiv \sigma_{a,S} \frac{\rho_U \overline{P_{s1}}}{\overline{E_R}\overline{\Sigma}_f}$. This average specific model has corresponding difficulties dealing with isotopes with large neutron absorption cross-section and experiencing power histories with lengthy shutdowns or large variations in specific power. As such a piecewise solution was again pursued. The piecewise solution for the atom concentration of the stable daughter monitor is

$$N_S^i(t) = \frac{\rho_U P_s^i}{\overline{E_R}\sigma_{a,S,eff}} \left[\frac{Y_{f,U235}^S}{1+R^{-1}} + \frac{Y_{f,Pu239}^S}{1+R} \right] (1 - e^{-\sigma_{a,S,eff}(t-t_{i-1})}) +$$
$$\lambda_R \left\{ \begin{array}{l} \frac{\rho_U P_s^i}{\overline{E_R}\lambda_{R,eff}} \left[\frac{Y_{f,U235}^R}{1+R^{-1}} + \frac{Y_{f,Pu239}^R}{1+R} \right] \left[\frac{(1 - e^{-\sigma_{a,S,eff}(t-t_{i-1})})}{\sigma_{a,S,eff}} + \frac{(e^{-\sigma_{a,S,eff}(t-t_{i-1})} - e^{-\lambda_{R,eff}(t-t_{i-1})})}{(\sigma_{a,S,eff} - \lambda_{R,eff})} \right] \\ + \frac{N_R^{i-1}(t_{i-1})(e^{-\lambda_{R,eff}(t-t_{i-1})} - e^{-\sigma_{a,S,eff}(t-t_{i-1})})}{(\sigma_{a,S,eff} - \lambda_{R,eff})} \end{array} \right\} \quad (23)$$
$$+ N_S^{i-1}(t_{i-1}) e^{-\sigma_{a,S,eff}(t-t_{i-1})}, \text{ for } t_{i-1} < t < t_i$$

where $\sigma_{a,S,eff} \equiv \sigma_{a,S} \frac{\rho_U P_s^i}{\overline{E}_R \overline{\Sigma}_f}$

$$N_S^i(t) = N_S^{i-1}(t_{i-1}) + N_R^{i-1}(t_{i-1})(1 - e^{-\lambda_R(t-t_{i-1})}) \quad (24)$$

E. Model Verification

These models were benchmarked against concentration values generated by TransLat for two sets of radioactive parent and stable daughter nuclide pairs. The cross-sections and yield values used were taken from the ORIGEN 2.2 PWRPUU library. ORIGEN 2.2 is the Oak Ridge Isotope Generation Code which uses a deterministic method for determining isotope generation and depletion and has been successfully benchmarked elsewhere.[34,35]

Several TransLat cases run were based on a PWR pin cell similar to those used in the benchmarking study described in Chapter II. Figure 8 illustrates the power histories simulated with TransLat.

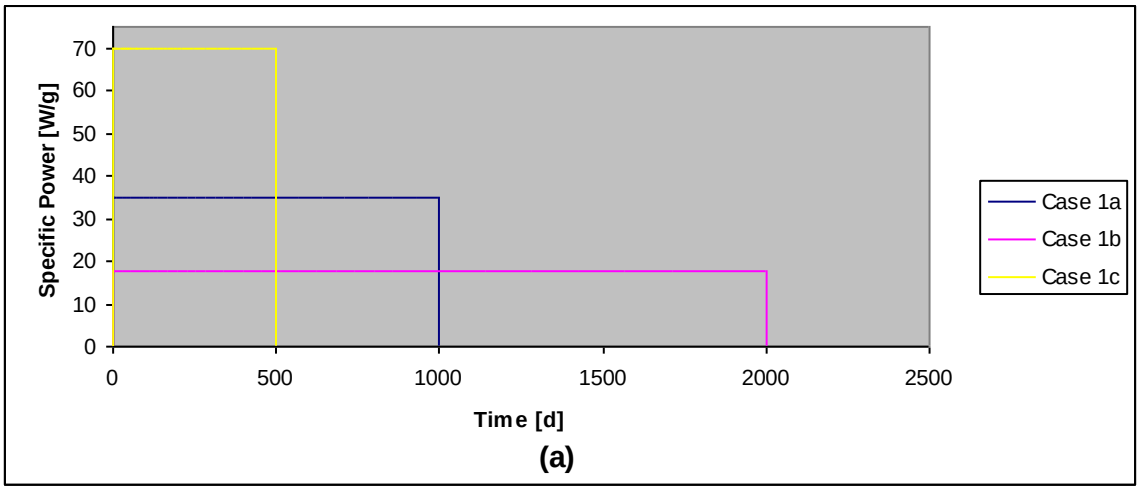

Figure 8. Reactor Power History Cases Run Using TransLat (a) Cases 1a, 1b, 1c; (b) Case 2; (c) Case 3; (d) Case 4; (e) Case 5; (f) Case 6.

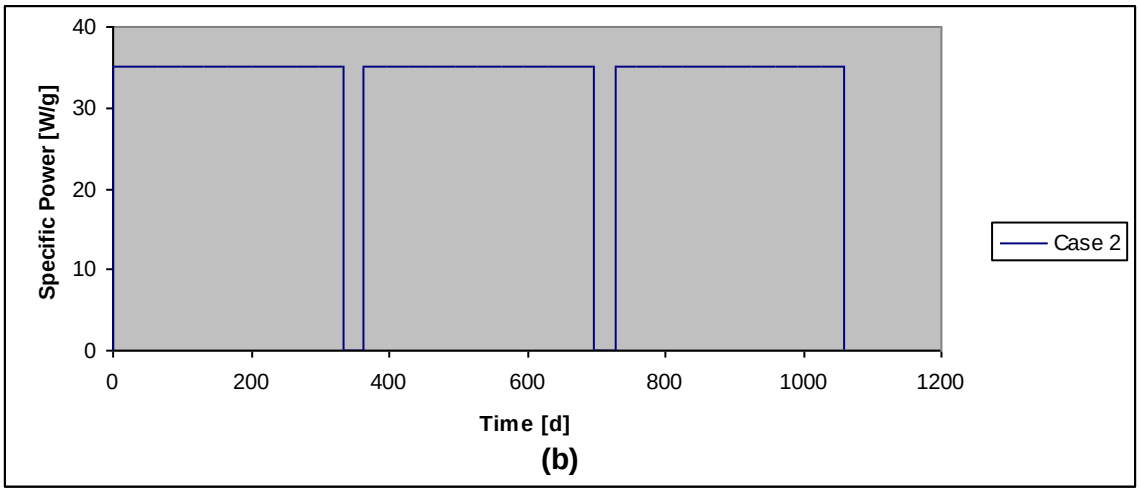

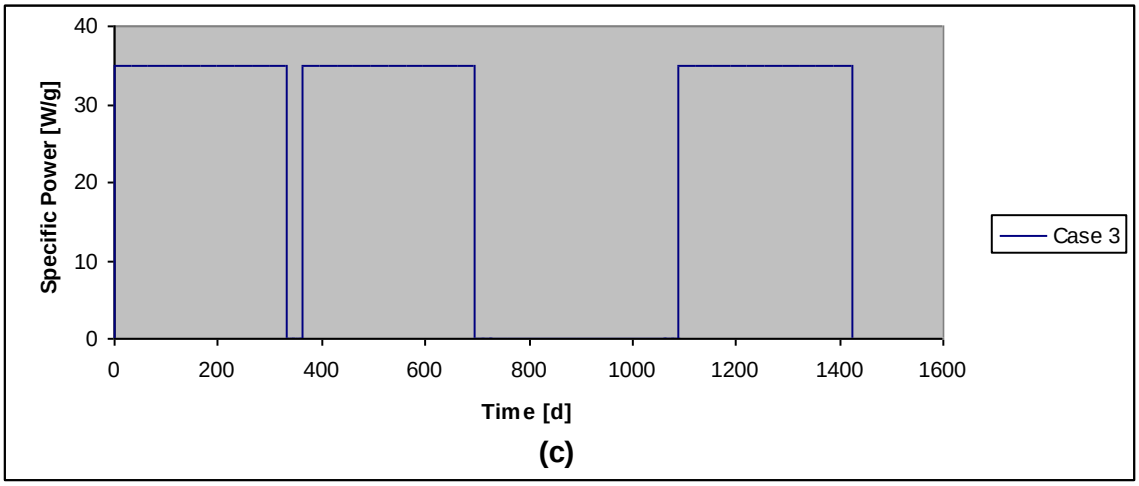

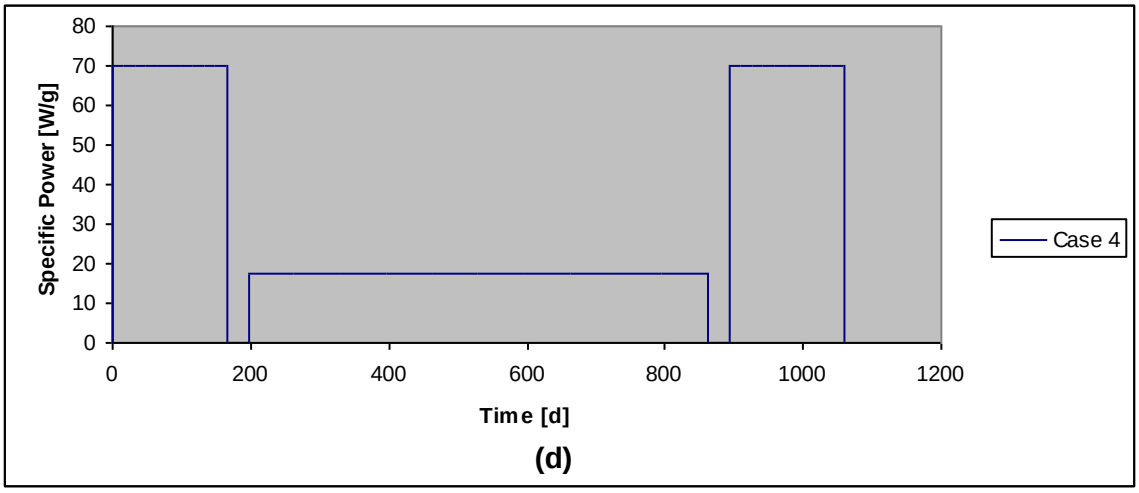

Figure 8. Continued.

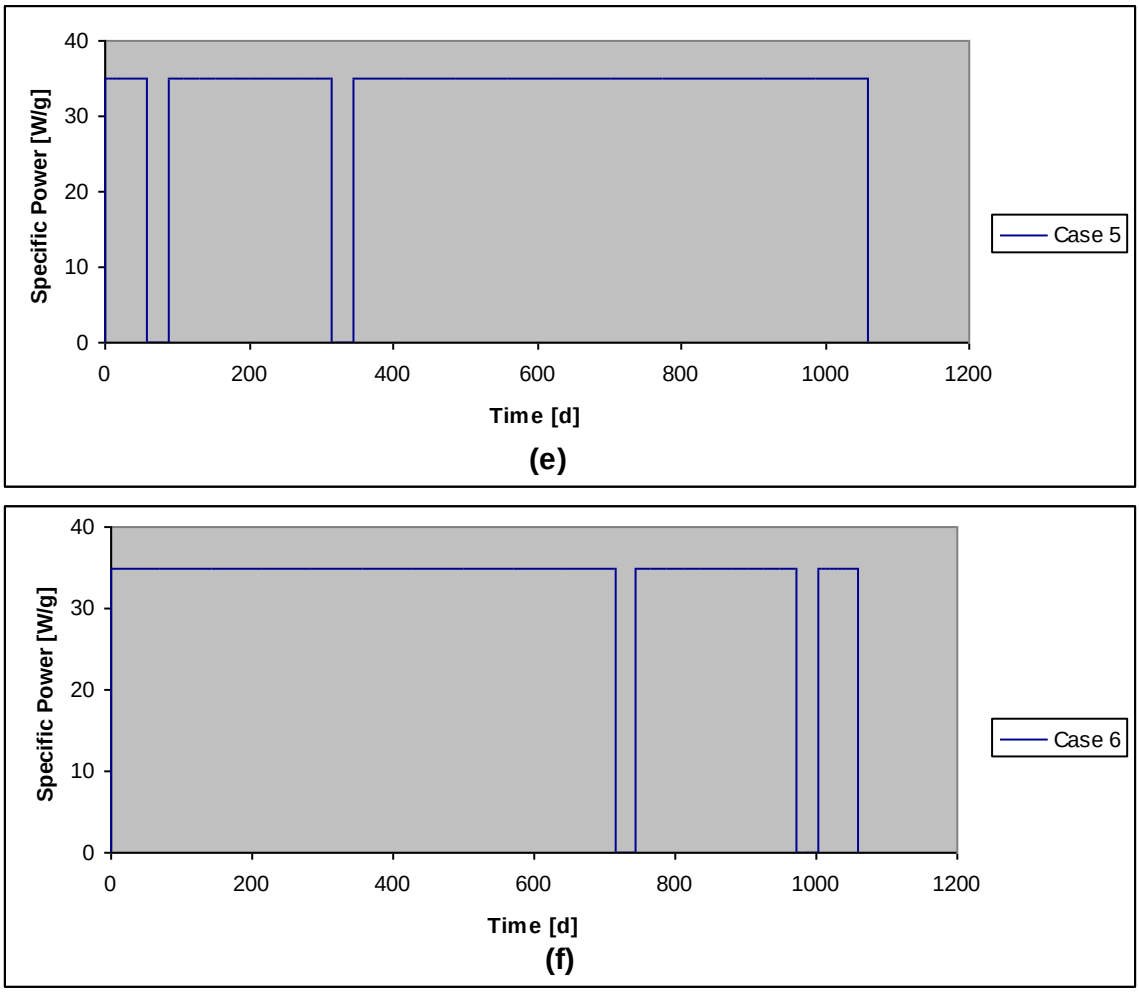

Figure 8. Continued.

All cases run have a final burnup of 35 GWD/MTU. The first three cases, Case 1a, Case 1b, and Case 1c are all straight burns with no shutdowns. Case 1a is the base case run with a constant specific power of 35 W/g. Case 1b and Case 1c halve and double the specific power of Case 1a to 17.5 W/g and 70 W/g respectively. Case 2 adds two thirty day shutdowns to the base case maintaining the original 35 W/g specific power. Case 3 adds an additional cooling cycle, of equal length to the burn cycles of Case 2, and an

additional thirty day shutdown period. This recreates a four-cycle core load where fuel assemblies experience a three burn cycle rotation with one cooling cycle out of the reactor. This is a common practice in the nuclear power industry.[36] Case 4 reverts to the shutdown scenario of Case 2, but varies the specific power from 70 W/g, 17.5 W/g, and back to 70 W/g for the burn cycles. It should be noted in Case 4 that the total burnup of each burn cycle remains the same while the actual of time of each burn cycle varies inversely with specific power. Case 5 and Case 6 vary from Case 2 by adjusting when the shutdowns occur. In Case 5 the shutdowns occur at fuel burnups of 2 GWD/MTU and 10 GWD/MTU whereas in Case 6 the shutdowns occur at 25 GWD/MTU and 33 GWD/MTU.

The larger concern for benchmarking of the analytic models was not accuracy, but instead behavior in response to power history variations. The analytic models derived are general and make several assumptions. Further the values of parameters obtained from ORIGEN 2.2 and used in the models are not necessarily equal to the values of the same parameters used by TransLat. Accuracy was also not necessary for the models to be useful. The models were intended to be used to construct a guide for identifying potential monitor isotopes. As long as the models yield results that behave similar to results from TransLat with respect to power history variations, the guides produced from the models will be applicable. Figure 9 compares the behavior of the models to the behavior of TransLat in response to the power history variations described for Cases 1-6 for the radioactive and stable daughter nuclide pairs Sr-90, Zr-90, Cs-137, and Ba-137.

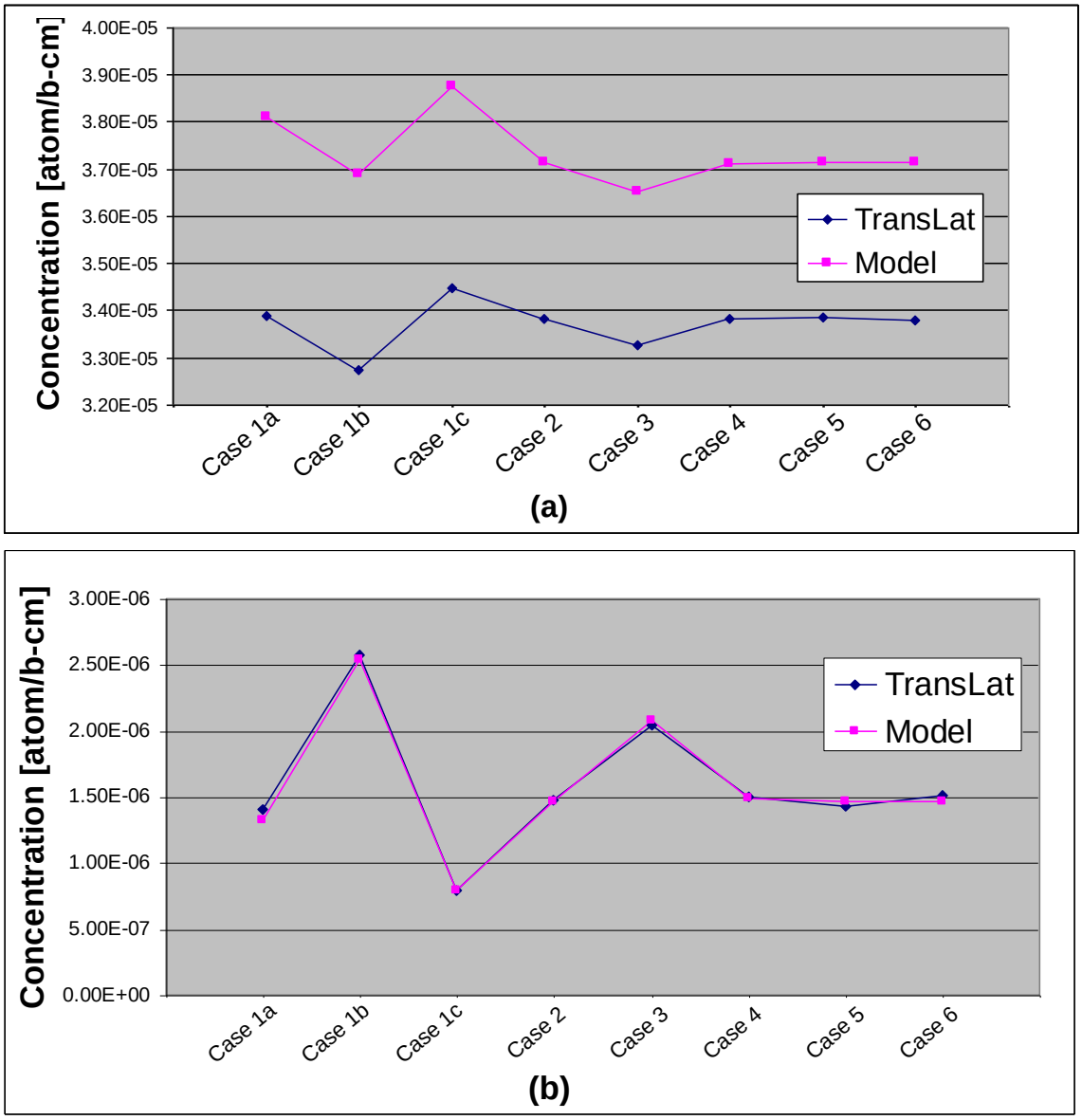

Figure 9. Model Benchmarking Results for (a) Sr-90, (b) Zr-90, (c) Cs-137, (d) Ba-137.

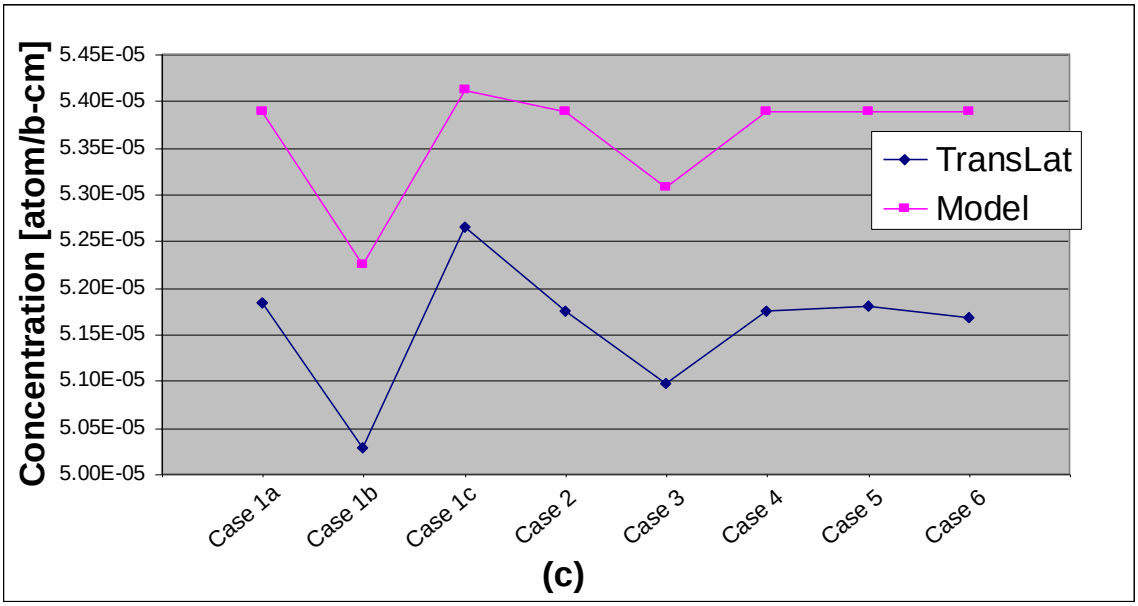

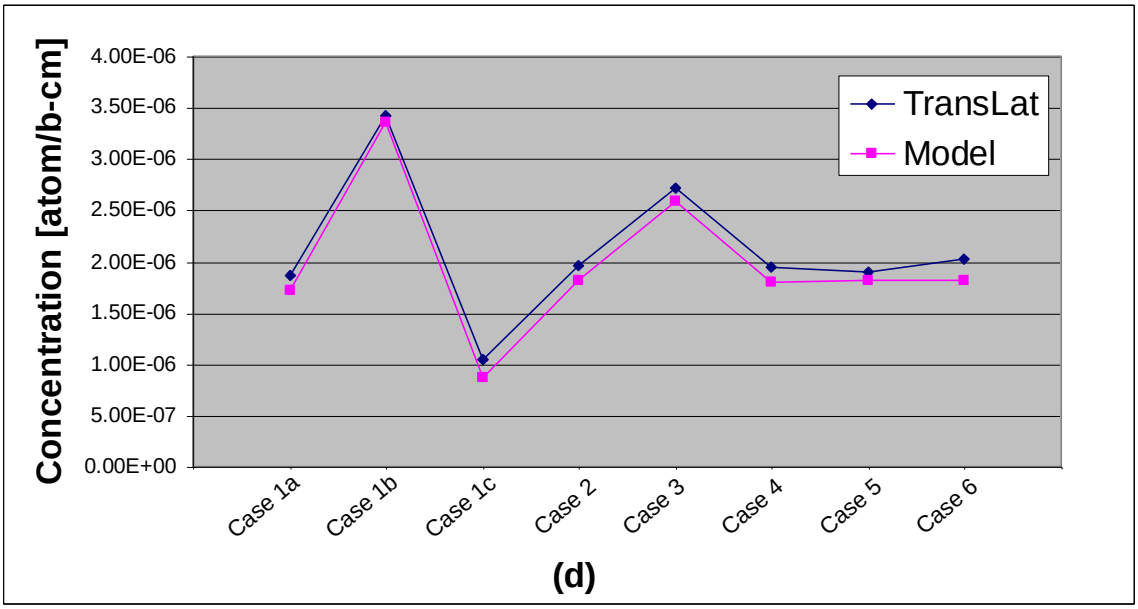

Figure 9. Continued.

As seen in Figure 9 the models follow the behavior of TransLat very closely and in the cases of Zr-90 and Ba-137 even have good accuracy as well. Tables with the numerical

data represented in Figure 9 are given in Appendix B. This validates the use of the derived models.

F. Monitor Selection Guide Development

The models developed above were used to generate a range of useful monitor properties to guide the selection and testing of actual fission product isotopes. In doing so an understanding of how the decay constant and cross-sections influence the concentration of potential monitors in response to power history variations was also developed. Table III shows the ranges of values for the decay constants and cross-sections of the potential monitor models used in this analysis.

Table III

Ranges of Parameters Varied for Potential Monitor Models

	Radioactive Monitor	Stable Monitor
Parent Half-Life [yr]	N/A	0.0055-40,000
Parent Cross-section [b]	N/A	1-10,000
Monitor Half-Life [yr]	0.0055-40,000	N/A
Monitor Cross-section [b]	1-10,000	1-10,000

While varying the parameters as described in Table III, both models were applied to power history scenarios which varied specific power and shutdown time. The total burnup for the power history scenarios was held constant at 35 GWd/MTU. The first power history scenario, shown in Figure 10, consisted of a single irradiation cycle with a

constant specific power and no shutdowns. The constant specific power was varied from 1–110 W/g. The second power history scenario, shown in Figure 11, consisted of three irradiation cycles of equal burnup with variable specific power and no shutdowns. The specific powers of the first and third cycles were held constant at 100 W/g while the second cycle specific power was varied from 10–100 W/g. The third power history scenario, shown in Figure 12, involved three burn cycles of equal burnup divided by shutdowns of variable duration. The total shutdown time was varied between 20 d – 2000 d and evenly divided between the two shutdowns. The specific power of each cycle for the third scenario was held constant at 35 W/g. Plots illustrating the results of the power history variation scenarios were included in Appendix C.

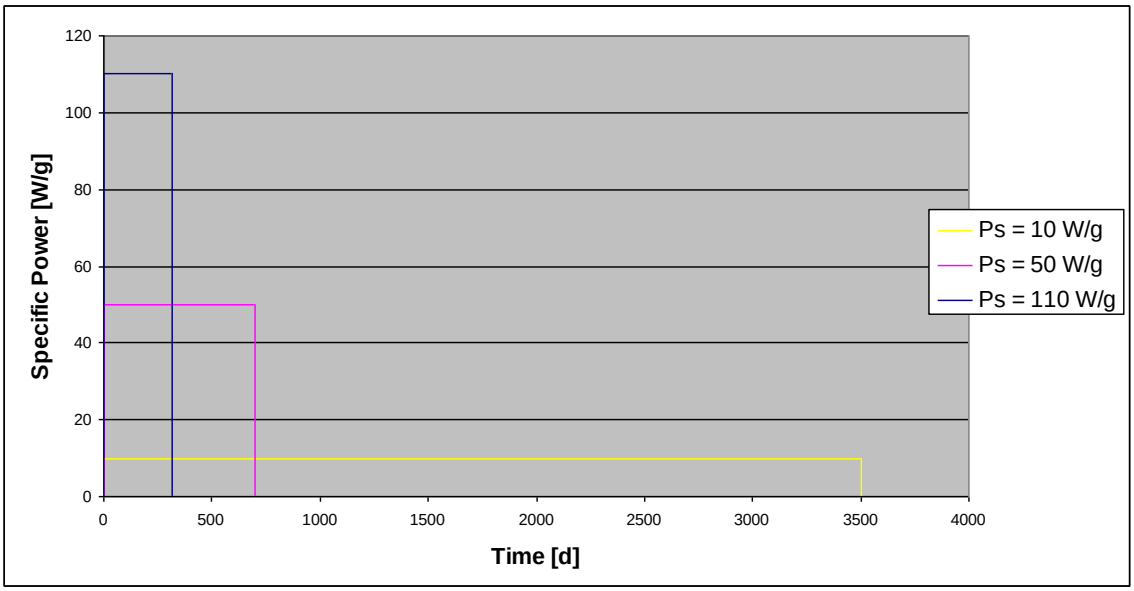

Figure 10. Power History Variation Scenario 1: Specific Power Constant during Reactor Operation.

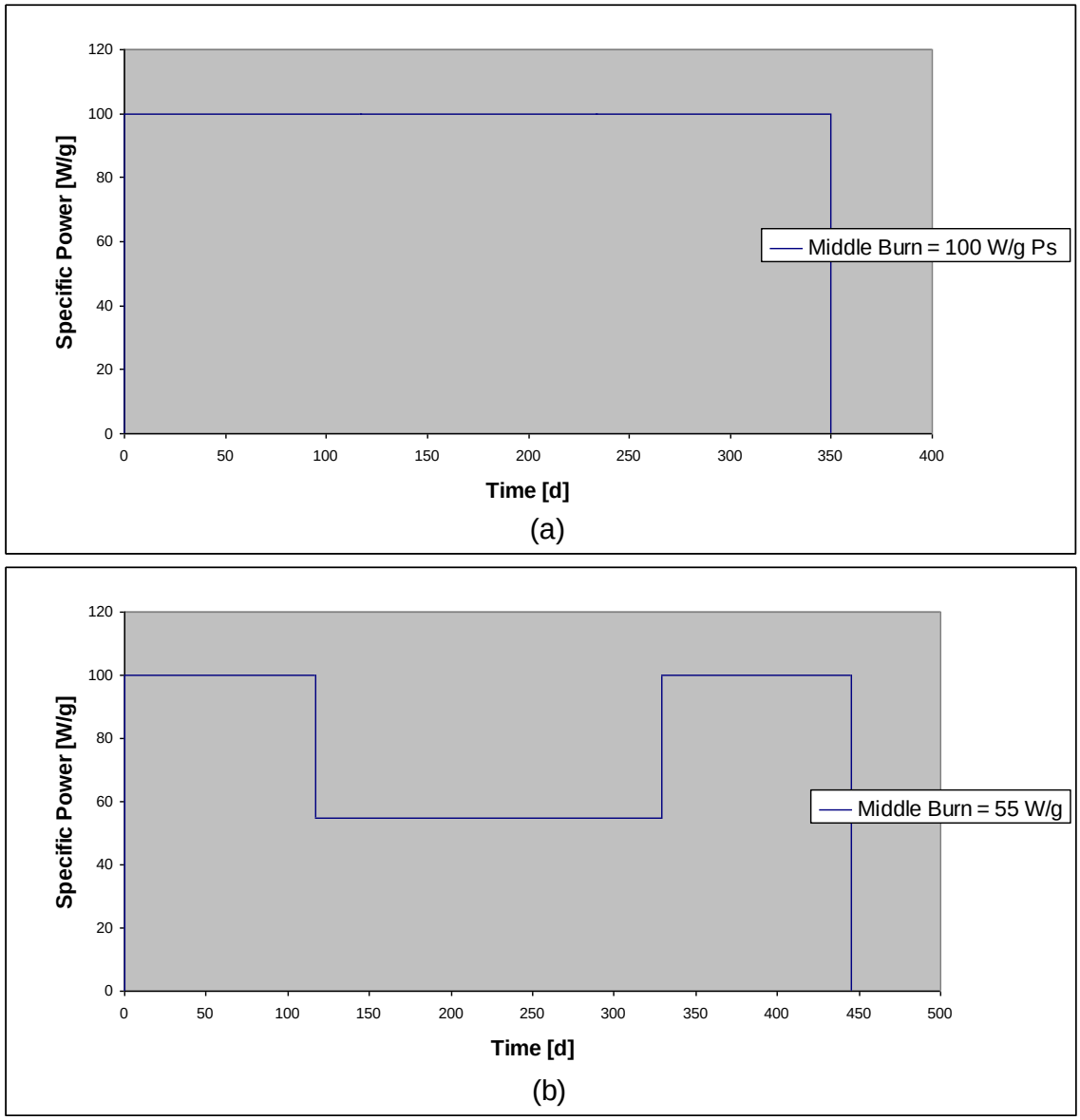

Figure 11. Power History Variation Scenario 2: Specific Power Varied during Reactor Operation (a) Maximum 2nd Cycle Specific Power, (b) Mean 2nd Cycle Specific Power, (c) Minimum 2nd Cycle Specific Power.

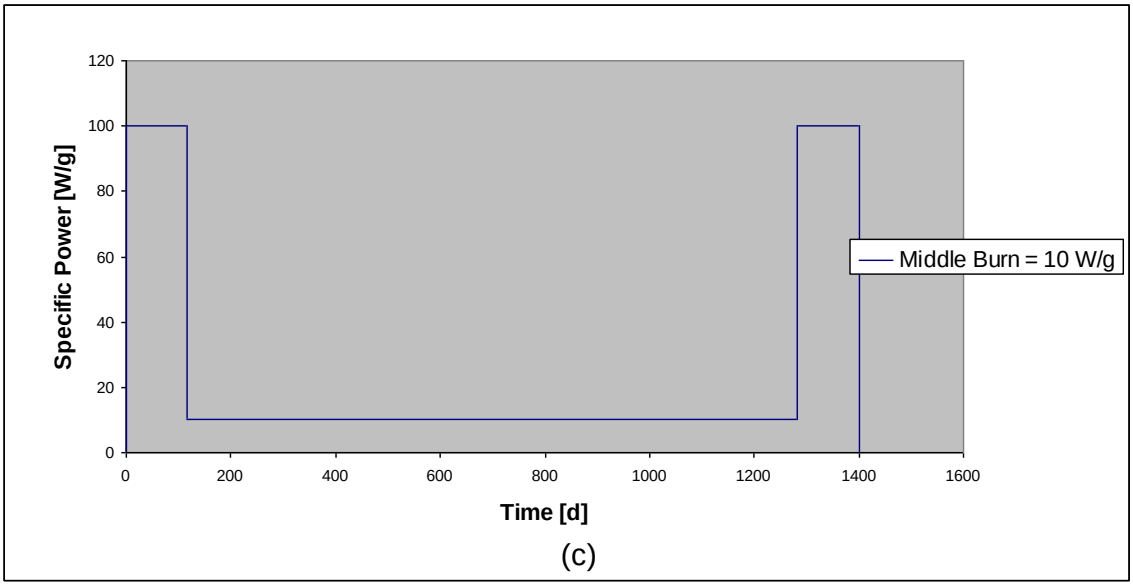

Figure 11. Continued.

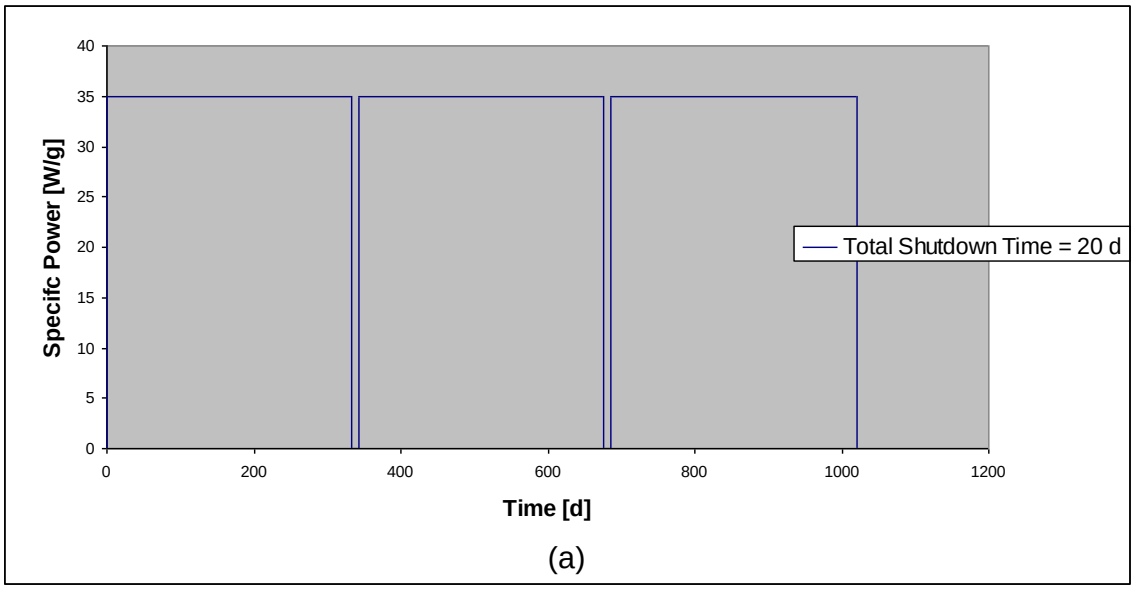

Figure 12. Power History Variation Scenario 3: Variable Shutdown Time divided between Two Shutdowns (a) Minimum Total Shutdown Time, (b) Mean Total Shutdown Time, (c) Maximum Total Shutdown Time.

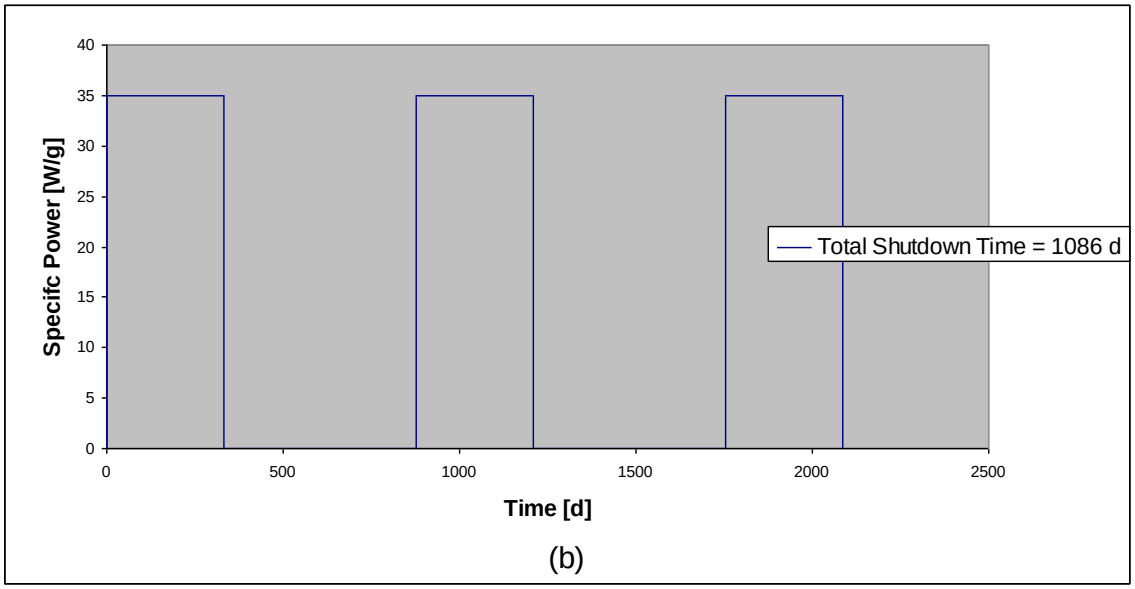

(b)

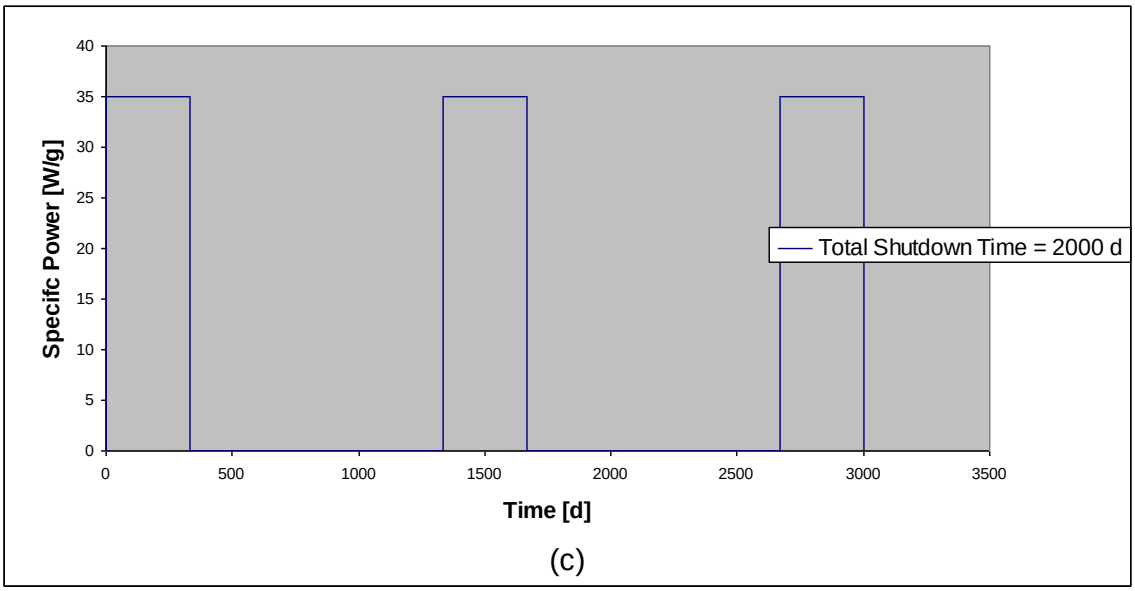

(c)

Figure 12. Continued.

G. Monitor Selection Guide

Differences in final monitor concentrations generated through the power history variation analyses led to identification of ideal values of monitor properties. Useful ranges of monitor properties are shown in Figure 13.

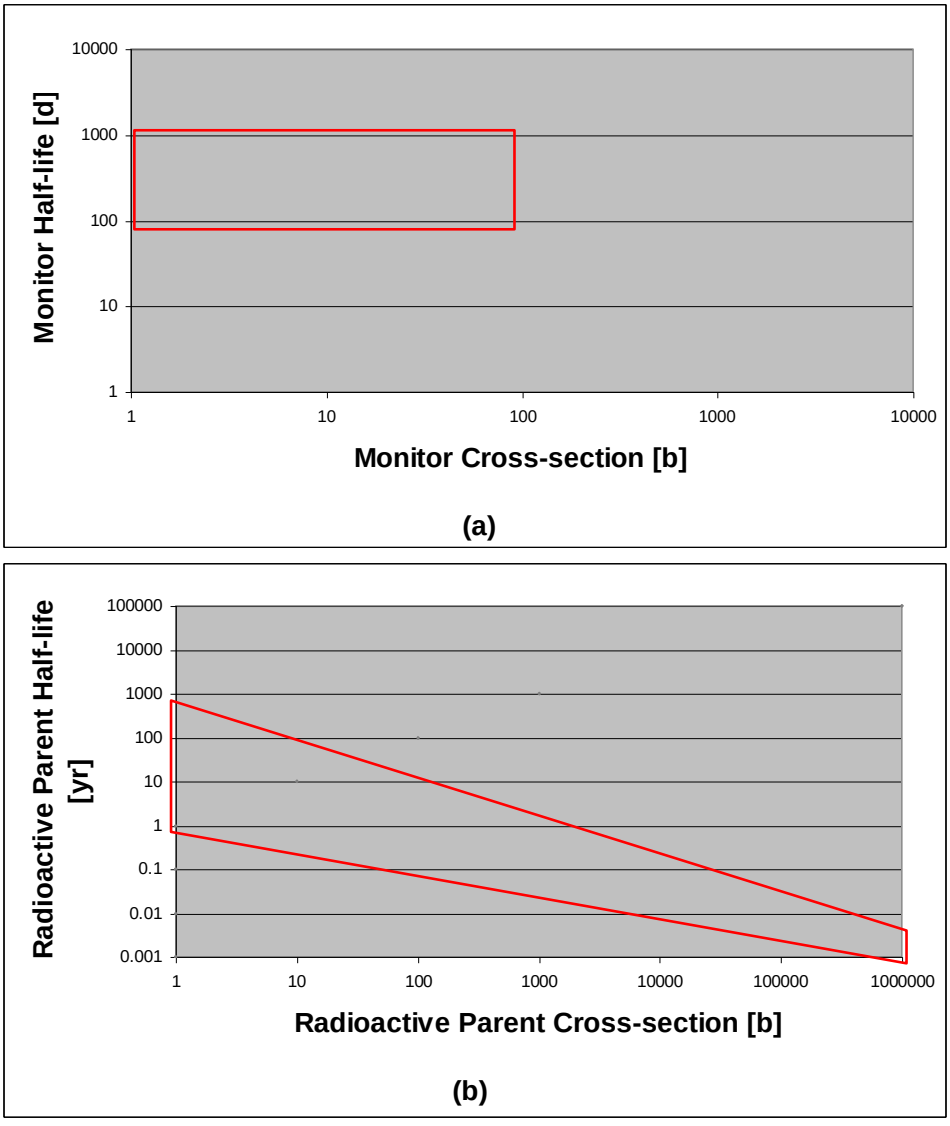

Figure 13. Useful Property Ranges for (a) Potential Radioactive Monitors and (b) Potential Stable Monitors.

H. Influence of Monitor Properties

The ranges of useful monitor properties are determined by the value of $\lambda_{R,eff}$, $\sigma_{a,S,eff}$, and the time duration of the irradiation. Since in all scenarios the final burnup was constant, the total amount of monitor isotope atoms produced was also constant. However, the amount of each isotope lost via absorption or decay or produced via parent decay varies depending on the specific power history. The implications of $\lambda_{R,eff}$ will be explored separately for the radioactive monitor and the stable monitor.

H.1 Radioactive Monitor

Concentration differences in radioactive monitors from variations in power history were found to be a result of an optimal destruction mechanism of the monitor. The destruction mechanism of the radioactive monitor is controlled by the effective decay constant $\lambda_{R,eff}$. If $\lambda_{R,eff}$ is too small, a negligible amount of destruction will occur and concentration will not vary with power history. However, if $\lambda_{R,eff}$ is too large the monitor will decay too rapidly leading to saturation of the monitor at the current specific power and loss of measurable signal after shutdown. A Figure of Merit (*FOM,R*) was defined for the radioactive monitor as

$$FOM,R = \frac{N_R^i\left(t_i, P_s^i = 10\ \text{W/g}\right) - N_R^i\left(t_i, P_s^i = 100\ \text{W/g}\right)}{N_R^i\left(t_i, P_s^i = 10\ \text{W/g}\right)} * 100 * N_R^i\left(t_i, P_s^i = 10\ \text{W/g}\right) \quad (25)$$

where the power history consists of a single irradiation cycle to 35 GWd/MTU. This *FOM,R* accounts for the increased percent difference for large values of $\lambda_{R,eff}$. This *FOM,R* is plotted against $\lambda_{R,eff}$ in Figure 14.

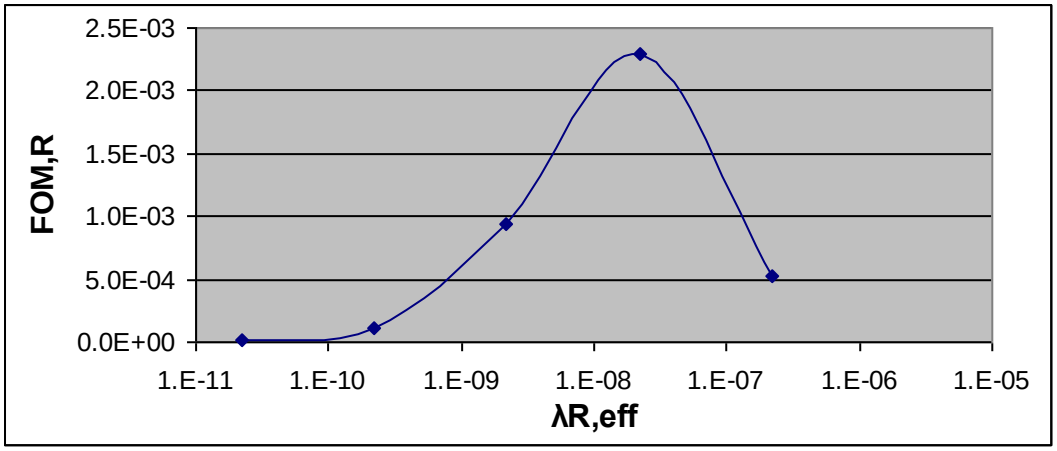

Figure 14. Optimal Range of $\lambda_{R,eff}$ for a Radioactive Monitor.

The limits shown in Figure 13(a) can be derived in part from Figure 14. The limits of $\lambda_{R,eff}$ may be directly applied to the monitor half-life. The influence of cross-section on radioactive monitor concentration is not as clear as cross-section coupled to specific power as seen in the definition of $\lambda_{R,eff}$. Substituting for specific power by $P_s^i = BU_i\left(t - t_{i-1}\right)^{-1}$ in Equation 19 and referring to the product $\lambda_{R,eff}(t - t_{i-1})$ one sees that if decay is negligible relative absorption, irradiation time will cancel:

$$\lambda_{R,eff}(t - t_{i-1}) = \frac{\sigma_{a,R}\rho_U BU_i}{\overline{E_R}\overline{\Sigma_f}}.$$

The result is that variations in specific power will not produce variations in monitor concentration. If decay is not relatively negligible then a large cross-section will shift $\lambda_{R,eff}$ above the useful range. As such minimal cross-sections are desirable and correspond to the limits of cross-section shown in Figure 13(a). It is noteworthy that the value of this optimal $\lambda_{R,eff}$ is approximately inversely proportional to the reactor period. It was seen that if reactor period is increased the limits of $\lambda_{R,eff}$ will be decreased.

H.2 Stable Monitor

Concentration differences in stable monitors from variations in power history were found to be a result of an optimal production mechanism from the decay of the monitor's radioactive parent. Production via parent decay is represented by the second term in Equation 23. In order for concentration differences to occur in the stable monitor, the rate of production via decay of the parent must be sufficiently limited so that irradiation time (as specified by specific power) determines the amount of production via decay. If the rate of decay is too fast, total time will not impact the amount of production. The properties of the radioactive parent determine the amount of stable monitor production via decay.

For an appropriate discussion of how the properties of the radioactive parent limit production via decay the parent destruction rate $\lambda_{R,eff}$ must be resolved into its components of decay, λ_R, and absorption, $\sigma_{a,R}$. λ_R directly limits production via

decay. There is thus a range of λ_R for which production will be sufficiently limited but not so limited that production will be negligible. The percent difference between final monitor concentrations produced from a single irradiation cycles to 35 GWd/MTU with specific powers of 10 W/g and 100 W/g is plotted against λ_R in Figure 15 for two values of $\sigma_{a,R}$: (a) $\sigma_{a,R}$ = 0.001 b and (b) 10,000 b.

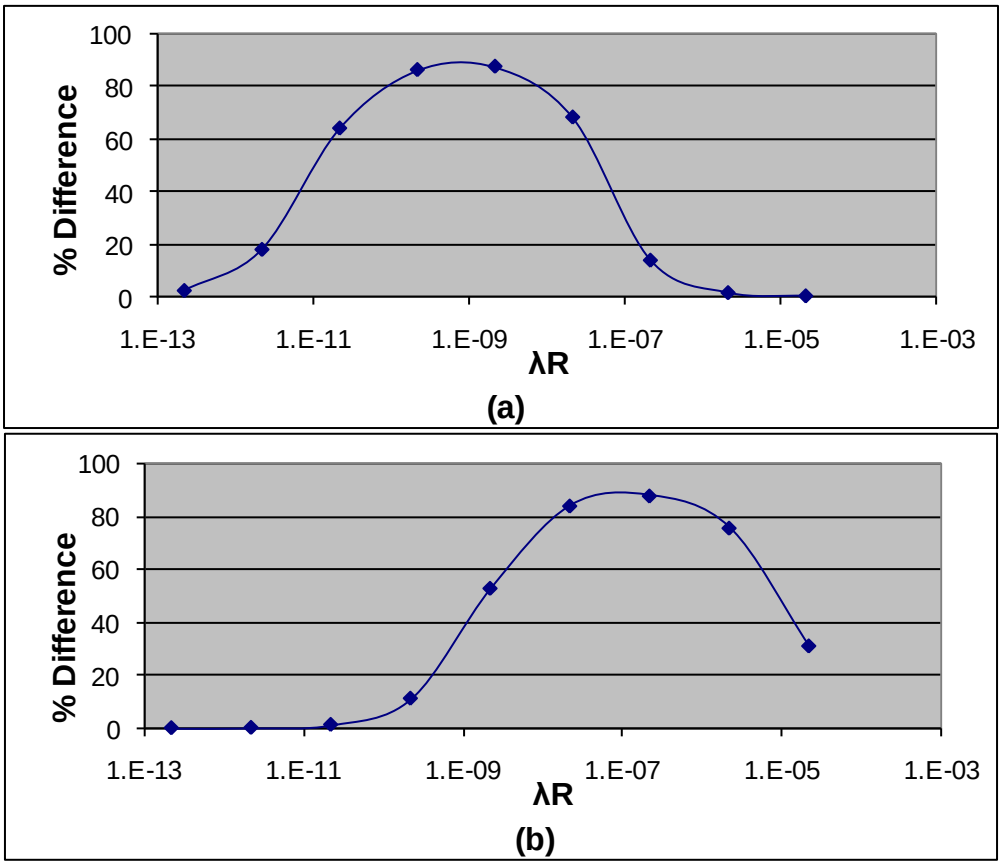

Figure 15. Optimal Range of λ_R for a Stable Monitor with (a) $\sigma_{a,R}$ = 0.001b and (b) 10,000b.

Neutron absorption by the radioactive parent serves as competition for production via decay. This competition serves to drive the useful range of λ_R to higher values. This is illustrated in Figure 15(b) by increasing the value of $\sigma_{a,R}$ to 10,000 b. The optimal range of parent half-life and $\sigma_{a,R}$ shown in Figure 13(b) reflect the useful range of λ_R as influenced by $\sigma_{a,R}$. Another affect of the competition provided by absorption is a boost in concentration experienced by the stable monitor as a result of reactor shutdowns.[15] This concept is illustrated by Figure 1.

If cross-section is large enough to move the useful parent property range to the far right of Figure 13(b), the presence of reactor shutdowns will no longer be reflected in the stable monitor concentration. In this case the useful parent half-life is so short that all parent atoms will immediately decay if not absorbed. Such a monitor would reflect only variations in non-zero specific power. The parent daughter pair of Xe-135 and Cs-135 exhibit the properties required of a specific power only monitor. Comparison of the Cs-135 concentration and the Sm-147 concentration which is highly influenced by reactor shutdowns (depicted in Figure 1) may directly isolate total shutdown time.

It was desired to understand the physical mechanisms by which differences in fission product concentrations were produced as a result of variations in reactor power history. To do this analytical monitor models were developed and their use validated with the lattice physics code TransLat. These models were then used to simulate various reactor power history scenarios to develop an understanding of the physical mechanisms involved. It was determined that the fission product concentrations may be altered as a result of variations in power history through two modes. The first mode requires an optimized saturation rate as determined by half-life for radioactive monitors or the absorption cross-section of stable monitors. The second mode acted by an optimal limitation of production via radioactive parent decay as controlled by the half-life and the absorption cross-section of the radioactive parent isotope. The optimal ranges of monitor and parent properties were used to guide the identification of actual fission products for testing as potential monitor isotopes. The confirmation of fission product monitor isotopes will be discussed in Chapter IV.

CHAPTER IV

POTENTIAL MONITORS

The power history cases described in section III.E were modeled using TransLat to allow for confirmation of monitor isotopes that could be used to verify spent fuel power history. Eight different power history cases were simulated. Using the results of Chapter III as a guide, the isotopic data produced by the TransLat case study was used to confirm potential monitors. The results of this study with suggested monitor ratios are reported in this chapter.

Based on the half-life ranges of potential radioactive monitors and the radioactive parents of potential stable monitors given, a potential monitor list was developed. Tables IV and V list potential radioactive and stable monitors respectively.[37]

Table IV

Potential Radioactive Monitors

Potential Monitor	Monitor Half-Life [d]
Ru-106	372.3
Ag-110m	249.8
Sn-119m	293
Sn-123	129.2
Sb-125	1006.67
Te-127m	109
Cs-134	753.725
Ce-144	284.6
Pm-147	957.541

Table V

Potential Stable Monitors

Potential Monitor	Radioactive Parent	Parent Half-Life [yr]
Rb-85	Kr-85	10.76
Zr-90	Sr-90	28.78
Pd-106	Ru-106	372.3
Sb-123	Sn-123	0.3540
Te-125	Sb-125	2.758
I-127	Te-127m	0.2986
Ba-134	Cs-134	2.065
Ba-137	Cs-137	30.07
Nd-144	Ce-144	0.7797
Sm-147	Pm-147	2.6234
Eu-151	Sm-151	90
Gd-154	Eu-154	8.593
Gd-155	Eu-155	4.75

TransLat results were used to determine the sensitivity of each potential monitor to changes in power history. Figure 16 and Figure 17 illustrate the percent difference with the base case for the potential monitor isotope concentration of the other cases. The monitor isotopes would likely be measured by mass spectroscopy. To avoid fractionation effects, each monitor will be measured relative to another isotope of the same element.[38] As such the figures relate the data as ratios which were selected to maximize the differences with the base case. Tables of the numerical data represented in the figures are given in Appendix D.

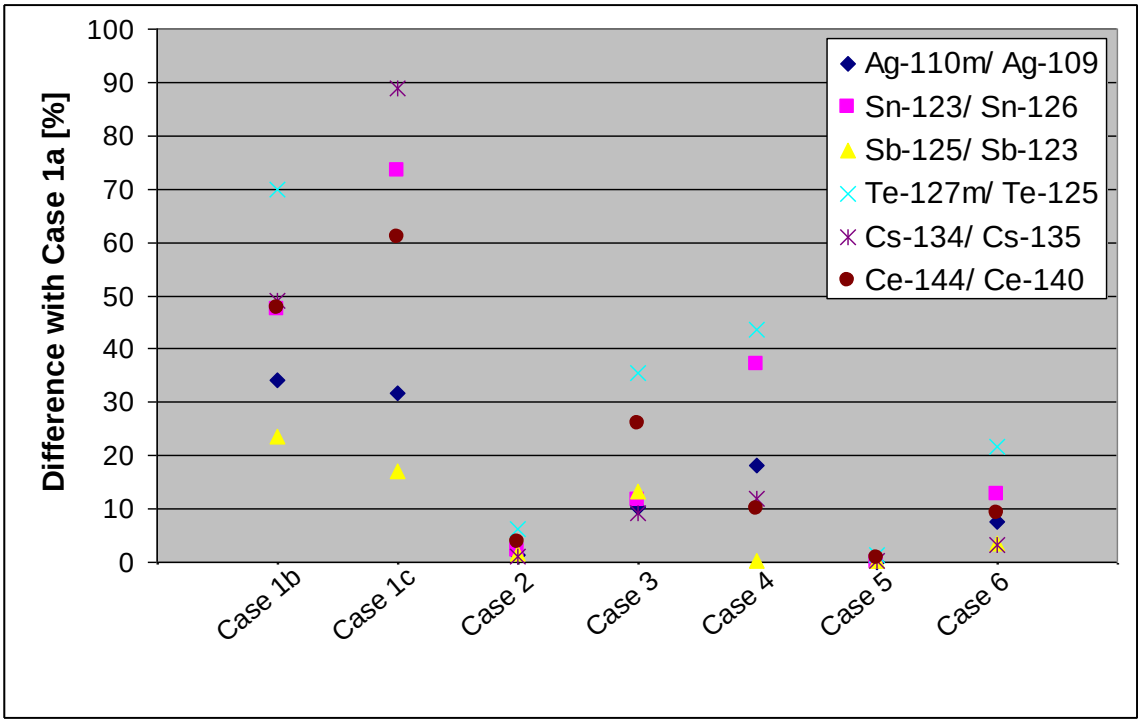

Figure 16. Results of TransLat Case Study for Potential Radioactive Monitors.

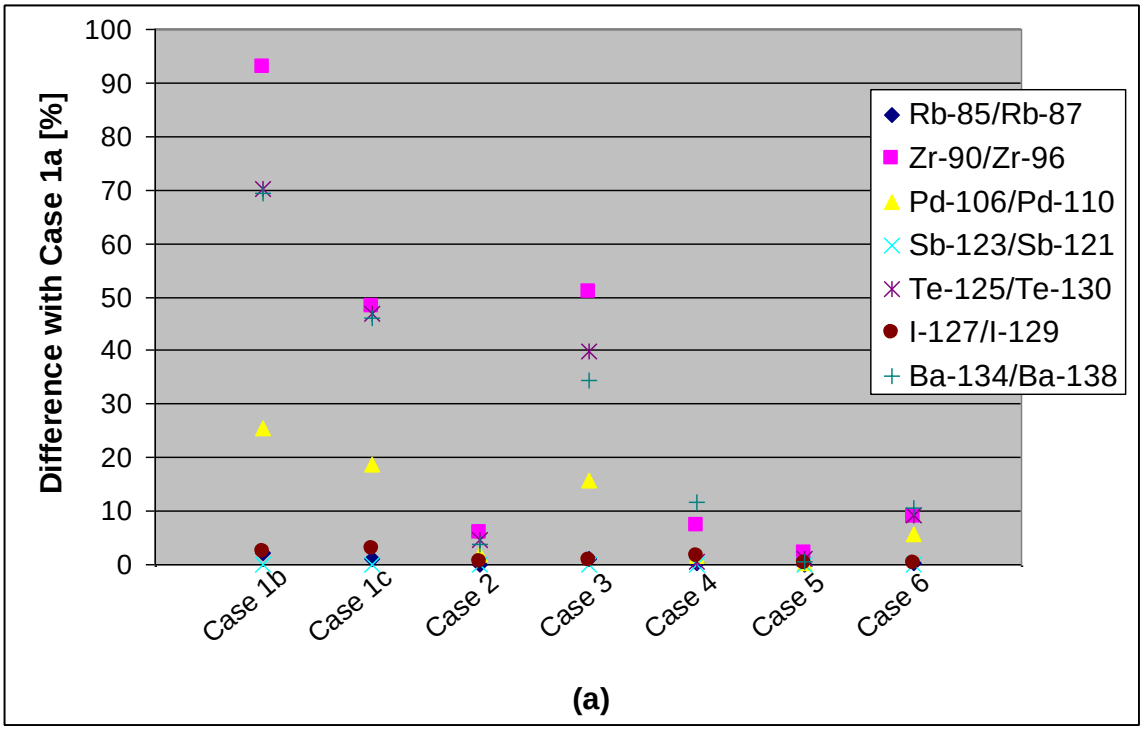

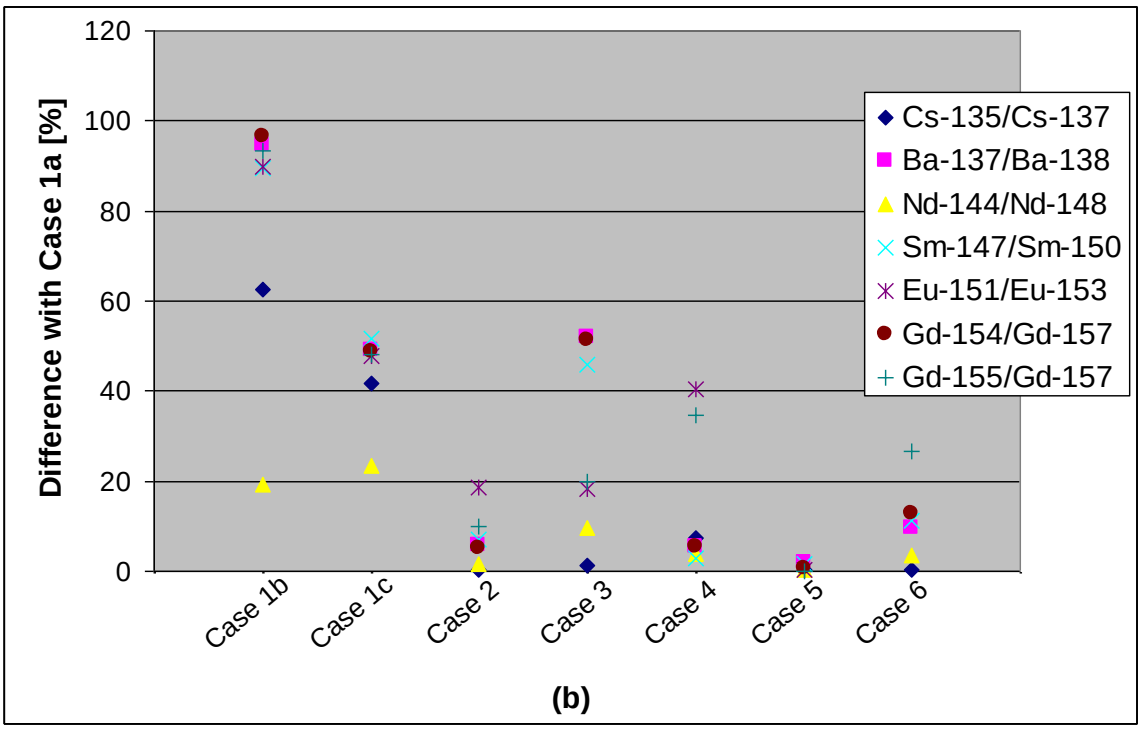

Figure 17. Results of TransLat Case Study for Potential Stable Monitor (a) Set 1 and (b) Set 2.

As seen in the Figures 16 and 17 above those potential monitors that do not show significant variation include Rb-85, Sb-123, and I-127. These three isotopes likely did not show variation because the radioactive parent responsible for the expected differences has multiple states with different half-lives. Thus the parent state with the half-life necessary for daughter variation was likely not the dominant parent state. As a result daughter concentration was controlled by a parent nuclide state without the necessary characteristics and the daughter behaved as such. Additionally, Sn-119m remains unconfirmed because it was not included in TransLat's nuclide library. A ratio including Pm-147 was not included because the element Pm has no stable isotopes. Thus, while it may be a useful signature, it's measurement via mass spectrometry would be complicated. Therefore, it was not considered as a monitor isotope.

The concept of using Cs-135 as a specific power only monitor was proven by the results shown in Figure 17. Significant differences for the Cs-135/Cs-137 ratio from Case 1a were seen for only the cases in which the specific power was adjusted: Case 1b, Case 1c, and Case 4. This makes Cs-135 unique among the other monitors and potentially very useful to the full characterization of reactor power history.

The Cs-135/Cs-137 monitor ratio may be used to isolate the specific power independent of any shutdowns during reactor operation. A generic mathematical representation of power history as a function of time may be written as

$$P_s(t) = \begin{Bmatrix} P_{s1},\ t_0 \le t < t_1 \\ P_{s2},\ t_1 \le t < t_2 \\ P_{s3},\ t_2 \le t < t_3 \\ P_{s4},\ t_3 \le t < t_4 \\ P_{s5},\ t_4 \le t < t_5 \\ P_{s6},\ t_5 \le t < t_6 \\ P_{s7},\ t_6 \le t < t_7 \end{Bmatrix}. \tag{26}$$

Full specification of $P_s(t)$ in this case requires the determination seven unknown specific powers and seven unknown times. Regardless if any of the individual specific powers are set to zero, as it is in the case of a reactor shutdown, the monitor ratios still depend on all intervals and specific powers shown in Equation 26. This is illustrated in the concentration models developed by Chapter III and the case study results presented above. However, due to the extremely short half-life of its parent Xe-135, the Cs-135 concentration does not depend on the shutdowns. Assuming $P_{s2} = P_{s4} = P_{s6} = 0$, i.e. shutdowns occurred; these specific powers can be removed from an equation describing the representative power history for the concentration of Cs-135. Further since the time intervals involved are no longer continuous they can be replaced by time differences, denoted t_b for burn time such that Equation 26 can be rewritten as

$$P_{s,Cs-135}(t) = \begin{Bmatrix} P_{s1},\ \text{for } t_{b1} \\ P_{s3},\ \text{for } t_{b2} \\ P_{s5},\ \text{for } t_{b3} \\ P_{s7},\ \text{for } t_{b4} \end{Bmatrix}. \tag{27}$$

The amount of unknowns has now been reduced from seven specific powers and seven times to four specific powers and four time durations. Not only is this a far simpler

system to solve, but it also can be used to gain information about the removed shutdowns. To illustrate this concept an abstract mathematical representation can be given as

$$\begin{Bmatrix} P_s(t) \\ Information \end{Bmatrix} - \begin{Bmatrix} P_{s,Cs-135}(t) \\ Information \end{Bmatrix} = \begin{Bmatrix} Shutdown \\ Information \end{Bmatrix}. \quad (28)$$

Using a signature based on a fission product whose concentration is highly dependent on shutdown time, such as Sm-147, for the first term in Equation 28 would optimize the extraction of shutdown information. A more detailed version of Equation 28 could serve as an additional basis for iteration in the applications of this work.

It was also found that ratios of a stable daughter to its radioactive parent provided significant sensitivity to changes in power history. This effect is caused by the inverse proportionality of their concentrations to changes in power history. This relationship was exploited using ratios of ratios. For example [Eu-151/Eu-153]/[Sm-151/Sm-147] is more sensitive to changes in power history than Eu-151/Eu-153. Figure 18 illustrates the differences of the double ratios with the base case. A table with the numerical data represented in Figure 18 is given in Appendix D.

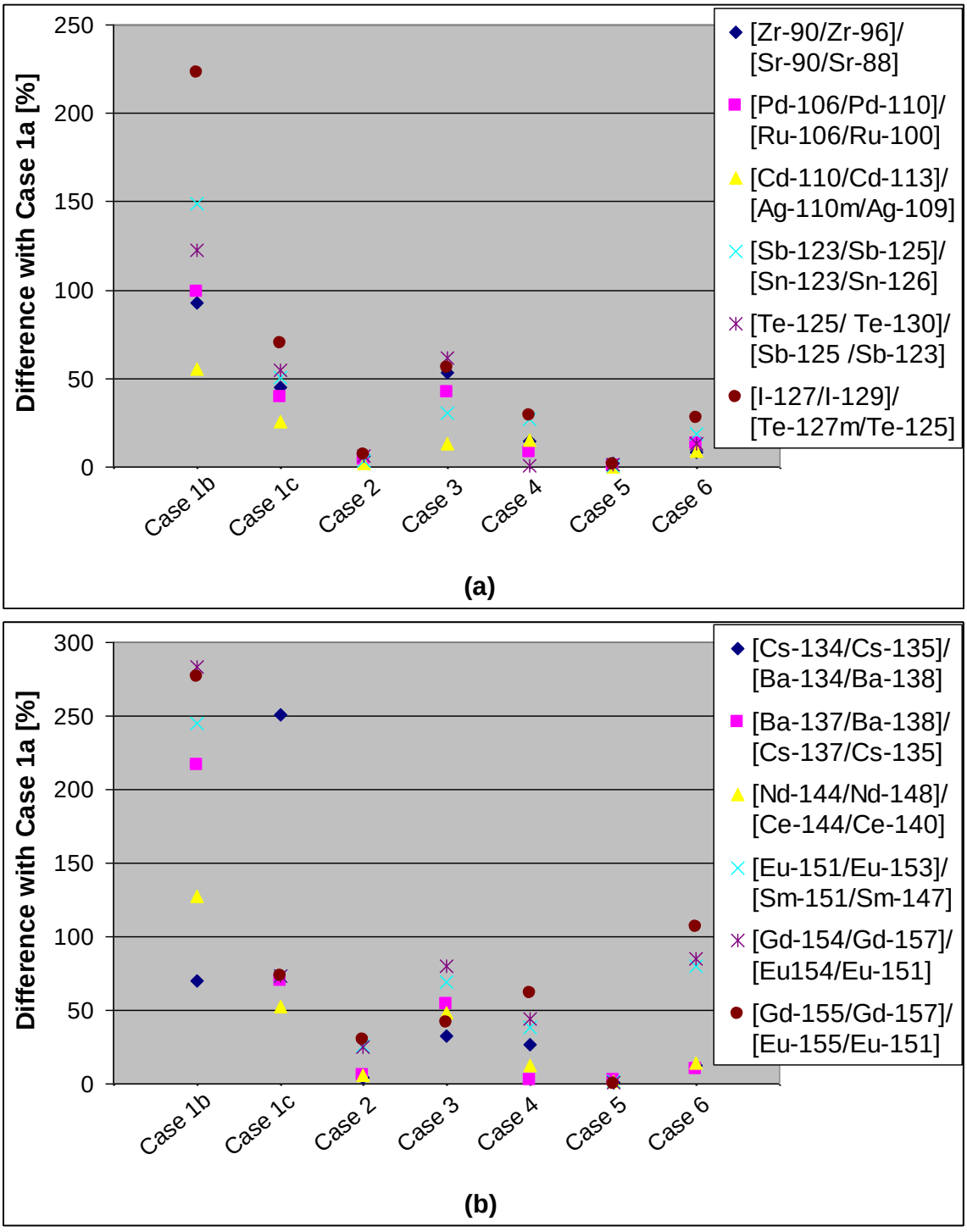

Figure 18. Results of Case Study for Double Ratio (a) Set 1 and (b) Set 2.

Significant differences with Case 1a are seen in the ratios listed for all but Case 5. This is a result of the early shutdowns effectively being buried by a long final burn cycle. However, all of the other cases show differences with Case 1a for at least several monitor ratios that are above the estimated error for TransLat. This proves the viability of the listed ratios as power history monitors.

Table VI lists the ratios with the most significant differences for use as power history signatures.

Table VI

Suggested Reactor Power History Signatures

Signature Type	Signature Ratio
Radioactive	Te-127m/ Te-125
	Ce-144/Ce-140
	Sn-123/Sn-126
Stable	Eu-151/Eu-153
	Gd-155/Gd-157
	Gd-154/Gd-157
	Sm-147/Sm-150
	Cs-135/Cs-133
Double	[Gd-155/Gd-157]/ [Eu-155/Eu-151]
	[Gd-154/Gd-157]/ [Eu-154/Eu-151]
	[Eu-151/Eu-153]/ [Sm-151/Sm-147]

It was desired to show that there were actual fission products that could serve as reactor power history monitors. Previously a range of ideal monitor properties was established

as a guide to selecting potential monitors. With potential monitors identified a case study involving eight different power histories was simulated with TransLat. This case study validated the use of the suggested monitors as power history verification signatures.

CHAPTER V

CONCLUSION

The goal of this thesis was to develop a method to uniquely identify a spent fuel assembly based on fission product signatures. Such a method would be useful as a transparency aid for international safeguards to help protect against possible diversions of spent nuclear fuel. The lattice physics code TransLat was benchmarked against available fission product isotopic data to validate its use in this work. In order to guide the search for potential monitors and as a tool for understanding the physics involved, concentration models were developed for both radioactive and stable monitors. Potential monitors identified were tested through a power history case study using TransLat. Monitors displaying a distinguishable concentration difference as a result of power history variations were catalogued and several such ratios displayed significant concentration differences. In conclusion of this study a discussion is given for a general system to apply the findings reported.

Based on the results of this study a verification regime could be developed for the identity of a given fuel assembly which uses the reactor operator's report for power history experienced by that fuel assembly. The first objective of the verification process would be to obtain the signature ratios listed in Table VI. The signatures are assumed to be determined by mass spectrometry analysis of spent fuel dissolutions obtained from commercial reprocessing facilities or other institutions conducting spent fuel analysis. A

system for obtaining such samples at a commercial facility must be developed that minimizes disruptions to the facility and costs incurred. Assuming such a system exists, the verification of power history and thus fuel assembly identity begins with obtaining the desired signatures from a spent fuel assembly.

The remaining task of the verification procedure is to generate expected signatures ratios for comparison with actual signature ratios measured in the spent fuel assembly. Using the power history provided in the reactor operator's report and the models developed in Chapter III, one may generate estimated signature ratios for comparison. However, doing so entirely based on the reactor operator's report creates unnecessary dependencies of other parameters used in the models of Chapter III. As described in Chapter I, methods exist for determination of final fuel burnup, initial enrichment, fuel age, and reactor type. Knowledge of burnup, enrichment, and reactor type allows for determination of the burnup averaged concentrations of U-235 and Pu-239 without referring to the reactor operator's report. Knowledge of the fuel age also allows for the correction of the ratios involved due to depletion or build-up as a result of radioactive decay during any post-irradiation cooling. Other parameters involved in the concentration models necessary are fission product yields and cross-sections. These parameters may be obtained from existing data libraries such as those used by ORIGEN 2.2. It is also possible to generate yields and cross-sections through physics codes such as TransLat with reactor models based on the obtainable parameters and assuming a generic power history, such as that given in the operator's report. Using burnup

averaged values for yields and cross-sections will reduce the importance of an accurate power history for the determination of these parameters. Though, if necessary the yields and cross-sections can be refined through an iterative process if the actual monitor ratios determined from the spent fuel diverge from those obtained using the power history from the operator's report. Extracting all possible information from the fuel itself as opposed to depending on the reactor operator's report eliminates excess degrees of freedom for the potential proliferator. With this in mind the verification method is simply comparing measured ratios against estimated ratios based on the power history provided by the reactor operator's report. Any inconsistencies merit further, more detailed investigation.

Another use of this work could be to independently determine a fuel assembly's power history without using the operator's report for verification. To do so would necessitate that all initial parameters be determined from the spent fuel as discussed above. After the desired power history signatures have been analyzed it may be possible to create an iterative scheme based on an assumed generic power history. Such a generic power history could consist of three irradiation cycles divided by two shutdowns in which the specific powers and the lengths of cycles were allowed to vary during iteration. However, prior to the full scale iteration it may be possible to isolate pieces of the power history independently. As mentioned in Chapter III, the concentration of fission products with short half-lives will saturate to the specific power of the final irradiation cycle. Though the signal would rapidly deteriorate, the specific power of the final irradiation cycle would be a useful origin for full power history characterization. As

discussed in Chapter IV, the Cs-135/Cs-137 signature could be used to isolate information about the shutdown time. With information about the final irradiation specific power and the shutdown time known, iteration on the generic power history system could be done until the estimated signature ratios matched the measured signature ratios to within specified tolerances. The full iteration system could involve several generic power histories with the overall best fit to all the measured signature ratios taken to be representative of the actual power history of the spent fuel assembly.

A fully functioning system for the identification of a spent fuel assembly based on its power history still requires much work to be done. Work to be done includes developing a deeper understanding of the power history monitor nuclides involved. Experimental validation of the concentration differences from actual fuel samples is desirable. Experimental validation could also help improve the models and codes used to calculate the monitor nuclides suggested here and enhance the distinguishing capability of the proposed verification system. Further it is likely that mass spectrometry measurement is not well developed for all the suggested monitors. The analysis techniques for obtaining the suggested ratios need to be refined and standardized especially if this system is to be employed on an international or commercial basis. Surely, other improvements and capabilities will need to be developed as part of the future identification system. However, the information given here demonstrates that such a system is possible and can serve as a guide for future efforts.

REFERENCES

1. U.S. Congress, Senate. Senate Select Committee on Intelligence. *Annual Threat Assessment of the Director of National Intelligence for the Senate Select Committee on Intelligence*. 110th Cong., 2nd sess., February 5, 2008.

2. U.S. Congress, 1995. Environmental Monitoring for Nuclear Safeguards. OTA-BP-ISS-168. Office of Technology Assessment.

3. J.C. Mark, "Explosive Properties of Reactor-Grade Plutonium," *Science & Global Security,* **4**, 111 (1993).

4. International Atomic Energy Agency, "Treaty on the Non-Proliferation of Nuclear Weapons." INFCIRC/140 (1970).

5. International Atomic Energy Agency, "Model Protocol Additional to the Agreement(s) Between State(s) and the International Atomic Energy Agency for the Application of Safeguards." INFCIRC/540 (1997).

6. D. Fischer, *History of the International Atomic Energy Agency: The First Forty Years*, IAEA, 9 (1997).

7. D. Fischer, *History of the International Atomic Energy Agency: The First Forty Years*, IAEA, 471 (1997).

8. International Atomic Energy Agency, "The Structure and Content of Agreements Between the Agency and States Required in Connection with the Treaty on the Non-Proliferation of Nuclear Weapons." INFCIRC/153 (1972).

9. *IAEA Safeguards Glossary 2001 Edition*, IAEA, 19 (2002).

10. P.J. Persiani, R.G. Bucher, "Implementation of Isotope Correlation Technique for Safeguards," ESARDA, 11th Annual Symposium on Safeguards and Nuclear Materials Management, Luxembourg, Luxembourg (1989).

11. R. Wellum, R. de Meester, K. Kammerichs, L. Koch, "The Categorization of Binary Isotope Correlations Derived from the Databank of the European Institute for Transuranium Elements," ESARDA, Symposium on the Isotopic Correlation & Its Application to the Nuclear Fuel Cycle, Stresa, Italy (1978).

12. L. Koch, A. Cricchio, F. Gerin, "Isotope Correlations of Heavy Isotopes and Fission Products for Consistency Checks and Data Generation," International Atomic Energy Agency Working Group on the Use of Isotopic Composition Data in Safeguards, Vienna, Austria (1972).

13. W.S. Charlton, "Monitors for the Prediction of Alternate Nuclear Material Concentrations for Pressurized Water Reactor Spent Fuel," *Nuclear Technology*, **136** (1), 24 (2001).

14. F.L. Lisman, W.J. Maeck, J.E. Rein, "Determination of Nuclear Fuel Burnup from Fission Product Analysis," *Nuclear Science and Engineering*, **42**, 215 (1970).

15. M. Scott, "Nuclear Forensics: Attributing the Source of Spent Fuel Used in an RDD Event," M.S. Thesis, Texas A&M University, College Station (2005).

16. W.S. Charlton, B.L. Fearey, C.W. Nakhleh, T.A. Parish, R.T. Perry, J. Poths, J.R. Quagliano, W.D. Stanbro, W.B. Wilson, "Operator Declaration Verification Technique for Spent Fuel at Reprocessing Facilities," *Nuclear Instruments and Methods in Physics Research*, **168 (**1), 98 (2000).

17. W.D. Stanbro, W.S. Charlton, P.H. Hemberger, J. Poths, T.L. Burr, B.L. Fearey, "Use of Stable Xenon Isotope Monitoring in Strengthened Safeguards at Large Reprocessing Plants," *Journal of the Institute of Nuclear Materials Management*, **28** (2), 22 (2000).

18. W.S. Charlton, J. Poths, "Capability of Ruthenium Isotopes in Distinguishing Spent Reactor Fuel Type and Burnup," *Journal of Nuclear Materials Management*, **31** (2), 5 (2003).

19. W.S. Charlton, "Burnup Determination and Age Dating of Spent Nuclear Fuel Using Noble Gas Isotopic Analysis," *Transactions of the American Nuclear Society*, **81**, 312 (1999).

20. J.E. McAninch, I.D. Proctor, N.J. Stoyer, K.J. Moody, "Viability of Long-Lived Fission Products as Signatures in Forensic Radiochemistry," UCRL-ID-126425, Lawrence Livermore National Laboratory (1997).

21. W.M. Stacey, *Nuclear Reactor Physics*, John Wiley & Sons, Inc., New York, New York, 201 (2001).

22. W.M. Stacey, *Nuclear Reactor Physics*, John Wiley & Sons, Inc., New York, New York, 295 (2001).

23. E.E. Lewis, W.F. Miller, *Computational Methods of Neutron Transport*, American Nuclear Society, Inc., La Grange Park, Illinois, 215 (1993).

24. T. Postma, J. Vujic, "The Method of Characteristics in General Geometry with Anisotropic Scattering," Proceedings of the International Conference on

Mathematics and Computation, Reactor Physics and Environmental Analysis in Nuclear Application, Madrid, Spain, **2**, 1215 (1999).

25. W.M. Stacey, *Nuclear Reactor Physics*, John Wiley & Sons, Inc., New York, New York, 357 (2001).

26. E.E. Lewis, W.F. Miller, *Computational Methods of Neutron Transport*, American Nuclear Society, Inc., La Grange Park, Illinois, 241 (1993).

27. T. Jevremovic, J. Vujic, K. Tsuda, "ANEMONA – a neutron transport code for the general geometry reactor assemblies based on the method of characteristics and R-function solid modeler," *Annals of Nuclear Energy*, **28**, 125 (2001).

28. "TransFX Computer Software Manuals: Advanced Particle Transport Software Using Three-Dimensional Deterministic Methods in Arbitrary Geometry," Transware Enterprises (2001).

29. S.P. Baker, "An evalutation of TransLat three-dimensional depletion-calculations," *Transactions of the American Nuclear Society*, **86**, 324 (2002).

30. S.P. Baker, "TransLat Benchmark of ANS Joint Benchmark Committee B&W Criticals," *Transactions of the American Nuclear Society*, **89**, 585 (2003).

31. "List of Reactors in SFCOMPO on WWW Ver.2," http://www.nea.fr/sfcompo/Ver.2/Eng/index.html (2008).

32. J.O. Barner, "Characterization of LWR Spent Fuel MCC-Approved Testing Material – ATM-101," PNL-5109 Rev. 1 UC-70, Pacific Northwest Laboratory (1985).

33. O.W. Hermann, S.M. Bowman, M.C. Brady, C.V. Parks, "Validation of the Scale System for PWR Spent Fuel Isotopic Composition Analyses," ORNL/TM-12667, Oak Ridge National Laboratory (1995).

34. A.G. Croff, "A User's Manual for the ORIGEN2 Computer Code," ORNL/TM-7175, Oak Ridge National Laboratory (1980).

35. W.S. Charlton, W.D. Stanbro, R.T. Perry, "Comparisons of HELIOS, ORIGEN2, and Monteburns Calculated 241Am and 243Am Concentrations to Measured Values for PWR, BWR, and VVER Spent Fuel," *J. Nuclear Science and Technology*, **37** (7), 615 (2000).

36. R.G. Cochran, N. Tsoulfanidis, *The Nuclear Fuel Cycle: Analysis and Management*, American Nuclear Society, Inc., 175 (1990).

37. E.M. Baum, H.D. Knox, T.R. Miller, "Nuclides and Isotopes 16th Edition," Knolls Atomic Power Laboratory (2002).

38. J.I.G. Alonso, D. Thoby-Schultzendorff, B. Giovanonne, J. Glatz, G. Pagliosa, L. Koch, "Characterization of Spent Nuclear Fuel Dissolver Solutions and Dissolution Residues by Inductively Coupled Plasma Mass Spectrometry," *Journal of Analytical Atomic Spectrometry*, **9** 1209 (1994).

APPENDIX A

Table VII

Modified Pin Cell Calculations for Calvert Cliffs No. 1 Pin Cell

	Actual Assembly Parameters	Modified Pin Cell Parameters
Rods per Assembly	176	--
Rod array	14*14	--
Rod Positions	196.000	--
Rod O.D. [cm]	1.118	1.118
Rod Area [cm^2]	0.982	0.982
Total Rod Area [cm^2]	172.777	--
Pin Pitch [cm]	1.470	1.551
Pin Cell Area [cm^2]	2.161	2.406
Assembly area [cm^2]	423.536	--
Total Moderator Area [cm^2]	250.759	--
Fuel to Moderator Ratio	0.689	0.689

Table VIII

Modified Pin Cell Calculations for Mihama Unit 3 Pin Cell

	Actual Assembly Parameters	Modified Pin Cell Parameters
Rods per Assembly	204	--
Rod array	15*15	--
Rod Positions	225	--
Rod O.D. [cm]	1.070	1.070
Rod Area [cm^2]	0.899	0.899
Total Rod Area [cm^2]	183.437	--
Pin Pitch [cm]	1.430	1.502
Pin Cell Area [cm^2]	2.045	2.255
Assembly area [cm^2]	460.103	--
Total Moderator Area [cm^2]	276.665	--
Fuel to Moderator Ratio	0.663	0.663

APPENDIX B

Table IX

Benchmarking Results of Piecewise Model for Sr-90

	TransLat	Model	% Error
Case 1a	3.39E-05	3.81E-05	-12.48
Case 1b	3.28E-05	3.69E-05	-12.68
Case 1c	3.45E-05	3.87E-05	-12.33
Case 2	3.38E-05	3.71E-05	-9.79
Case 3	3.33E-05	3.65E-05	-9.77
Case 4	3.38E-05	3.71E-05	-9.74
Case 5	3.39E-05	3.71E-05	-9.65
Case 6	3.38E-05	3.71E-05	-9.91

Table X

Benchmarking Results of Piecewise Model for Zr-90

	TransLat	Model	% Error
Case 1a	1.40E-06	1.32E-06	5.56
Case 1b	2.58E-06	2.54E-06	1.44
Case 1c	7.92E-07	6.96E-07	12.07
Case 2	1.48E-06	1.47E-06	0.82
Case 3	2.05E-06	2.08E-06	-1.47
Case 4	1.50E-06	1.48E-06	0.89
Case 5	1.43E-06	1.47E-06	-2.41
Case 6	1.52E-06	1.47E-06	3.39

Table XI

Benchmarking Results of Piecewise Model for Cs-137

	TransLat	Model	% Error
Case 1a	5.18E-05	5.39E-05	-3.94
Case 1b	5.03E-05	5.22E-05	-3.90
Case 1c	5.26E-05	5.41E-05	-2.79
Case 2	5.17E-05	5.39E-05	-4.12
Case 3	5.10E-05	5.31E-05	-4.14
Case 4	5.17E-05	5.39E-05	-4.14
Case 5	5.18E-05	5.39E-05	-3.99
Case 6	5.17E-05	5.39E-05	-4.25

Table XII

Benchmarking Results of Piecewise Model for Ba-137

	TransLat	Model	% Error
Case 1a	1.86E-06	1.72E-06	7.29
Case 1b	3.43E-06	3.36E-06	1.97
Case 1c	1.05E-06	8.66E-07	17.25
Case 2	1.95E-06	1.81E-06	7.16
Case 3	2.72E-06	2.59E-06	4.63
Case 4	1.95E-06	1.80E-06	7.38
Case 5	1.89E-06	1.81E-06	4.05
Case 6	2.02E-06	1.81E-06	10.13

APPENDIX C

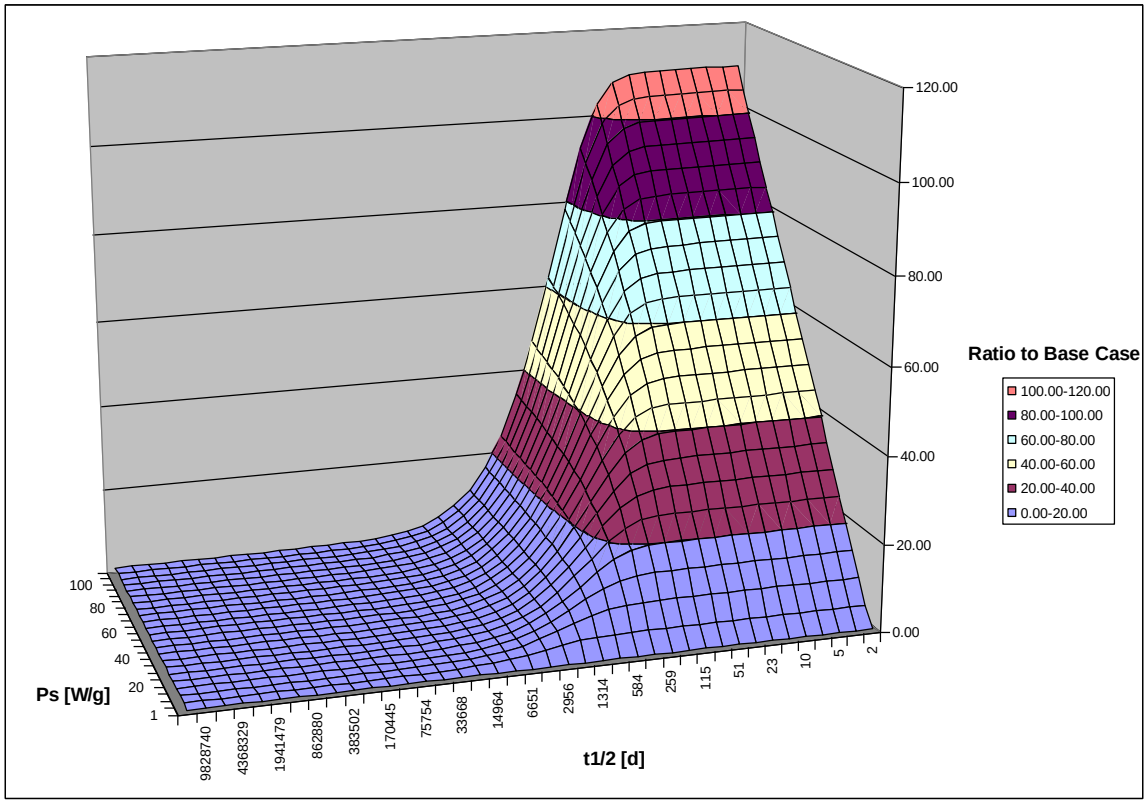

Figure 19. Radioactive Nuclide Concentration Ratio to Base Case of Ps = 1 W/g, $\sigma_{a,R}$ = 1 b for Each Half-life for a Single Burn Cycle of Constant Specific Power.

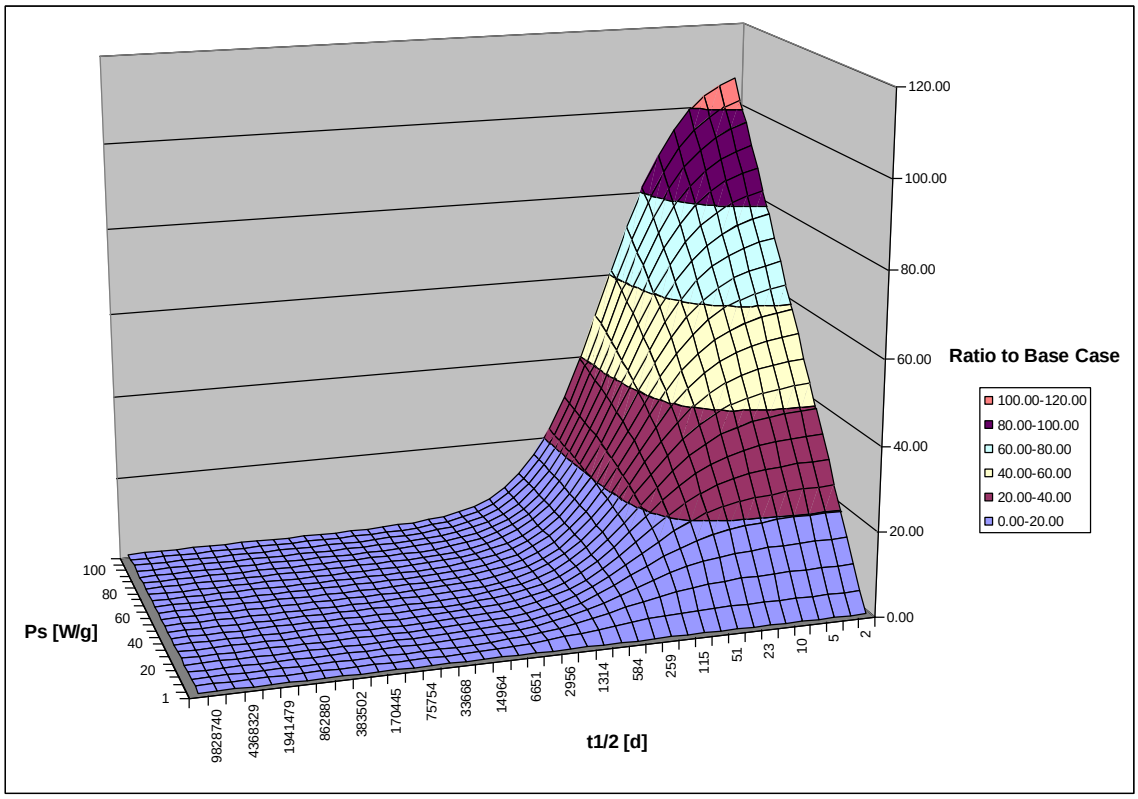

Figure 20. Radioactive Nuclide Concentration Ratio to Base Case of Ps = 1 W/g, $\sigma_{a,R}$ = 100 b for Each Half-life for a Single Burn Cycle of Constant Specific Power.

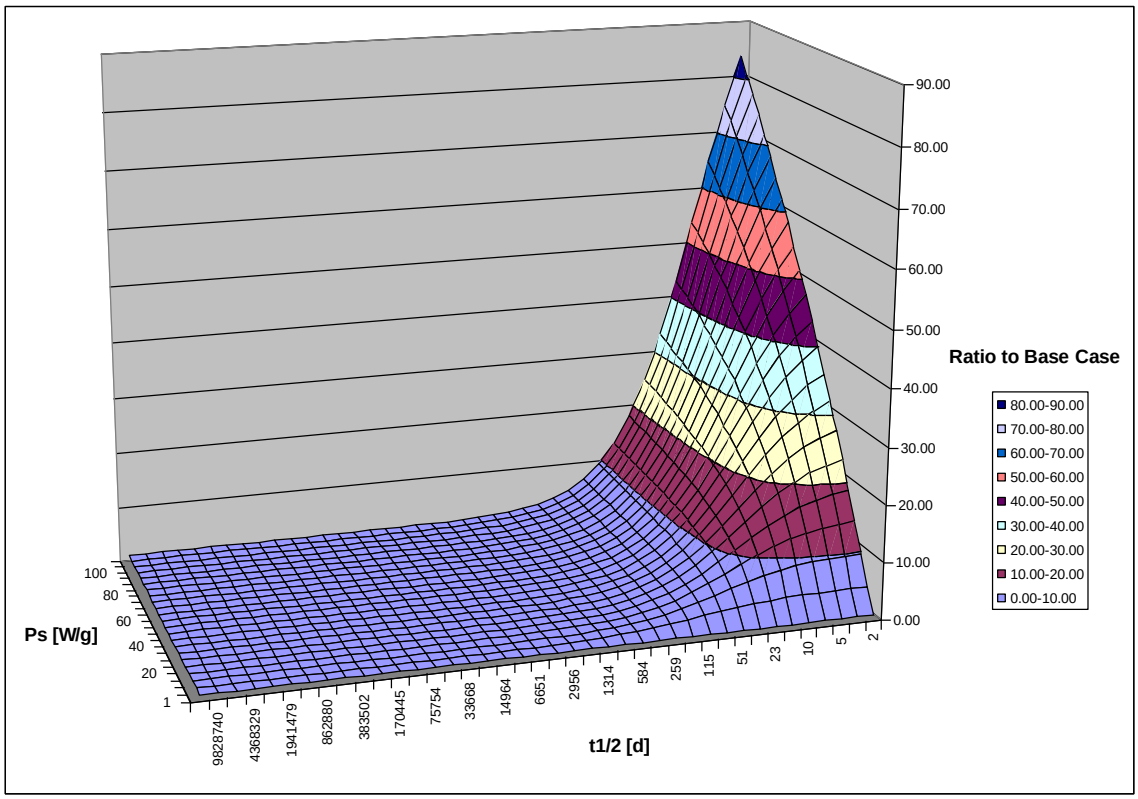

Figure 21. Radioactive Nuclide Concentration Ratio to Base Case of Ps = 1 W/g, $\sigma_{a,R}$ = 1000 b for Each Half-life for a Single Burn Cycle of Constant Specific Power.

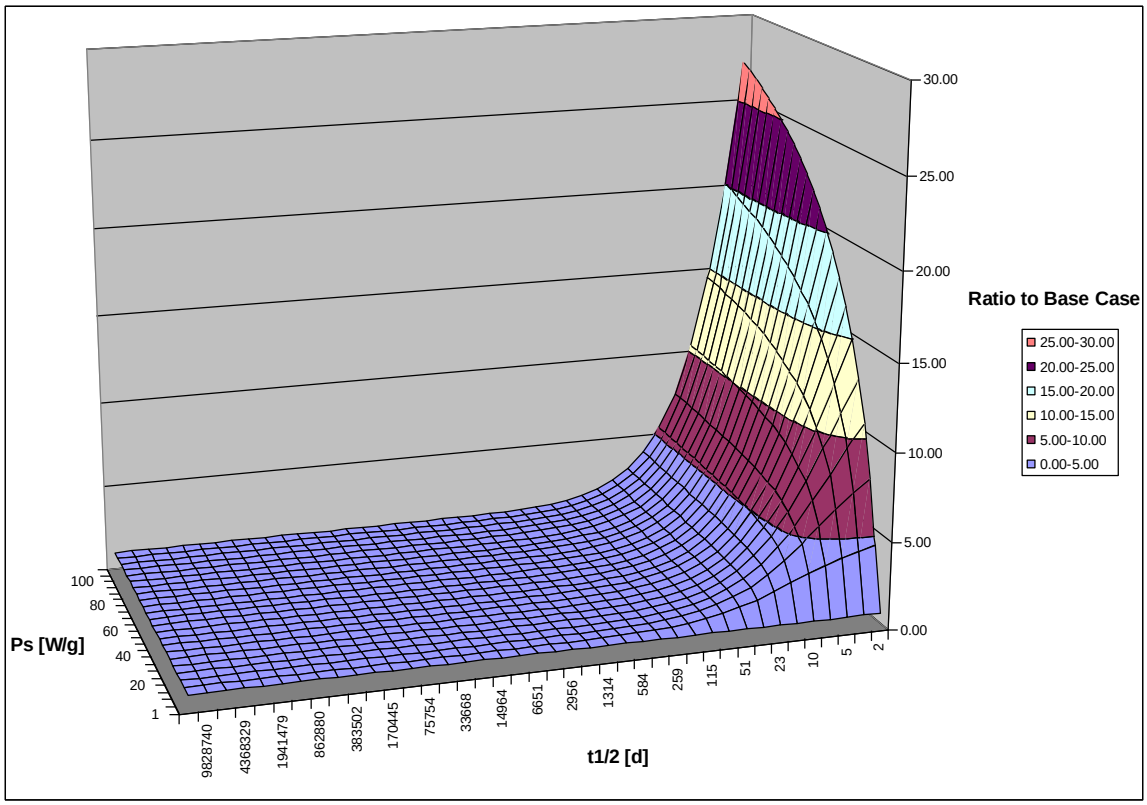

Figure 22. Radioactive Nuclide Concentration Ratio to Base Case of Ps = 1 W/g, $\sigma_{a,R}$ = 10,000 b for Each Half-life for a Single Burn Cycle of Constant Specific Power.

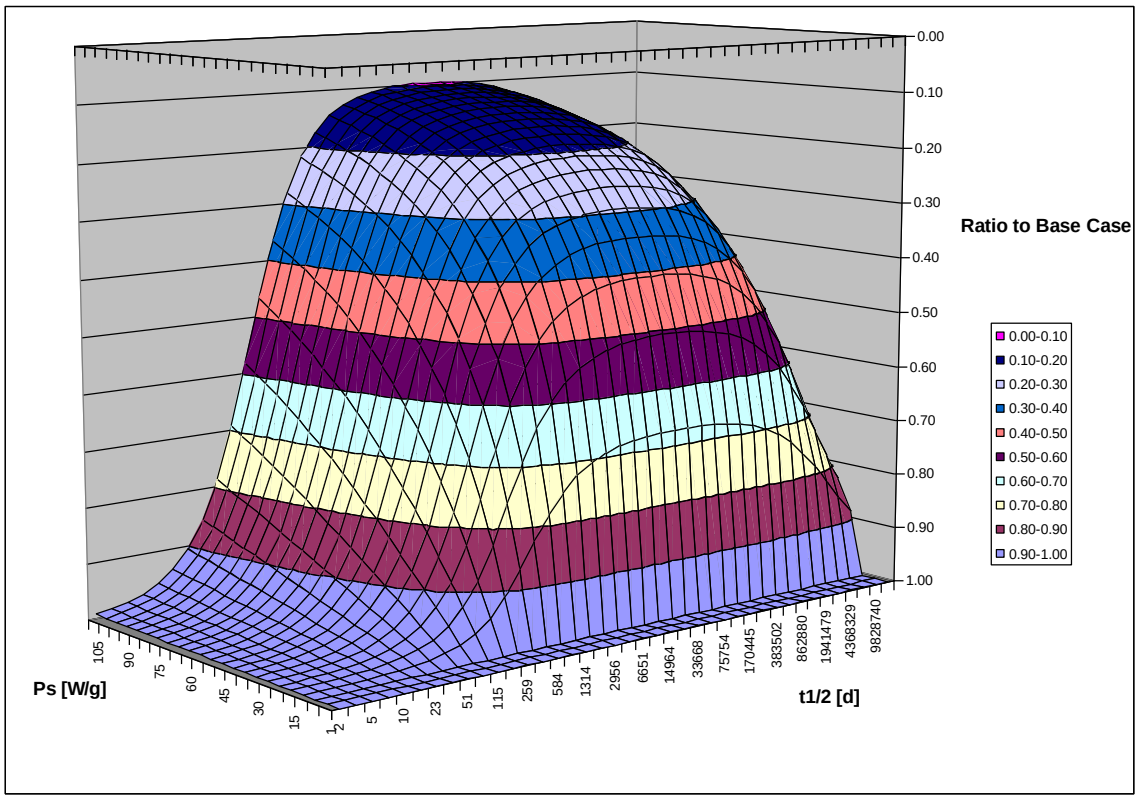

Figure 23. Stable Nuclide Concentration Ratio to Base Case of Ps = 10 W/g, $\sigma_{a,R}$ = 1 b, $\sigma_{a,S}$ = 1 b for Each Half-life of Radioactive Parent for a Single Burn Cycle of Constant Specific Power.

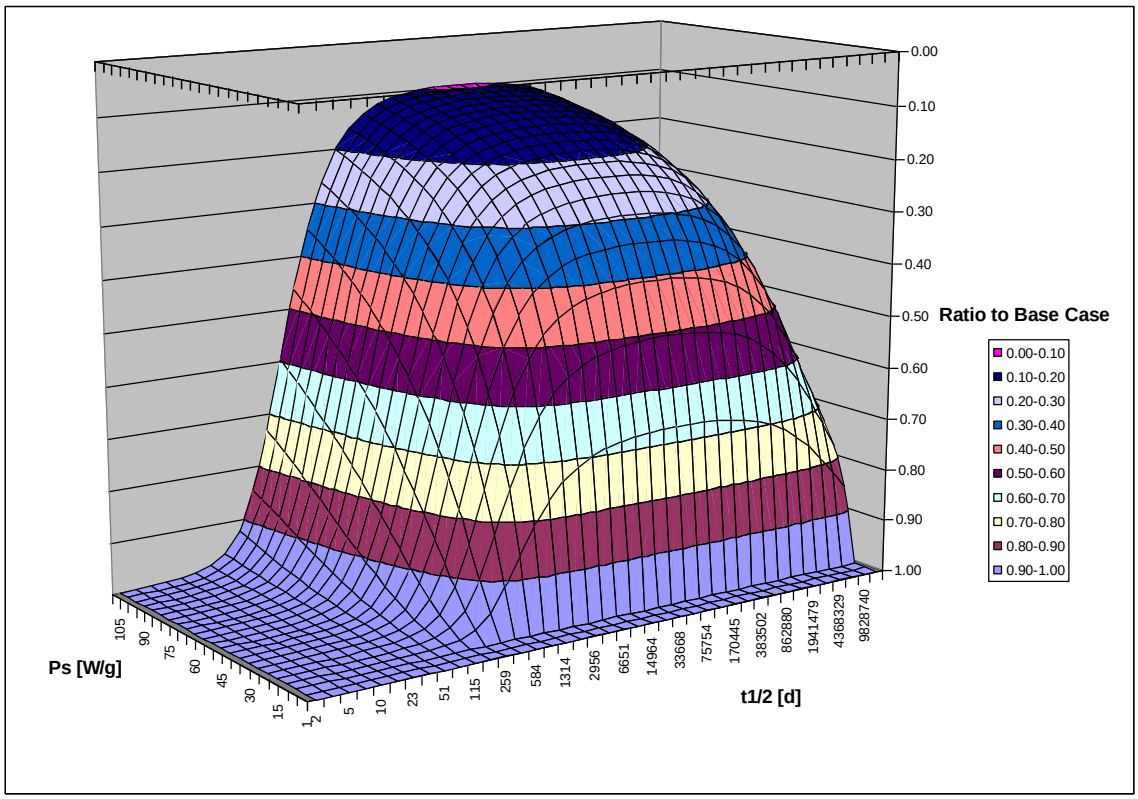

Figure 24. Stable Nuclide Concentration Ratio to Base Case of Ps = 10 W/g, $\sigma_{a,R}$ = 1 b, $\sigma_{a,S}$ = 100 b for Each Half-life of Radioactive Parent for a Single Burn Cycle of Constant Specific Power.

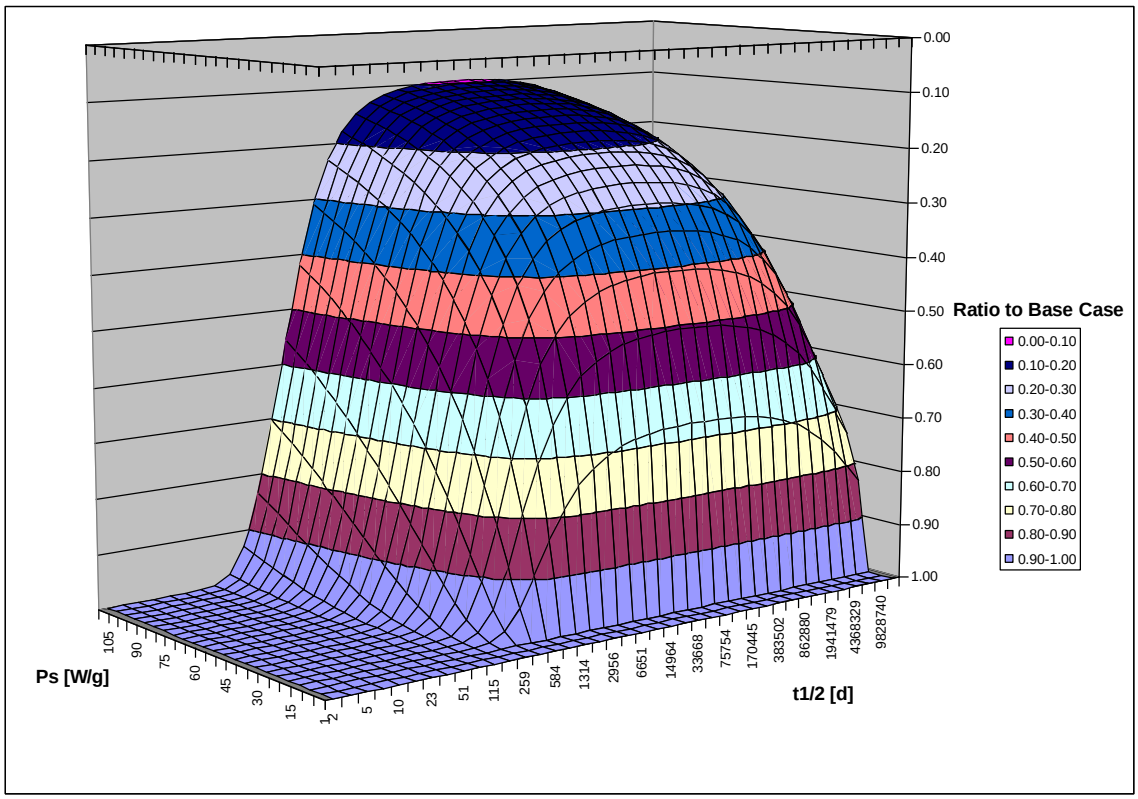

Figure 25. Stable Nuclide Concentration Ratio to Base Case of Ps = 10 W/g, $\sigma_{a,R}$ = 1 b, $\sigma_{a,S}$ = 1000 b for Each Half-life of Radioactive Parent for a Single Burn Cycle of Constant Specific Power.

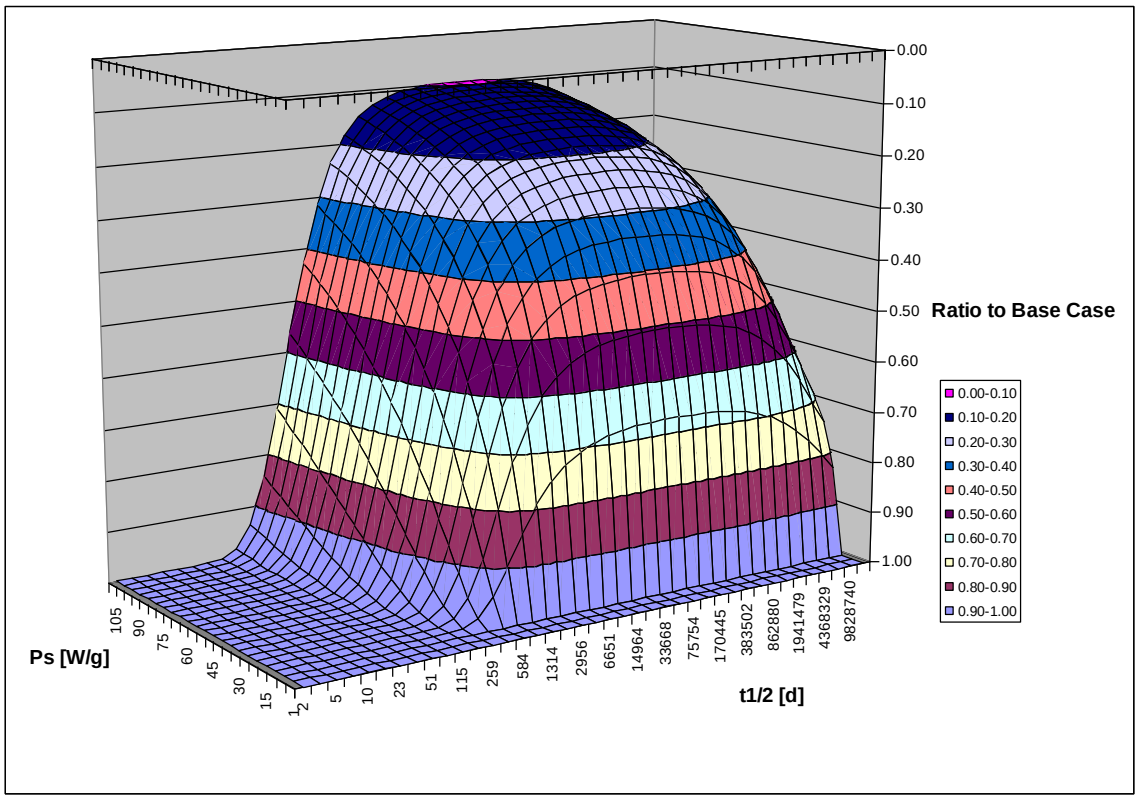

Figure 26. Stable Nuclide Concentration Ratio to Base Case of Ps = 10 W/g, $\sigma_{a,R}$ = 1 b, $\sigma_{a,S}$ = 10000 b for Each Half-life of Radioactive Parent for a Single Burn Cycle of Constant Specific Power.

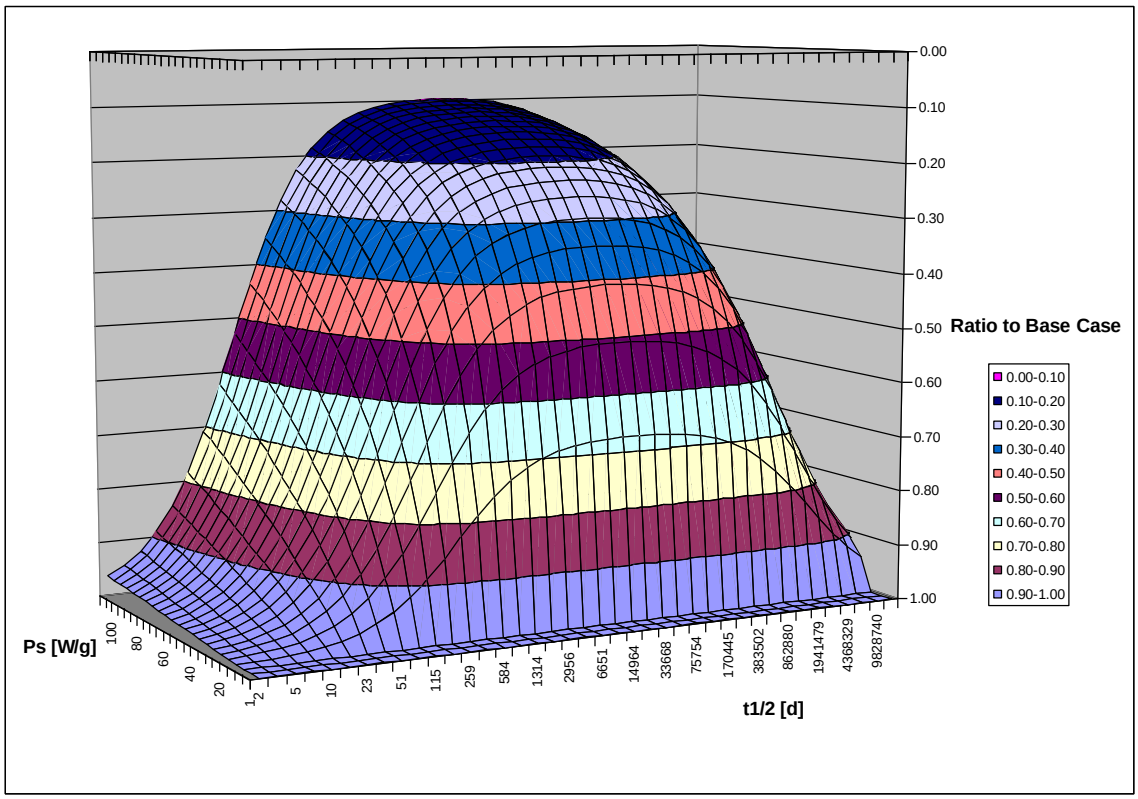

Figure 27. Stable Nuclide Concentration Ratio to Base Case of Ps = 10 W/g, $\sigma_{a,R}$ = 100 b, $\sigma_{a,S}$ = 1 b for Each Half-life of Radioactive Parent for a Single Burn Cycle of Constant Specific Power.

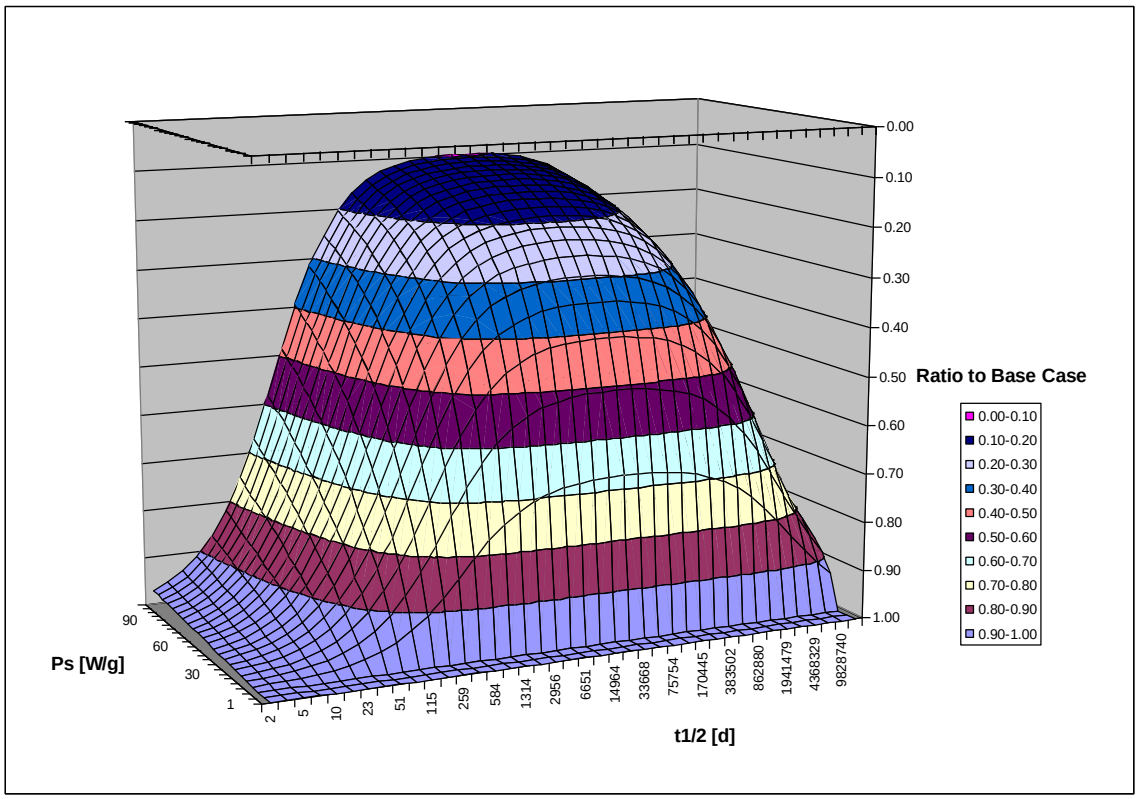

Figure 28. Stable Nuclide Concentration Ratio to Base Case of Ps = 10 W/g, $\sigma_{a,R}$ = 100 b, $\sigma_{a,S}$ = 100 b for Each Half-life of Radioactive Parent for a Single Burn Cycle of Constant Specific Power.

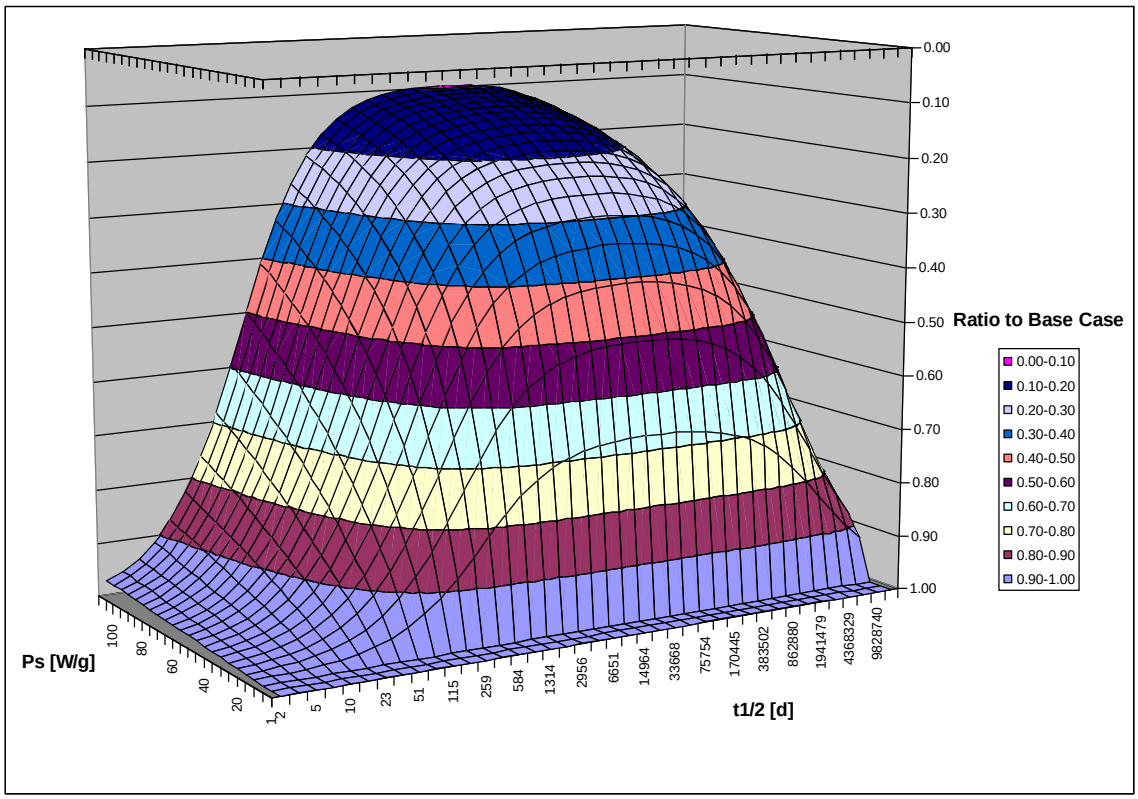

Figure 29. Stable Nuclide Concentration Ratio to Base Case of Ps = 10 W/g, $\sigma_{a,R}$ = 100 b, $\sigma_{a,S}$ = 1000 b for Each Half-life of Radioactive Parent for a Single Burn Cycle of Constant Specific Power.

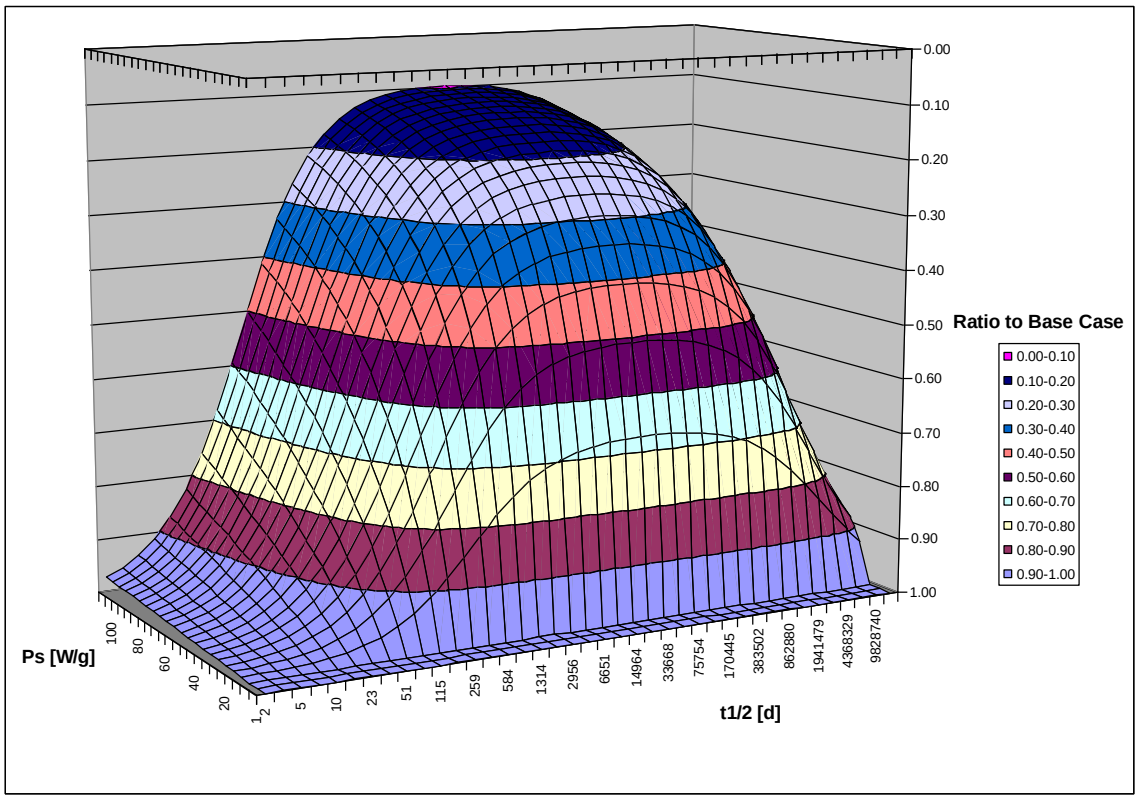

Figure 30. Stable Nuclide Concentration Ratio to Base Case of Ps = 10 W/g, $\sigma_{a,R}$ = 100 b, $\sigma_{a,S}$ = 10000 b for Each Half-life of Radioactive Parent for a Single Burn Cycle of Constant Specific Power.

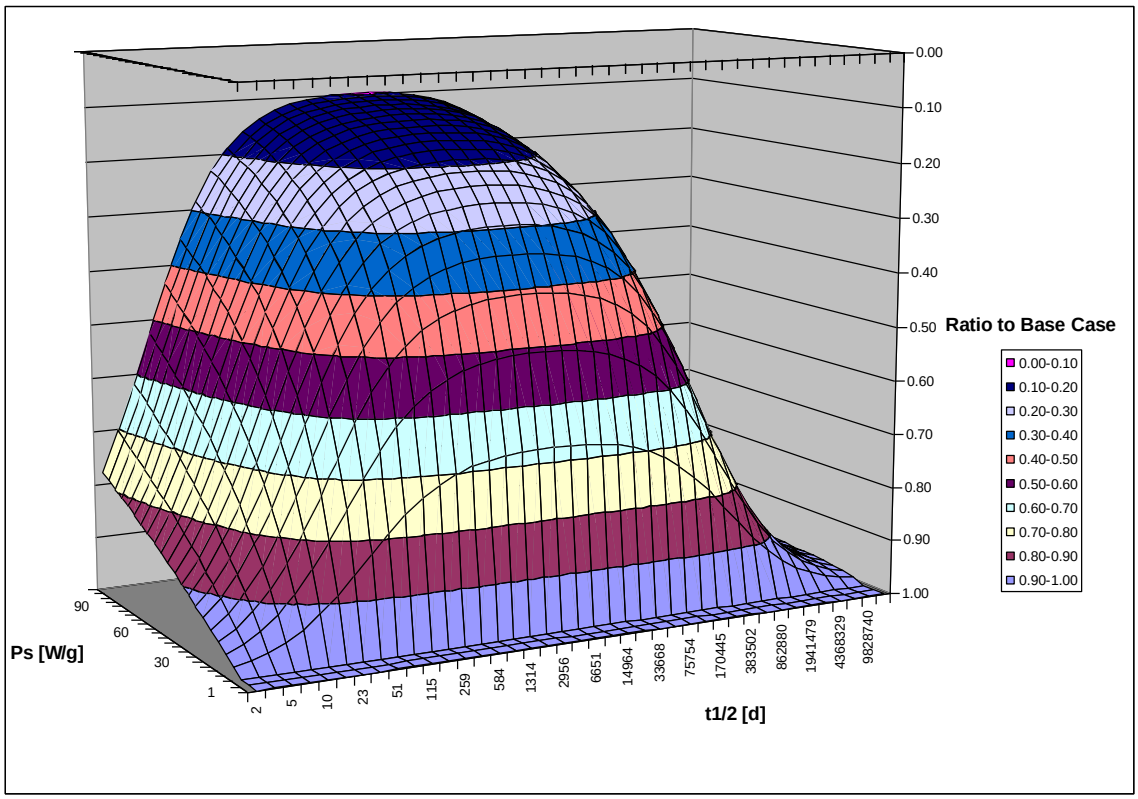

Figure 31. Stable Nuclide Concentration Ratio to Base Case of Ps = 10 W/g, $\sigma_{a,R}$ = 1000 b, $\sigma_{a,S}$ = 1 b for Each Half-life of Radioactive Parent for a Single Burn Cycle of Constant Specific Power.

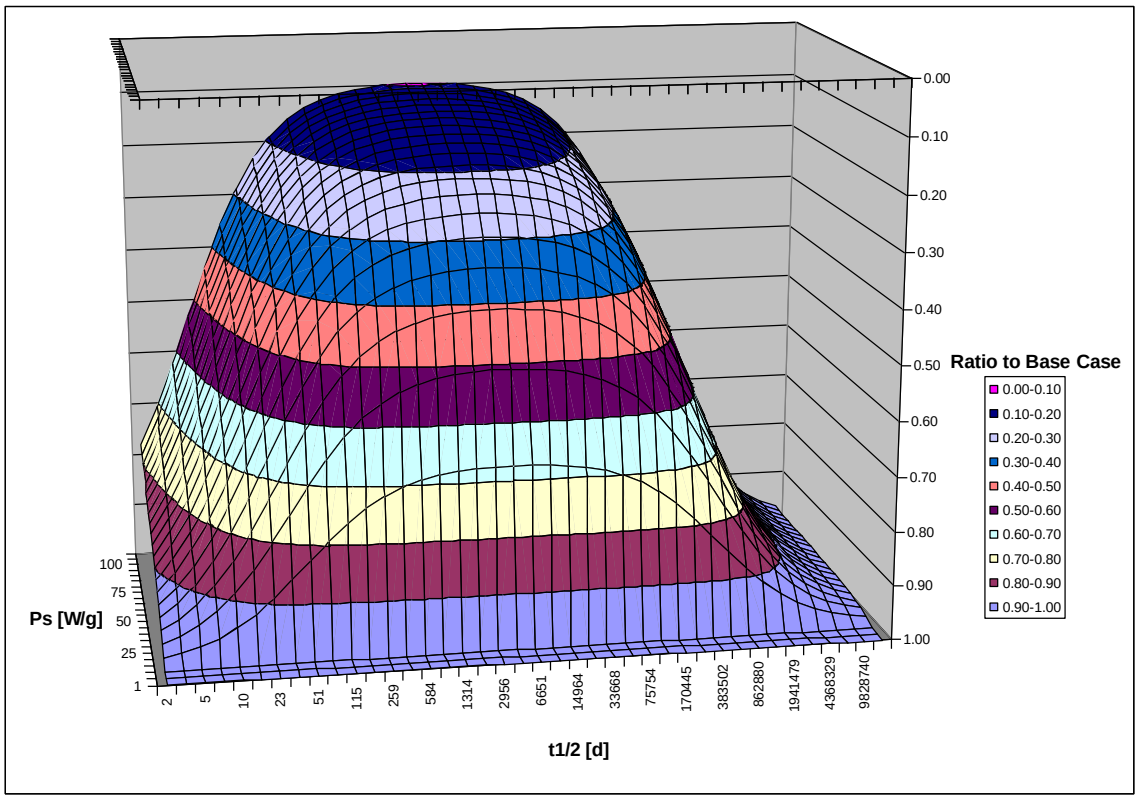

Figure 32. Stable Nuclide Concentration Ratio to Base Case of Ps = 10 W/g, $\sigma_{a,R}$ = 1000 b, $\sigma_{a,S}$ = 100 b for Each Half-life of Radioactive Parent for a Single Burn Cycle of Constant Specific Power.

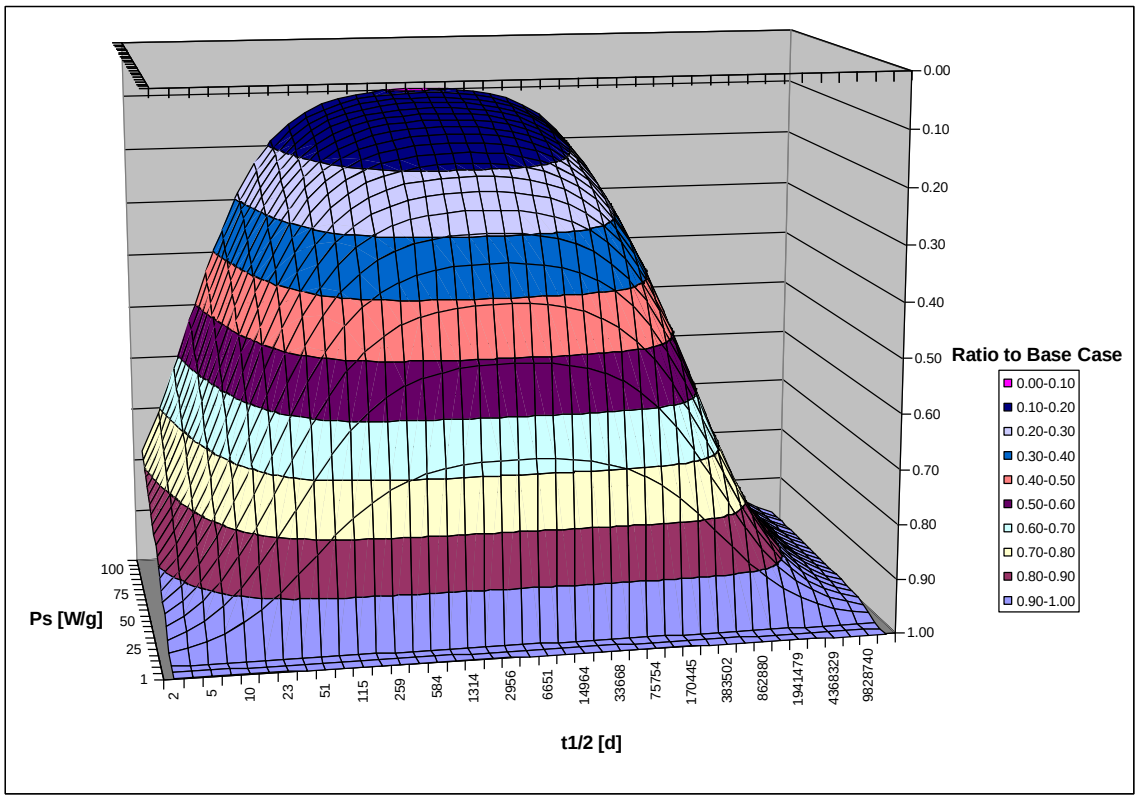

Figure 33. Stable Nuclide Concentration Ratio to Base Case of Ps = 10 W/g, $\sigma_{a,R}$ = 1000 b, $\sigma_{a,S}$ = 1000 b for Each Half-life of Radioactive Parent for a Single Burn Cycle of Constant Specific Power.

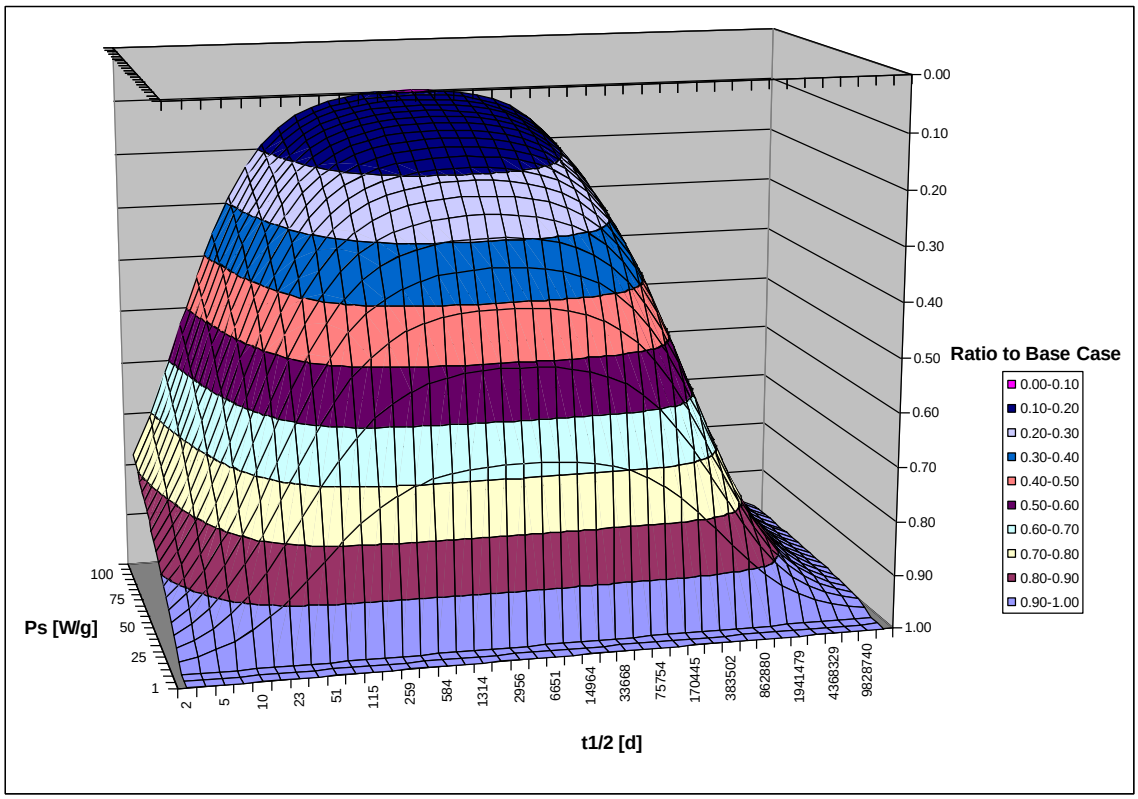

Figure 34. Stable Nuclide Concentration Ratio to Base Case of Ps = 10 W/g, $\sigma_{a,R}$ = 1000 b, $\sigma_{a,S}$ = 10000 b for Each Half-life of Radioactive Parent for a Single Burn Cycle of Constant Specific Power.

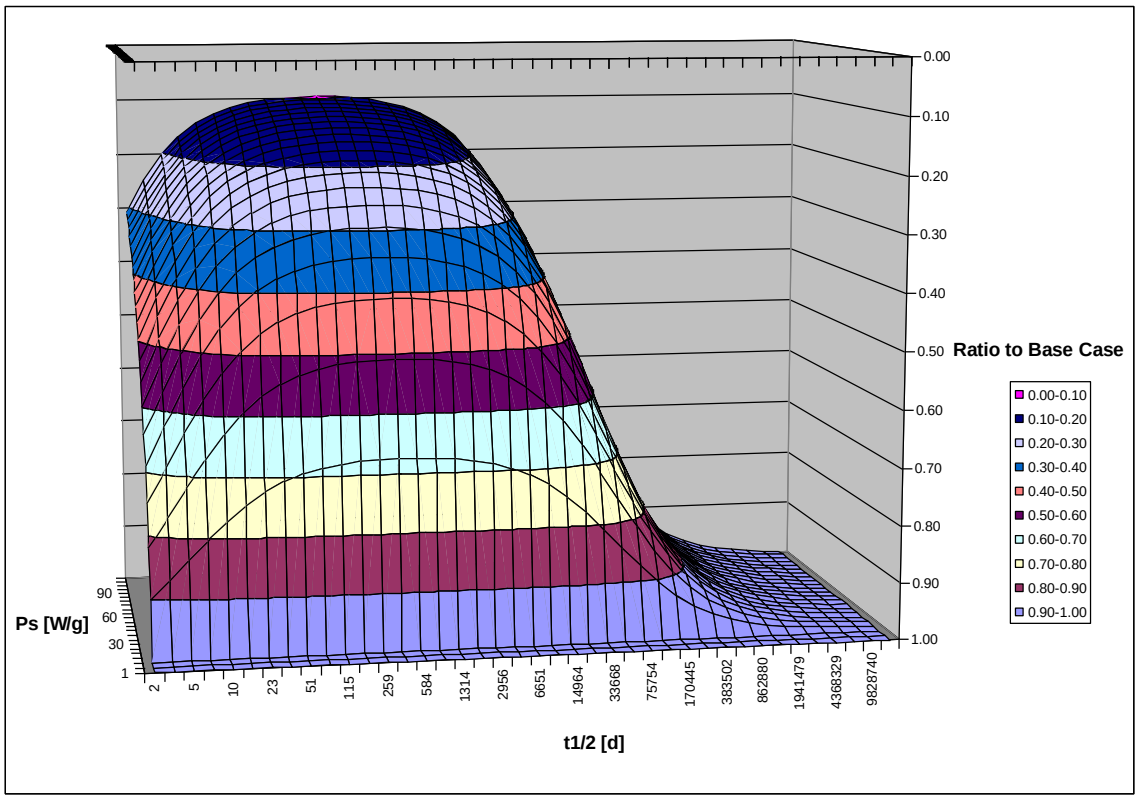

Figure 35. Stable Nuclide Concentration Ratio to Base Case of Ps = 10 W/g, $\sigma_{a,R}$ = 10,000 b, $\sigma_{a,S}$ = 1 b for Each Half-life of Radioactive Parent for a Single Burn Cycle of Constant Specific Power.

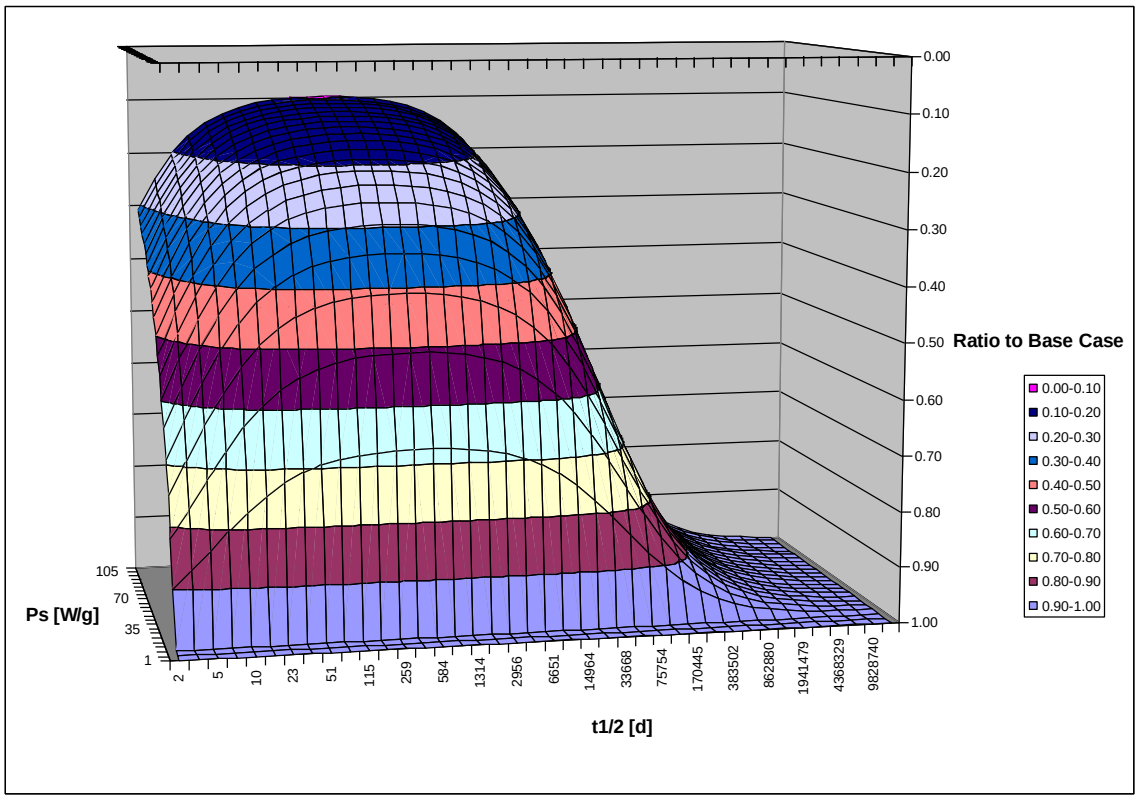

Figure 36. Stable Nuclide Concentration Ratio to Base Case of Ps = 10 W/g, $\sigma_{a,R}$ = 10,000 b, $\sigma_{a,S}$ = 100 b for Each Half-life of Radioactive Parent for a Single Burn Cycle of Constant Specific Power.

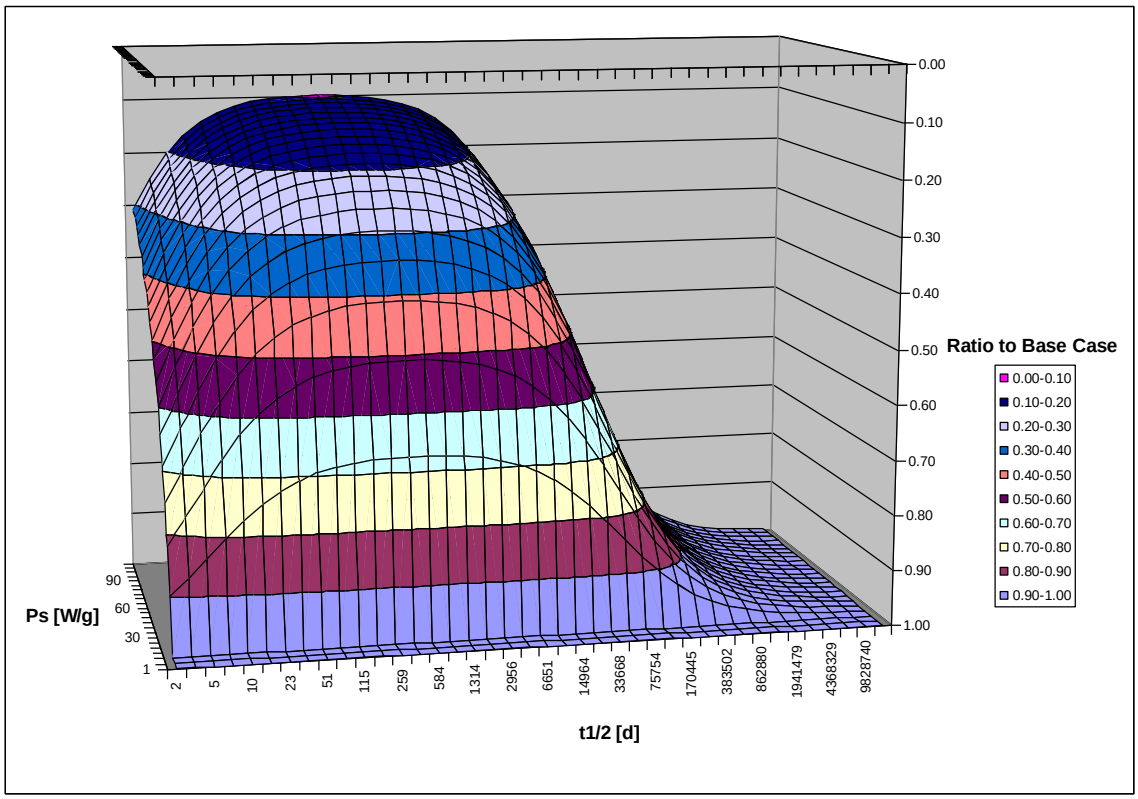

Figure 37. Stable Nuclide Concentration Ratio to Base Case of Ps = 10 W/g, $\sigma_{a,R}$ = 10,000 b, $\sigma_{a,S}$ = 1000 b for Each Half-life of Radioactive Parent for a Single Burn Cycle of Constant Specific Power.

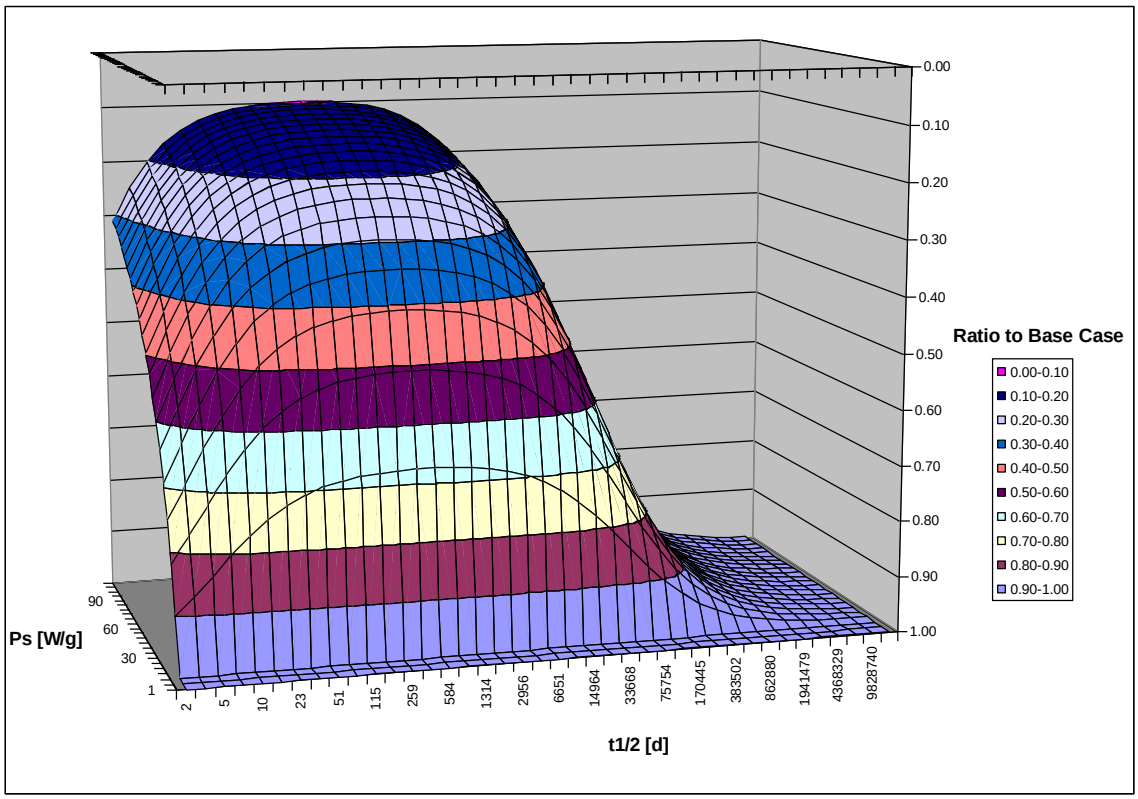

Figure 38. Stable Nuclide Concentration Ratio to Base Case of Ps = 10 W/g, $\sigma_{a,R}$ = 10,000 b, $\sigma_{a,S}$ = 10,000 b for Each Half-life of Radioactive Parent for a Single Burn Cycle of Constant Specific Power.

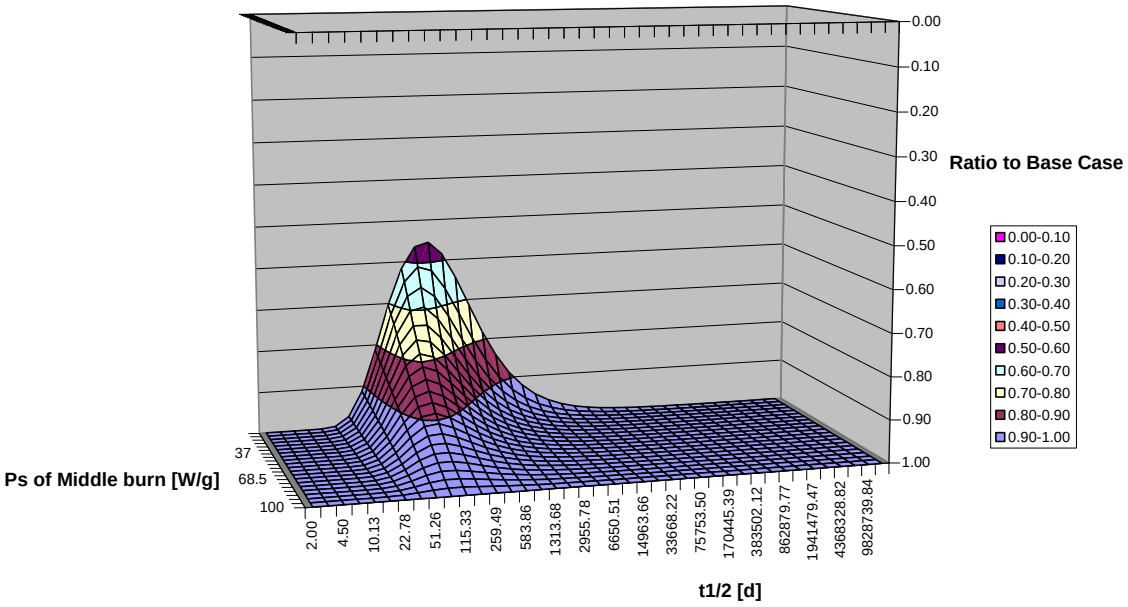

Figure 39. Radioactive Nuclide Concentration Ratio to Base Case of 2nd Burn Ps = 100 W/g, $\sigma_{a,R}$ = 1 b for Each Half-life of Radioactive Parent for Three Burn Cycles of Equal Burnup with Constant Specific Power of 100 W/g for the 1st and 3rd cycles and Variable Specific Power for the 2nd cycle.

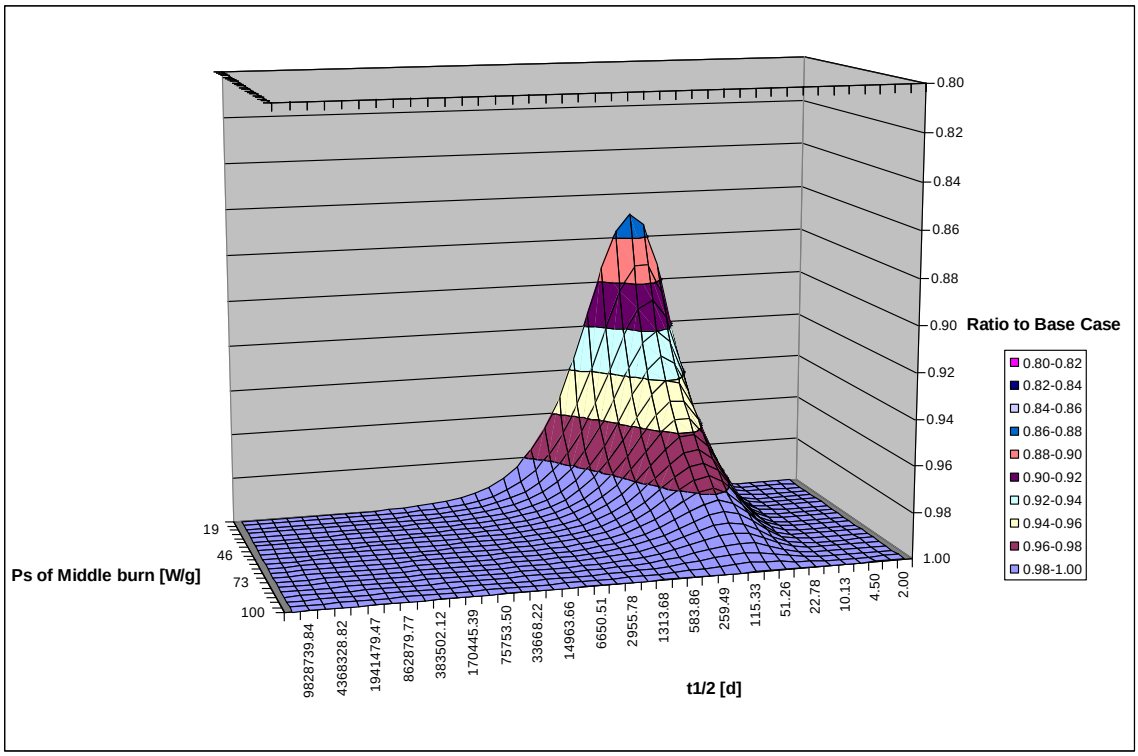

Figure 40. Radioactive Nuclide Concentration Ratio to Base Case of 2nd Burn Ps = 100 W/g, $\sigma_{a,R}$ = 100 b for Each Half-life of Radioactive Parent for Three Burn Cycles of Equal Burnup with Constant Specific Power of 100 W/g for the 1st and 3rd Cycles and Variable Specific Power for the 2nd Cycle.

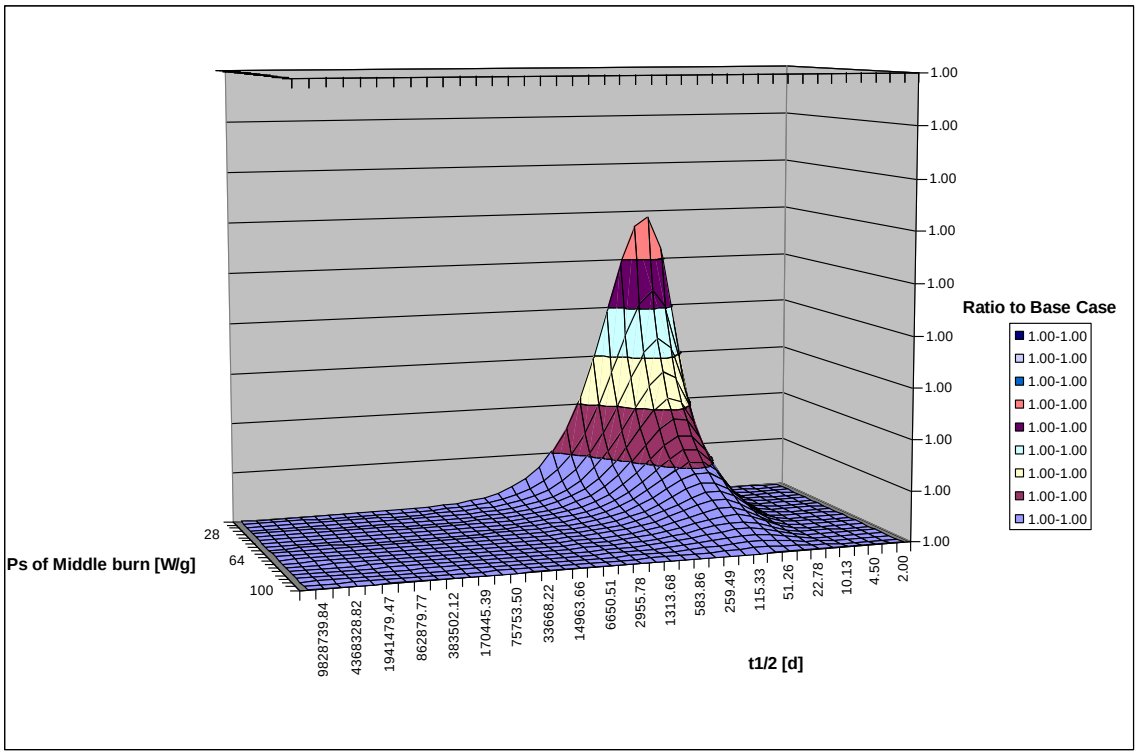

Figure 41. Radioactive Nuclide Concentration Ratio to Base Case of 2nd Burn Ps = 100 W/g, $\sigma_{a,R}$ = 1000 b for Each Half-life of Radioactive Parent for Three Burn Cycles of Equal Burnup with Constant Specific Power of 100 W/g for the 1st and 3rd Cycles and Variable Specific Power for the 2nd Cycle.

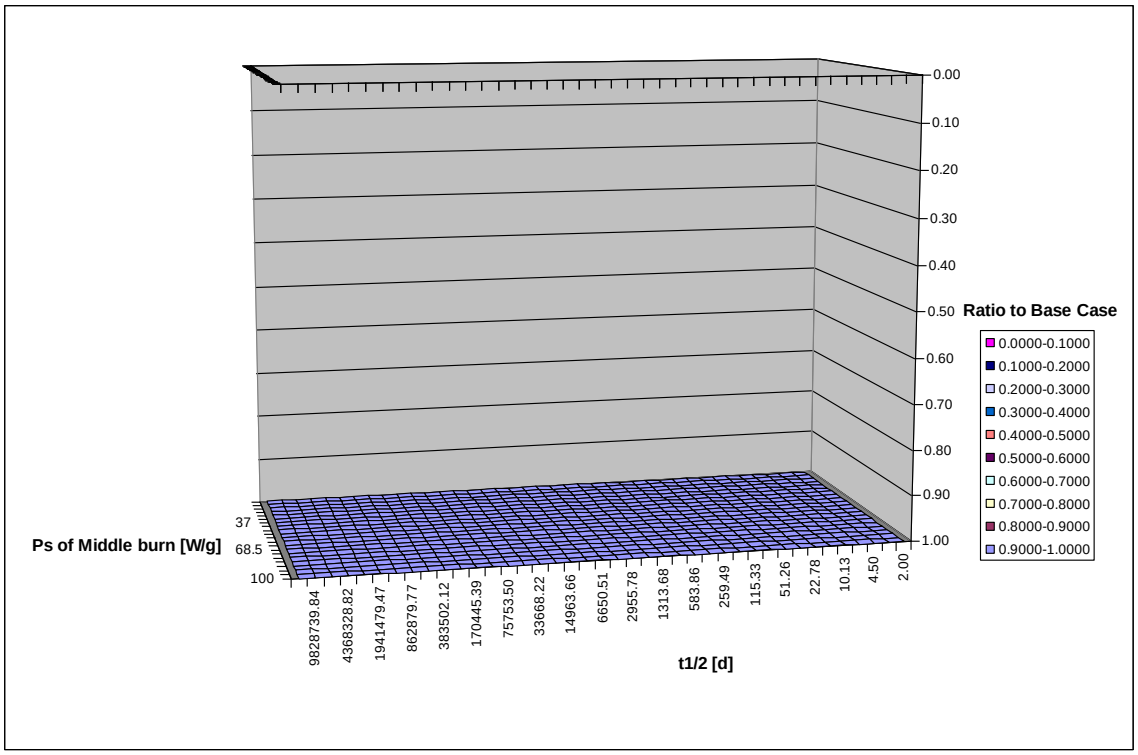

Figure 42. Radioactive Nuclide Concentration Ratio to Base Case of 2nd Burn Ps = 100 W/g, $\sigma_{a,R}$ = 10000 b for Each Half-life of Radioactive Parent for Three Burn Cycles of Equal Burnup with Constant Specific Power of 100 W/g for the 1st and 3rd Cycles and Variable Specific Power for the 2nd Cycle.

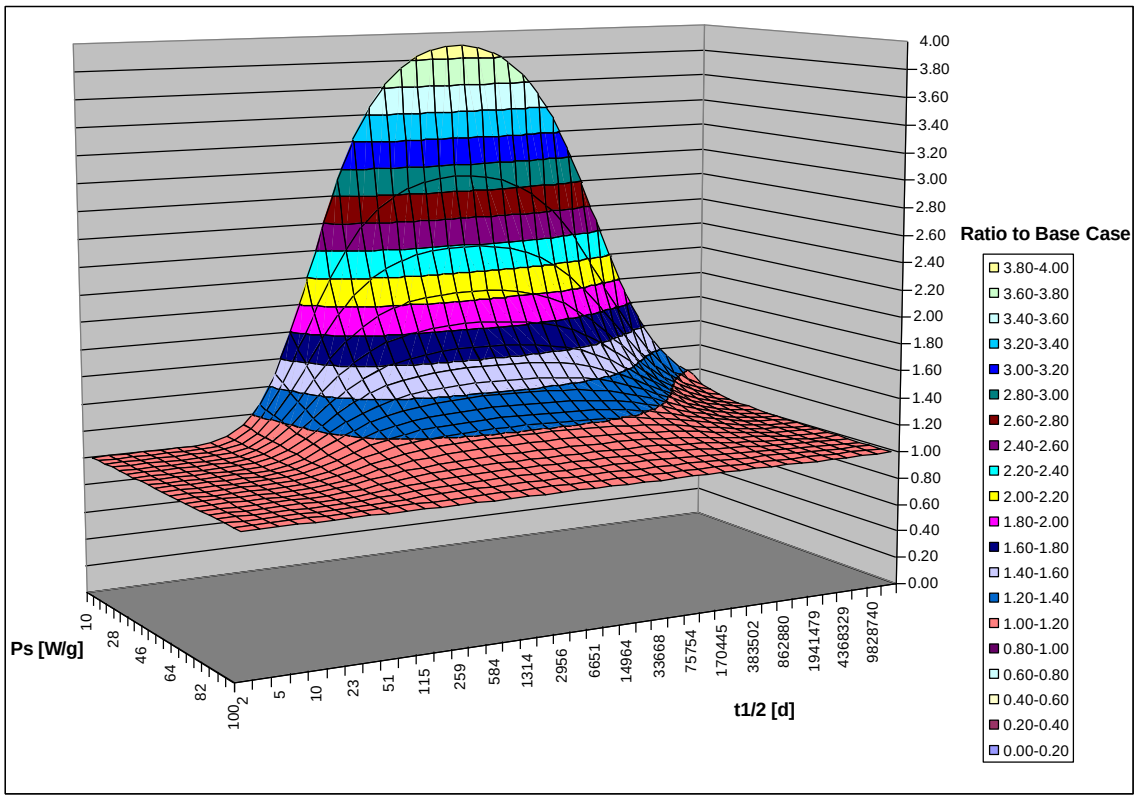

Figure 43. Stable Nuclide Concentration Ratio to Base Case of 2nd Burn Ps = 100 W/g, $\sigma_{a,R}$ = 1 b, $\sigma_{a,S}$ = 1 b for Each Half-life of Radioactive Parent for Three Burn Cycles of Equal Burnup with Constant Specific Power of 100 W/g for the 1st and 3rd Cycles and Variable Specific Power for the 2nd Cycle.

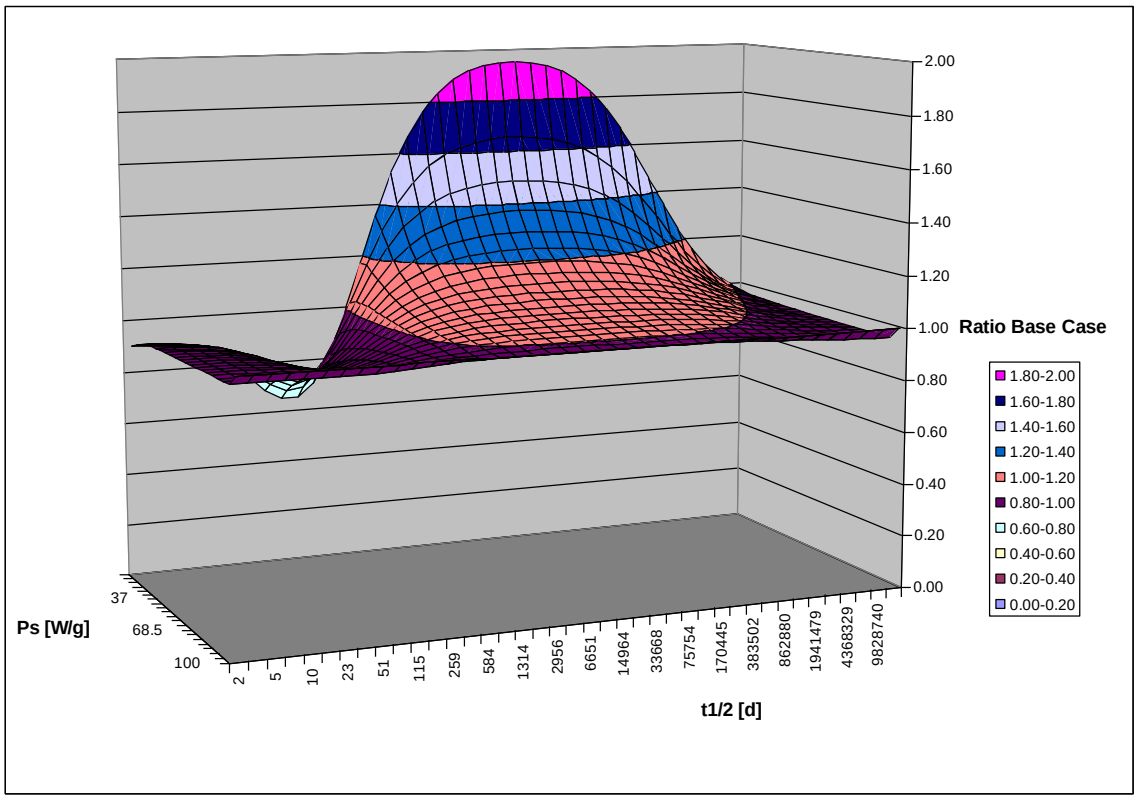

Figure 44. Stable Nuclide Concentration Ratio to Base Case of 2nd Burn Ps = 100 W/g, $\sigma_{a,R}$ = 1 b, $\sigma_{a,S}$ = 100 b for Each Half-life of Radioactive Parent for Three Burn Cycles of Equal Burnup with Constant Specific Power of 100 W/g for the 1st and 3rd Cycles and Variable Specific Power for the 2nd Cycle.

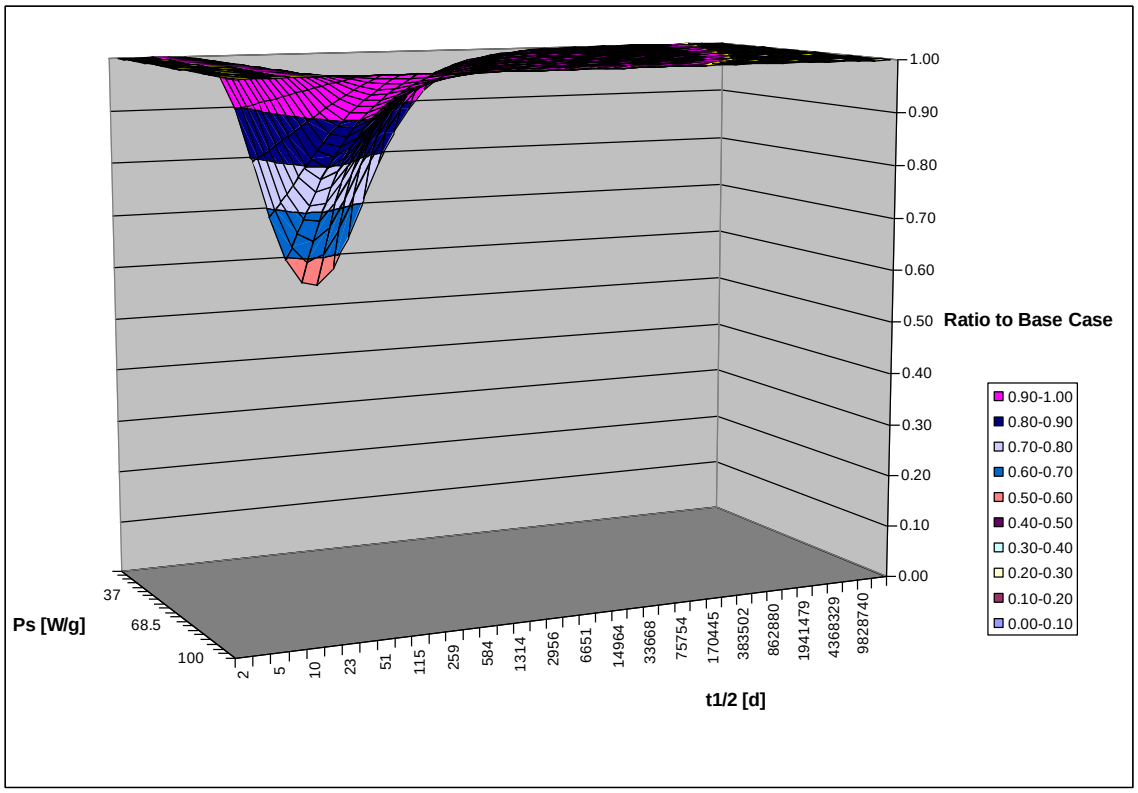

Figure 45. Stable Nuclide Concentration Ratio to Base Case of 2nd Burn Ps = 100 W/g, $\sigma_{a,R}$ = 1 b, $\sigma_{a,S}$ = 1000 b for Each Half-life of Radioactive Parent for Three Burn Cycles of Equal Burnup with Constant Specific Power of 100 W/g for the 1st and 3rd Cycles and Variable Specific Power for the 2nd Cycle.

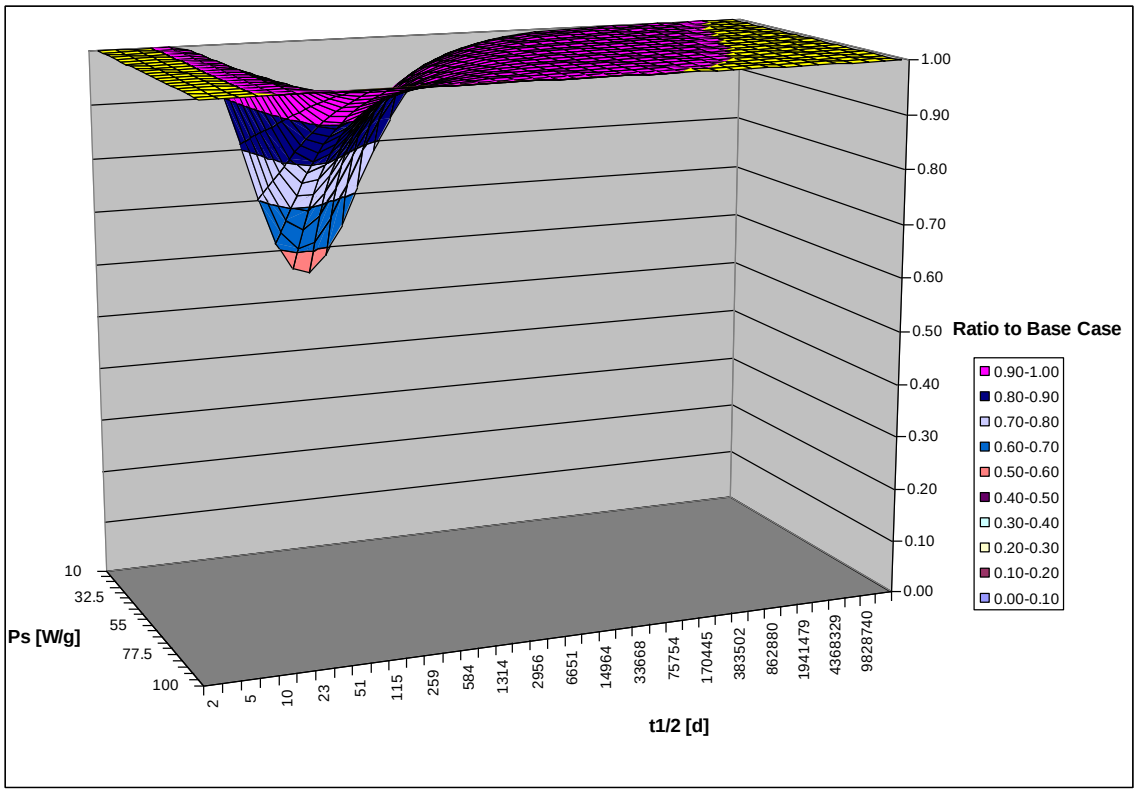

Figure 46. Stable Nuclide Concentration Ratio to Base Case of 2nd Burn Ps = 100 W/g, $\sigma_{a,R}$ = 1 b, $\sigma_{a,S}$ = 10,000 b for Each Half-life of Radioactive Parent for Three Burn Cycles of Equal Burnup with Constant Specific Power of 100 W/g for the 1st and 3rd Cycles and Variable Specific Power for the 2nd Cycle.

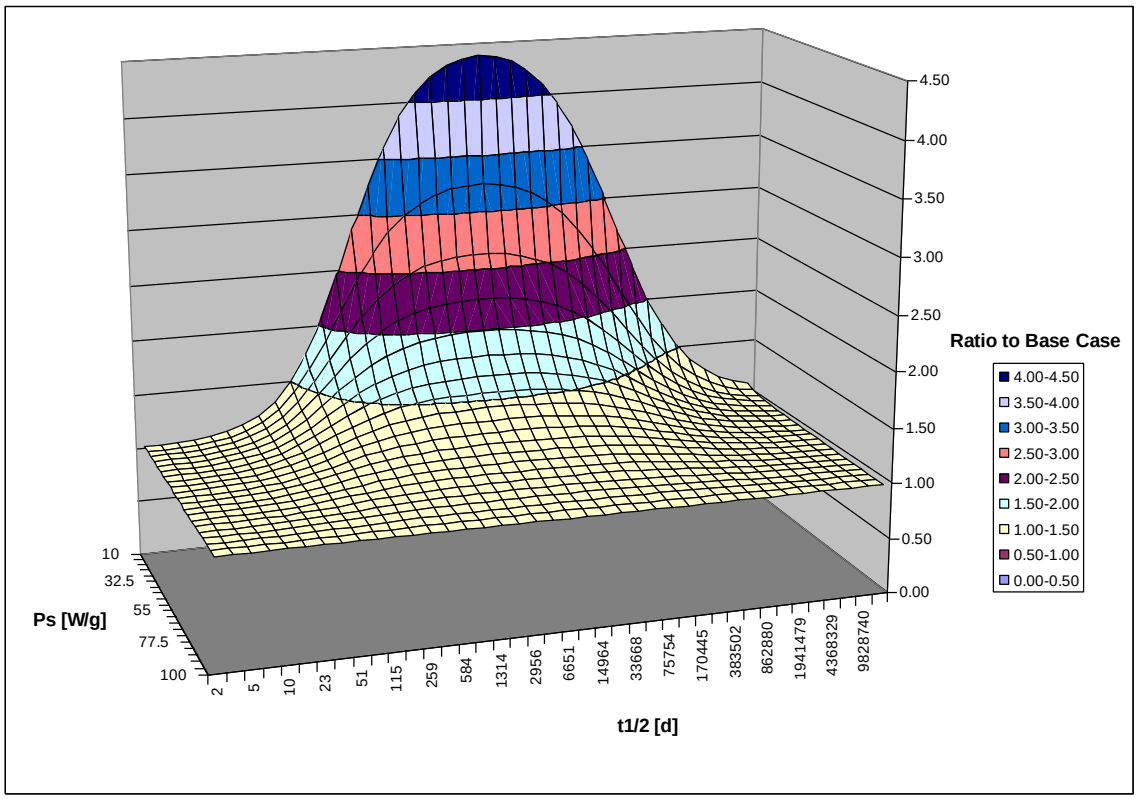

Figure 47. Stable Nuclide Concentration Ratio to Base Case of 2nd Burn Ps = 100 W/g, $\sigma_{a,R}$ = 100 b, $\sigma_{a,S}$ = 1 b for Each Half-life of Radioactive Parent for Three Burn Cycles of Equal Burnup with Constant Specific Power of 100 W/g for the 1st and 3rd Cycles and Variable Specific Power for the 2nd Cycle.

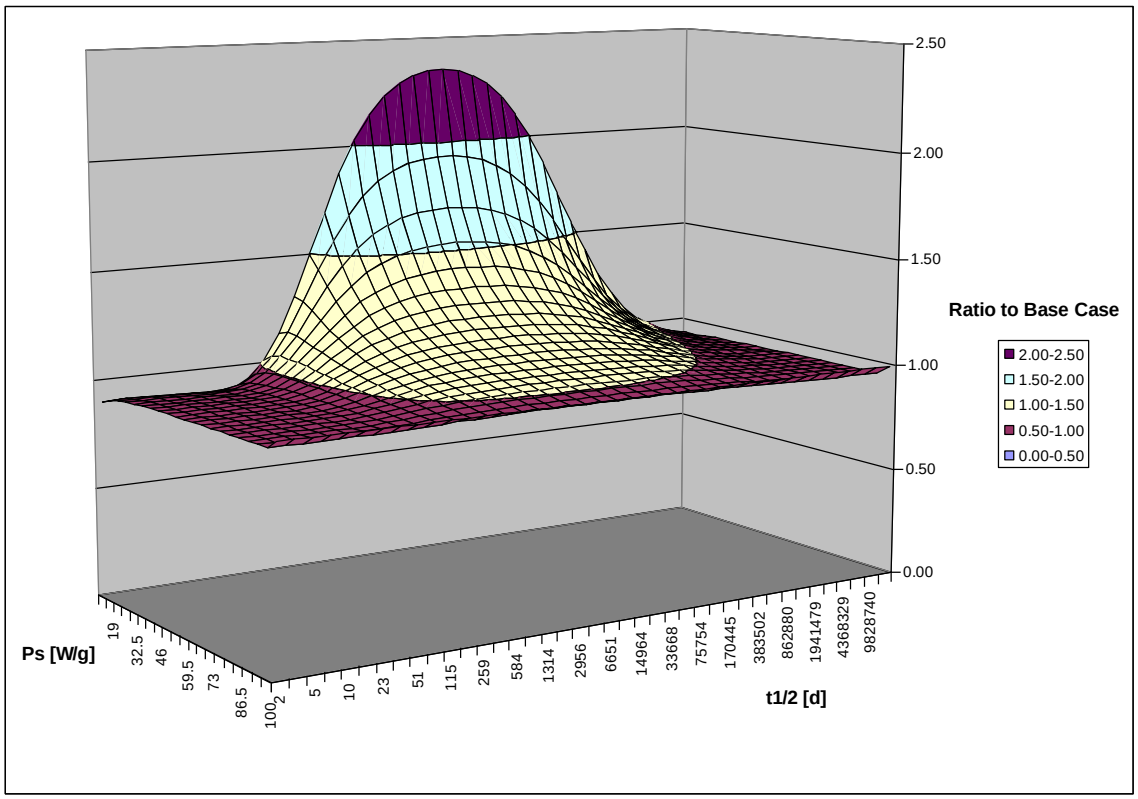

Figure 48. Stable Nuclide Concentration Ratio to Base Case of 2nd Burn Ps = 100 W/g, $\sigma_{a,R}$ = 100 b, $\sigma_{a,S}$ = 100 b for Each Half-life of Radioactive Parent for Three Burn Cycles of Equal Burnup with Constant Specific Power of 100 W/g for the 1st and 3rd Cycles and Variable Specific Power for the 2nd Cycle.

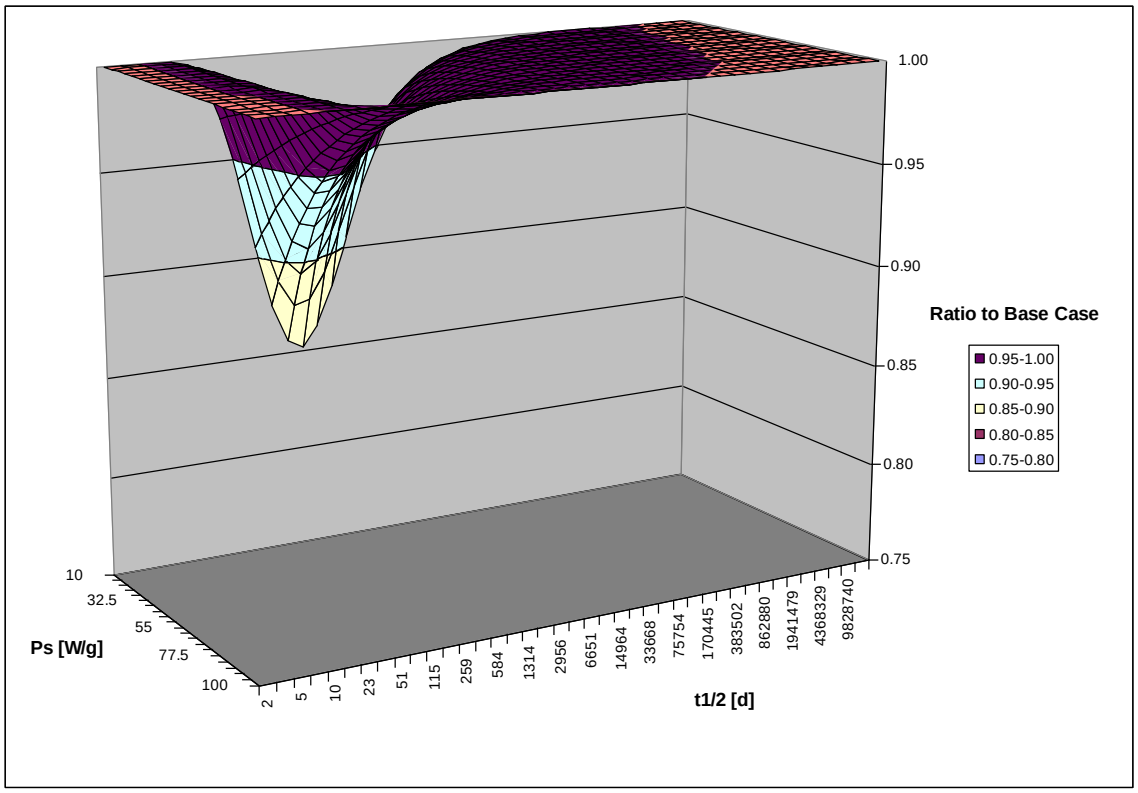

Figure 49. Stable Nuclide Concentration Ratio to Base Case of 2nd Burn Ps = 100 W/g, $\sigma_{a,R}$ = 100 b, $\sigma_{a,S}$ = 1000 b for Each Half-life of Radioactive Parent for Three Burn Cycles of Equal Burnup with Constant Specific Power of 100 W/g for the 1st and 3rd Cycles and Variable Specific Power for the 2nd Cycle.

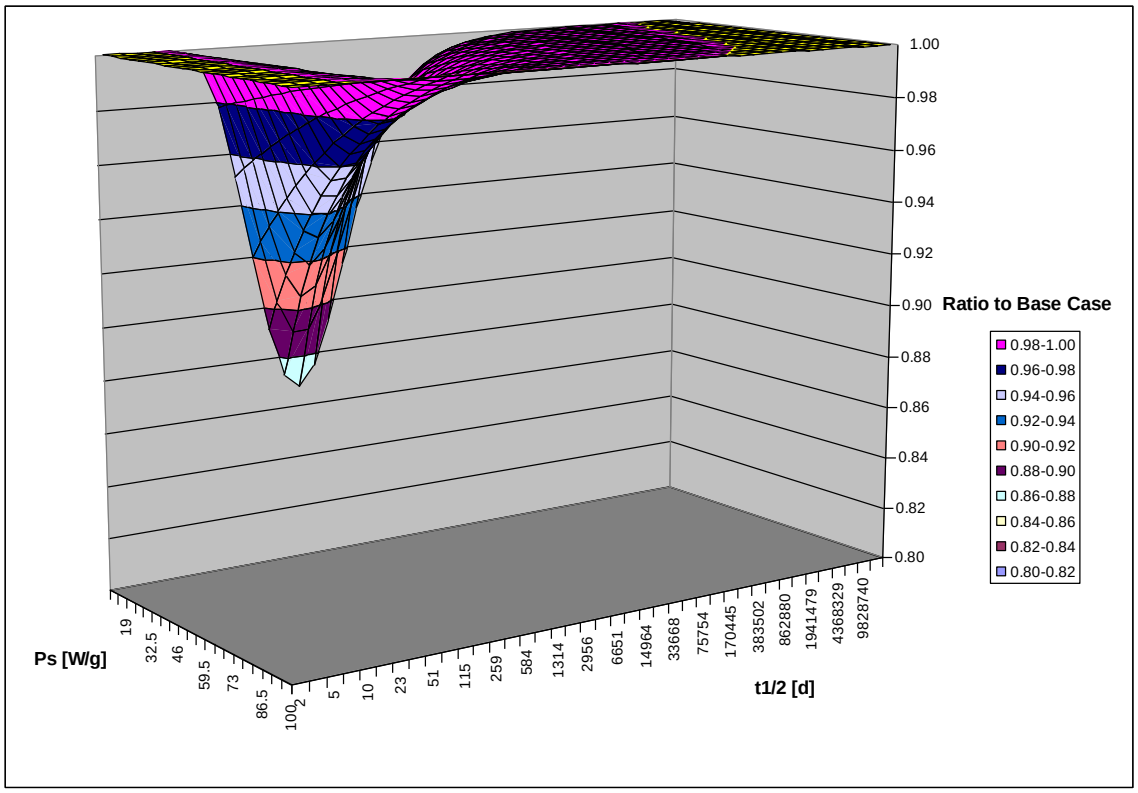

Figure 50. Stable Nuclide Concentration Ratio to Base Case of 2nd Burn Ps = 100 W/g, $\sigma_{a,R}$ = 100 b, $\sigma_{a,S}$ = 10000 b for Each Half-life of Radioactive Parent for Three Burn Cycles of Equal Burnup with Constant Specific Power of 100 W/g for the 1st and 3rd Cycles and Variable Specific Power for the 2nd Cycle.

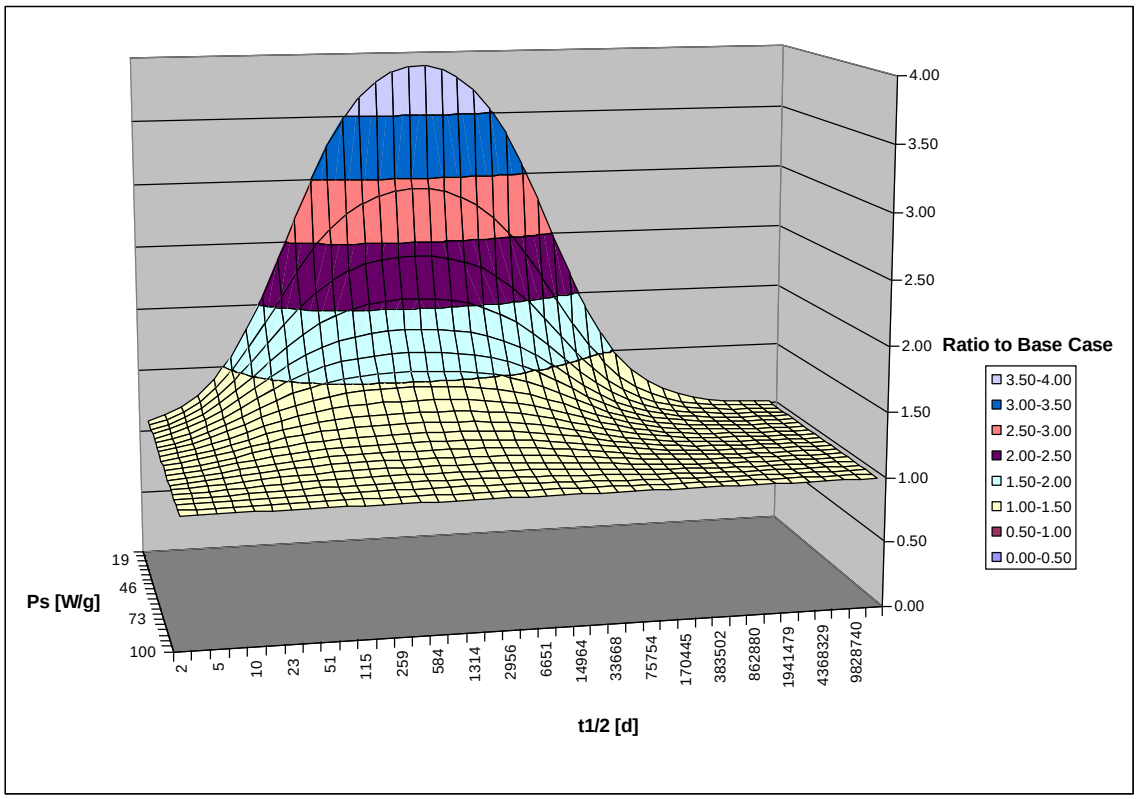

Figure 51. Stable Nuclide Concentration Ratio to Base Case of 2nd Burn Ps = 100 W/g, $\sigma_{a,R}$ = 1000 b, $\sigma_{a,S}$ = 1 b for Each Half-life of Radioactive Parent for Three Burn Cycles of Equal Burnup with Constant Specific Power of 100 W/g for the 1st and 3rd Cycles and Variable Specific Power for the 2nd Cycle.

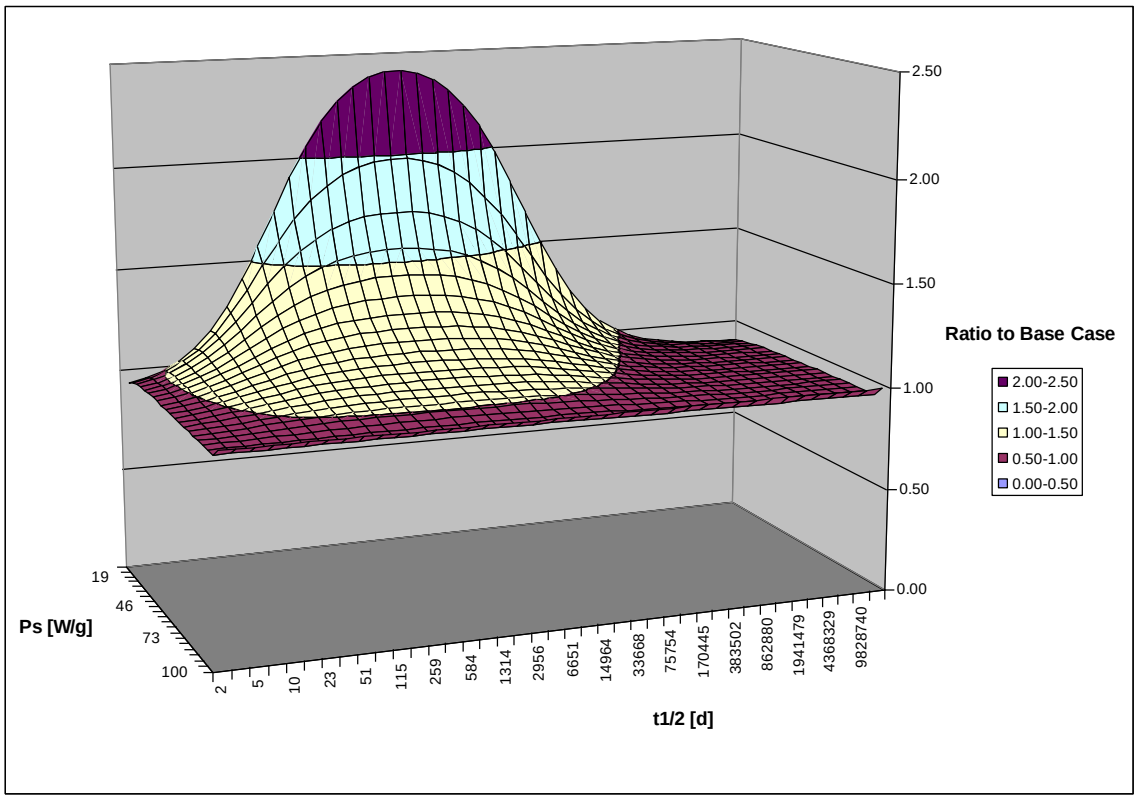

Figure 52. Stable Nuclide Concentration Ratio to Base Case of 2nd Burn Ps = 100 W/g, $\sigma_{a,R}$ = 1000 b, $\sigma_{a,S}$ = 100 b for Each Half-life of Radioactive Parent for Three Burn Cycles of Equal Burnup with Constant Specific Power of 100 W/g for the 1st and 3rd Cycles and Variable Specific Power for the 2nd Cycle.

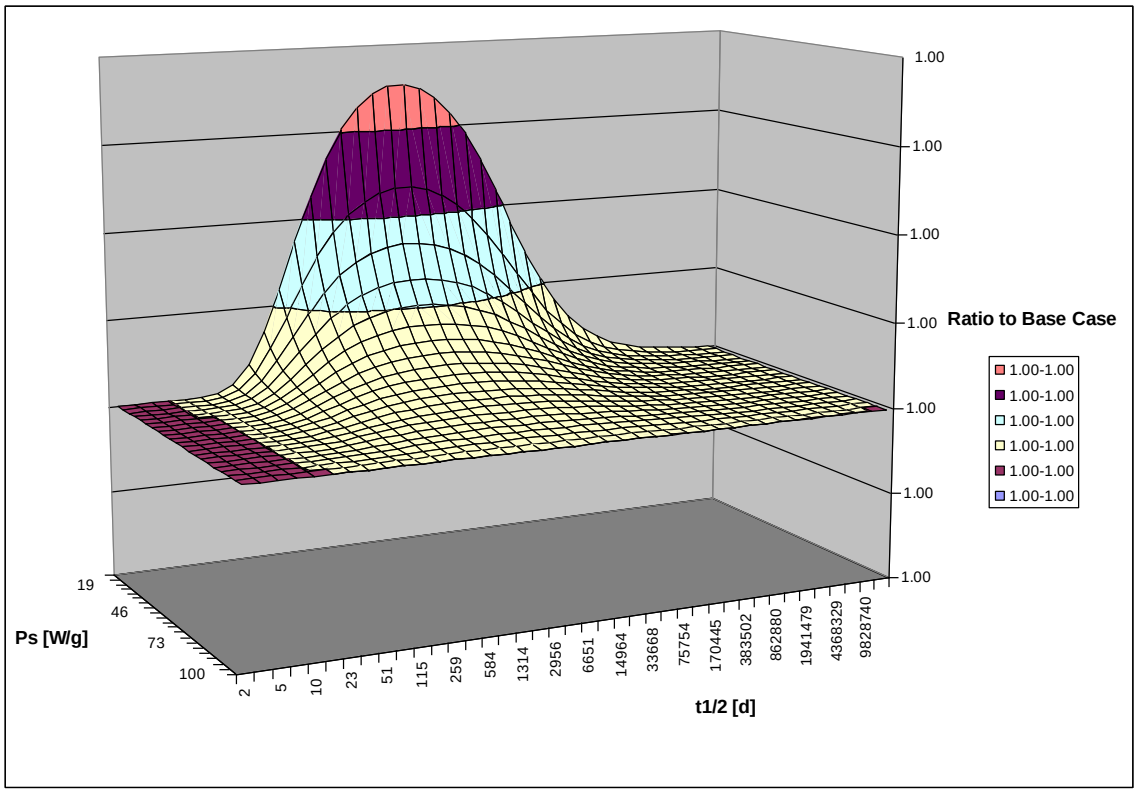

Figure 53. Stable Nuclide Concentration Ratio to Base Case of 2nd Burn Ps = 100 W/g, $\sigma_{a,R}$ = 1000 b, $\sigma_{a,S}$ = 1000 b for Each Half-life of Radioactive Parent for Three Burn Cycles of Equal Burnup with Constant Specific Power of 100 W/g for the 1st and 3rd Cycles and Variable Specific Power for the 2nd Cycle.

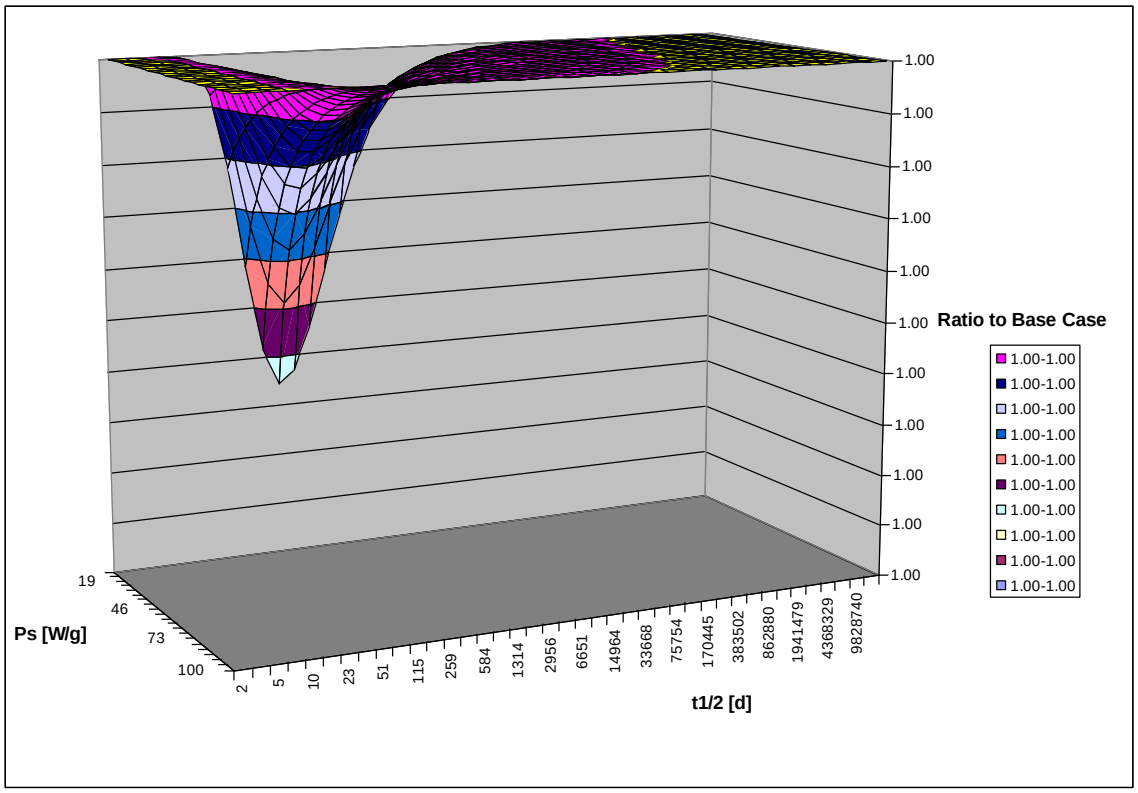

Figure 54. Stable Nuclide Concentration Ratio to Base Case of 2nd Burn Ps = 100 W/g, $\sigma_{a,R}$ = 1000 b, $\sigma_{a,S}$ = 10000 b for Each Half-life of Radioactive Parent for Three Burn Cycles of Equal Burnup with Constant Specific Power of 100 W/g for the 1st and 3rd Cycles and Variable Specific Power for the 2nd Cycle.

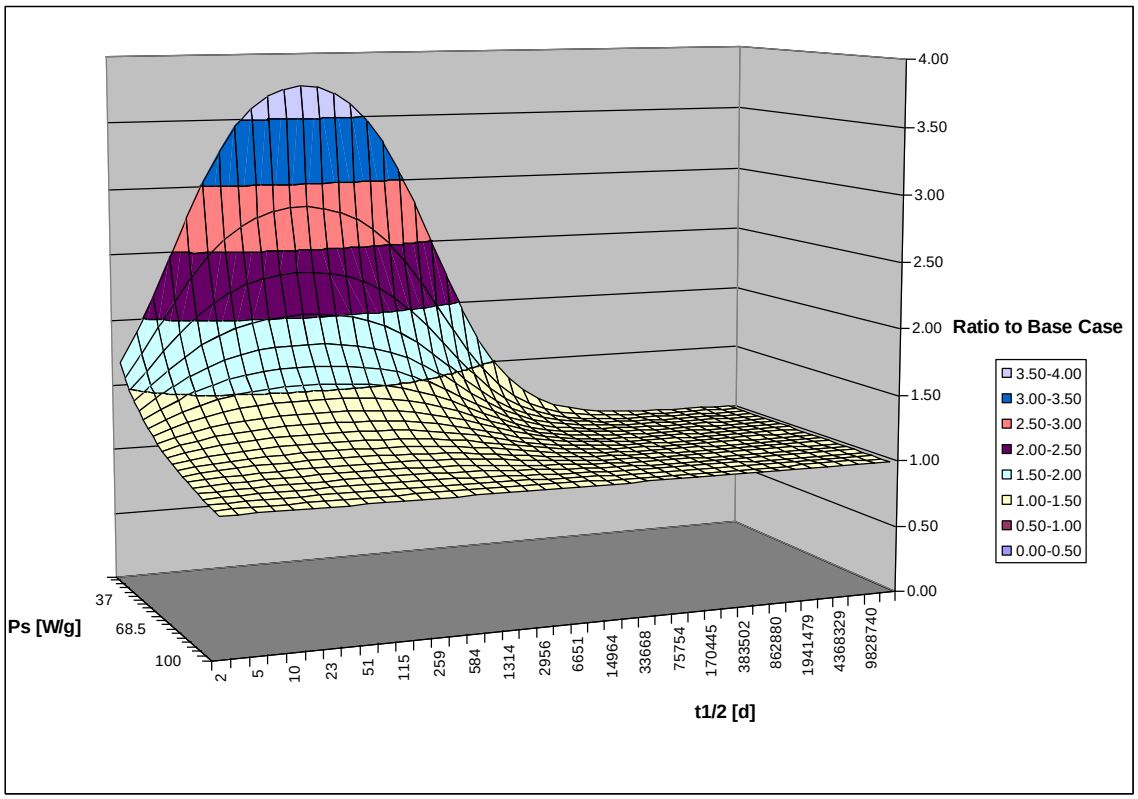

Figure 55. Stable Nuclide Concentration Ratio to Base Case of 2nd Burn Ps = 100 W/g, $\sigma_{a,R}$ = 10,000 b, $\sigma_{a,S}$ = 1 b for Each Half-life of Radioactive Parent for Three Burn Cycles of Equal Burnup with Constant Specific Power of 100 W/g for the 1st and 3rd Cycles and Variable Specific Power for the 2nd Cycle.

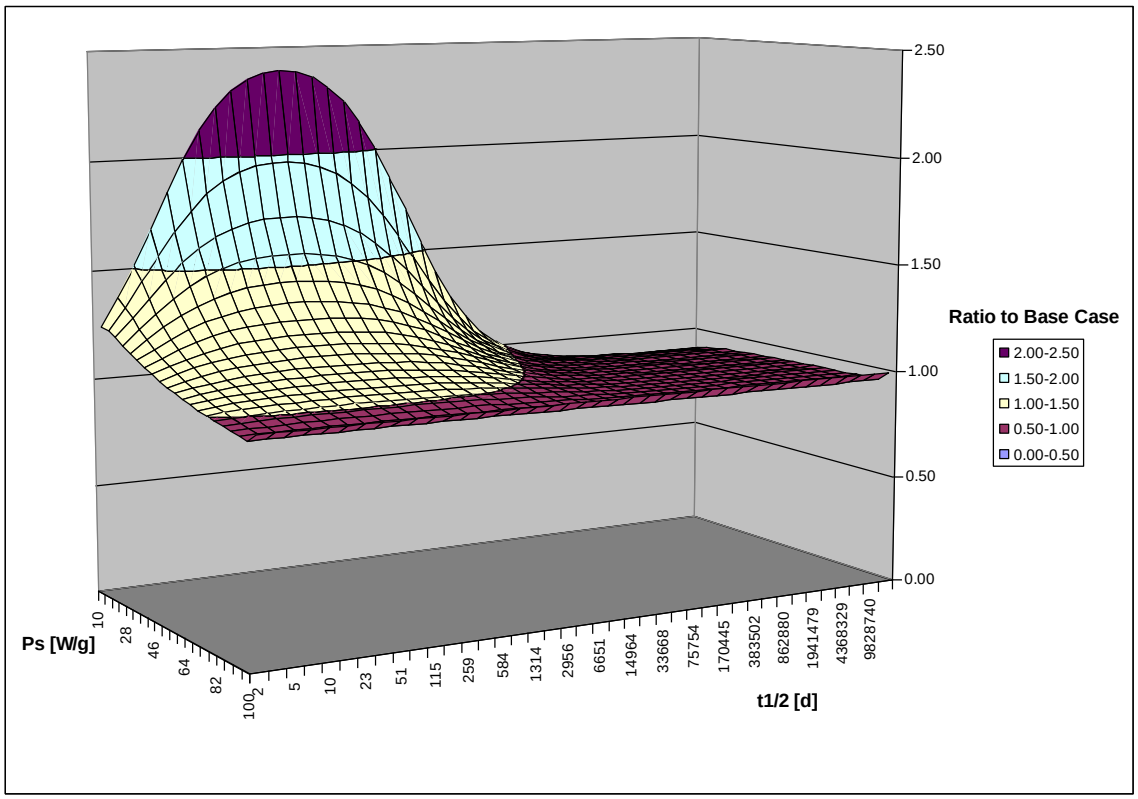

Figure 56. Stable Nuclide Concentration Ratio to Base Case of 2nd Burn Ps = 100 W/g, $\sigma_{a,R}$ = 10,000 b, $\sigma_{a,S}$ = 100 b for Each Half-life of Radioactive Parent for Three Burn Cycles of Equal Burnup with Constant Specific Power of 100 W/g for the 1st and 3rd Cycles and Variable Specific Power for the 2nd Cycle.

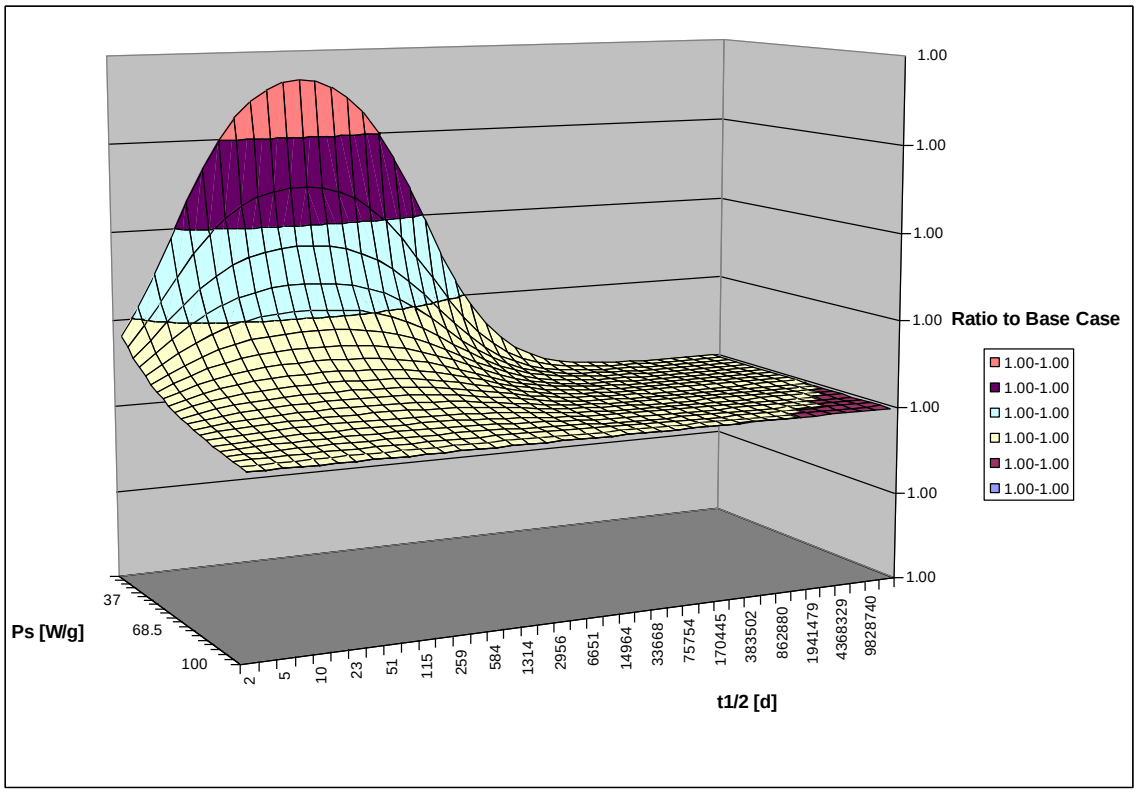

Figure 57. Stable Nuclide Concentration Ratio to Base Case of 2nd Burn Ps = 100 W/g, $\sigma_{a,R}$ = 10,000 b, $\sigma_{a,S}$ = 1000 b for Each Half-life of Radioactive Parent for Three Burn Cycles of Equal Burnup with Constant Specific Power of 100 W/g for the 1st and 3rd Cycles and Variable Specific Power for the 2nd Cycle.

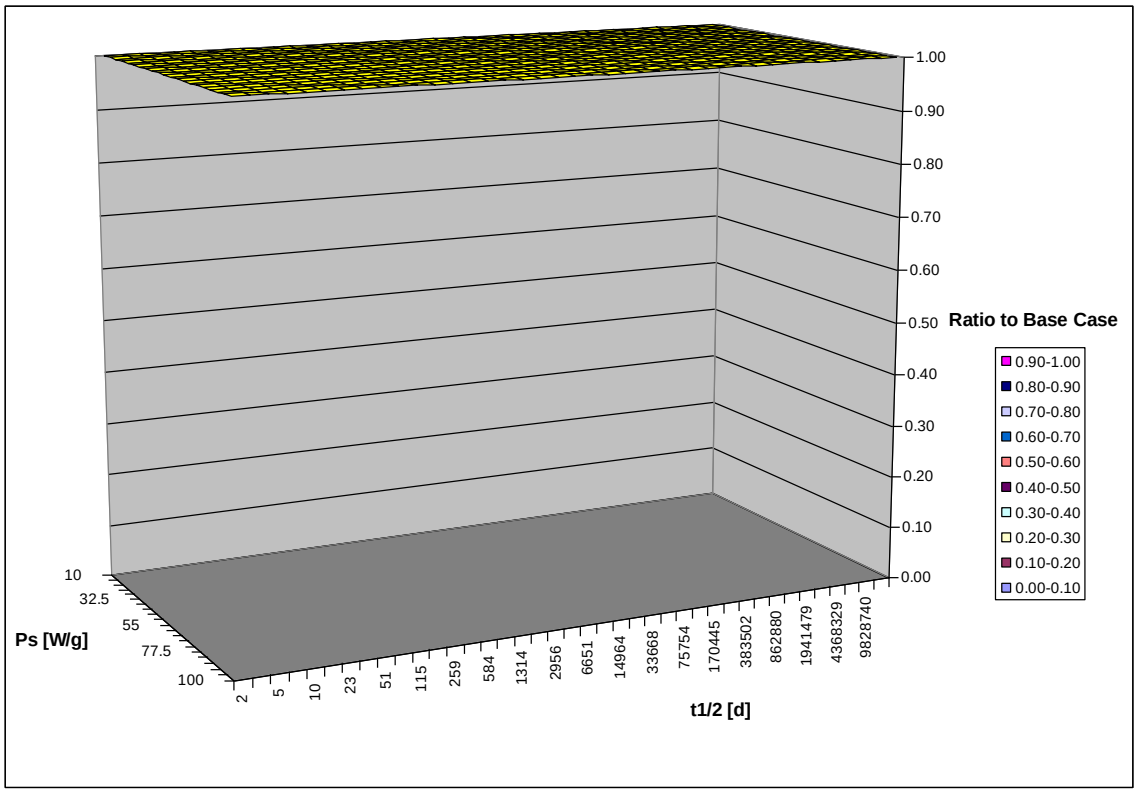

Figure 58. Stable Nuclide Concentration Ratio to Base Case of 2nd Burn Ps = 100 W/g, $\sigma_{a,R}$ = 10,000 b, $\sigma_{a,S}$ = 10,000 b for Each Half-life of Radioactive Parent for Three Burn Cycles of Equal Burnup with Constant Specific Power of 100 W/g for the 1st and 3rd Cycles and Variable Specific Power for the 2nd Cycle.

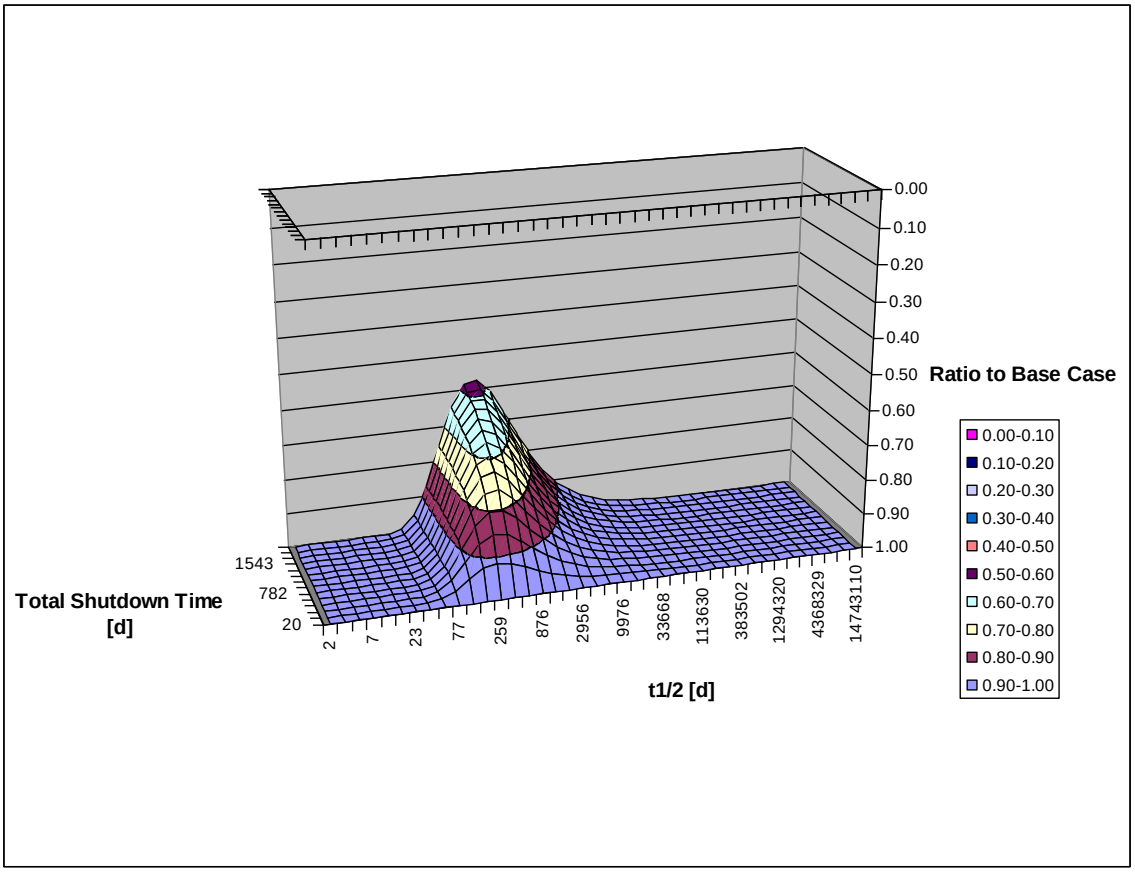

Figure 59. Radioactive Nuclide Concentration Ratio to Base Case of a Three Cycle Power History with Three Burn Cycles of Equal Length, a Constant Ps = 35 W/g for All Burn Cycles, and 20 Days of Total Shutdown Time Divided Evenly Between Two Shutdowns Separating the Burn Cycles and $\sigma_{a,R}$ = 1 b for Each Half-life of Radioactive Parent.

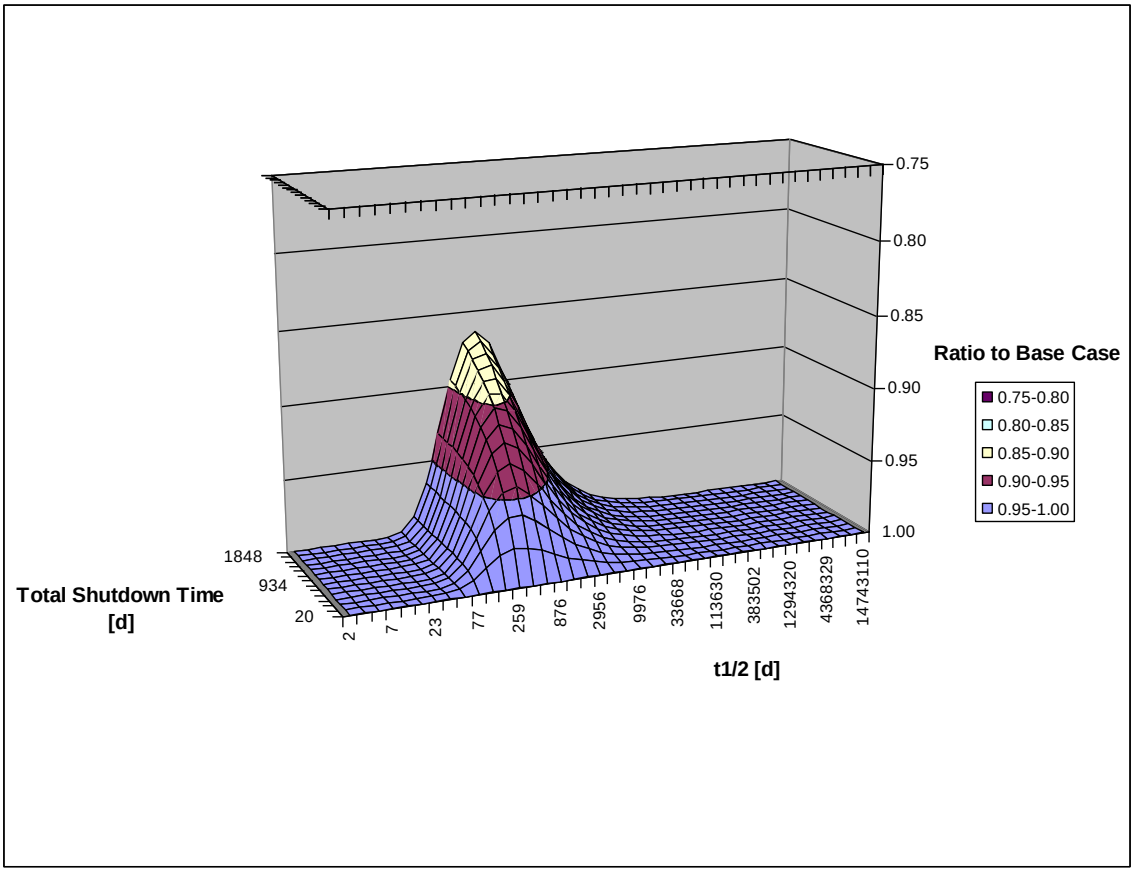

Figure 60. Radioactive Nuclide Concentration Ratio to Base Case of a Three Cycle Power History with Three Burn Cycles of Equal Length, a Constant Ps = 35 W/g for All Burn Cycles, and 20 days of Total Shutdown Time Divided Evenly Between Two Shutdowns Separating the Burn Cycles and $\sigma_{a,R}$ = 100 b for Each Half-life of Radioactive Parent.

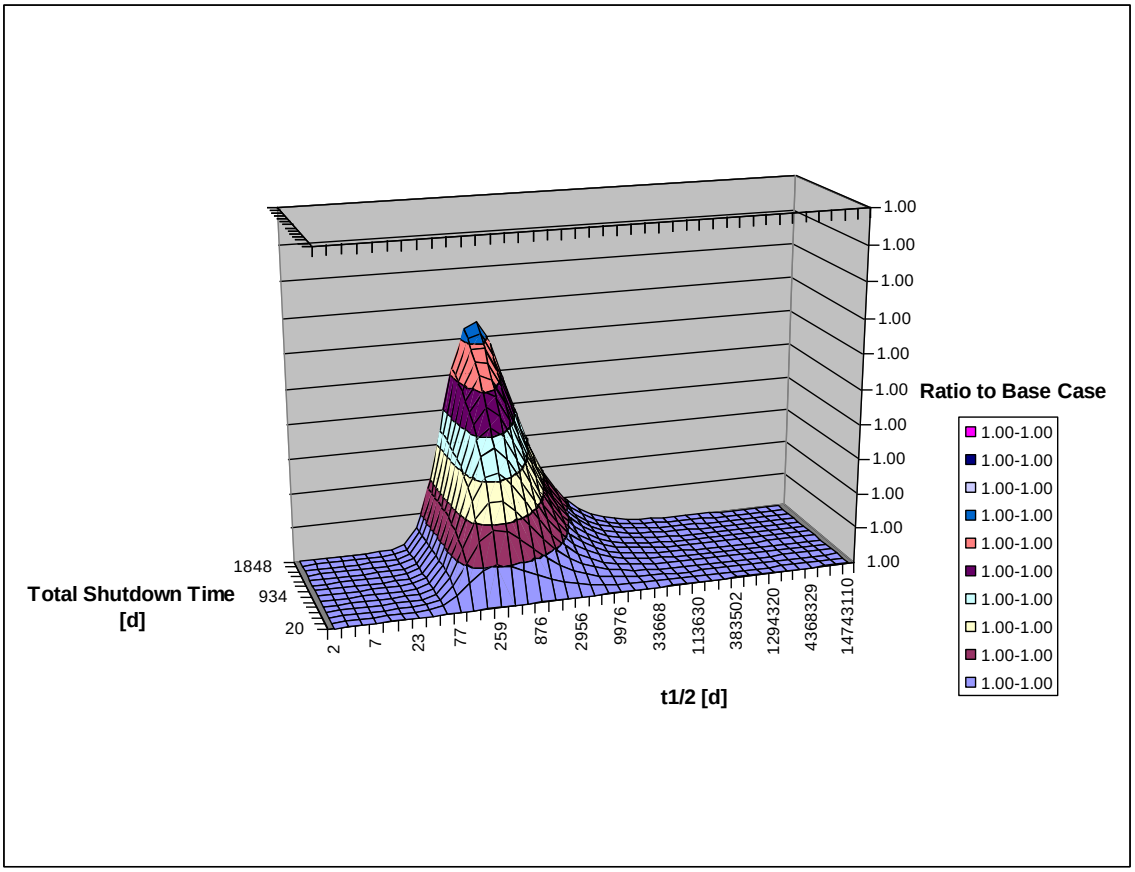

Figure 61. Radioactive Nuclide Concentration Ratio to Base Case of a Three Cycle Power History with Three Burn Cycles of Equal Length, a Constant Ps = 35 W/g for All Burn Cycles, and 20 days of Total Shutdown Time Divided Evenly Between Two Shutdowns Separating the Burn Cycles and $\sigma_{a,R}$ = 1000 b for Each Half-life of Radioactive Parent.

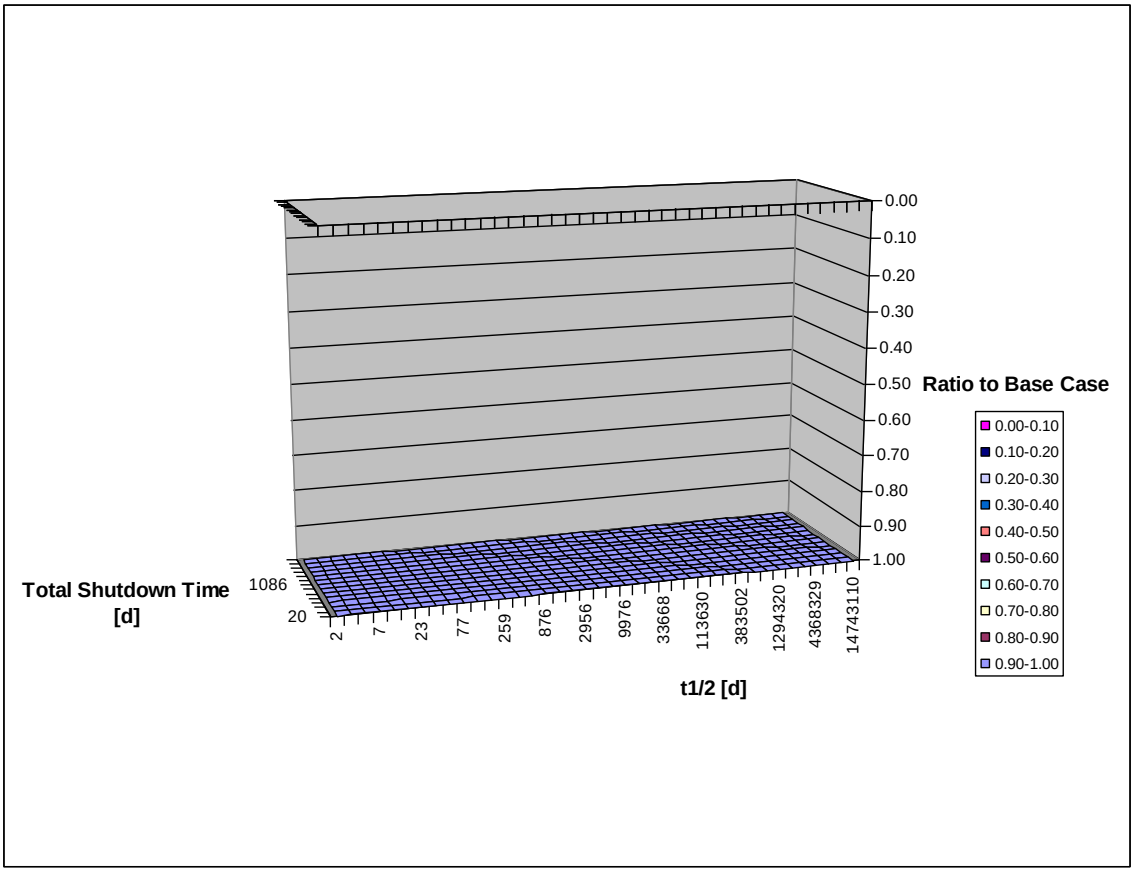

Figure 62. Radioactive Nuclide Concentration Ratio to Base Case of a Three Cycle Power History with Three Burn Cycles of Equal Length, a Constant Ps = 35 W/g for All Burn Cycles, and 20 days of Total Shutdown Time Divided Evenly Between Two Shutdowns Separating the Burn Cycles and $\sigma_{a,R}$ = 10000 b for Each Half-life of Radioactive Parent.

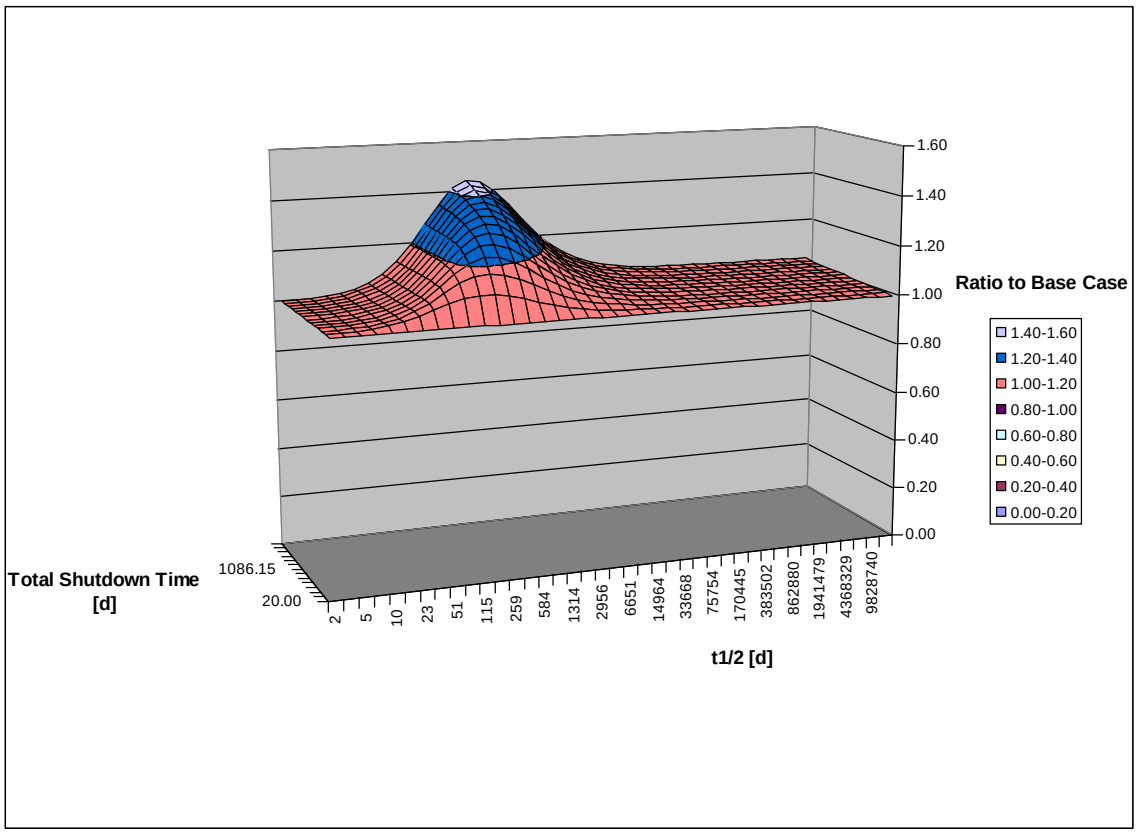

Figure 63. Stable Nuclide Concentration Ratio to Base Case of a Three Cycle Power History with Three Burn Cycles of Equal Length, a Constant Ps = 35 W/g for All Burn Cycles, and 20 days of Total Shutdown Time Divided Evenly Between Two Shutdowns Separating the Burn cycles, $\sigma_{a,R}$ = 1 b, and $\sigma_{a,S}$ = 1 b for Each Half-life of Radioactive Parent.

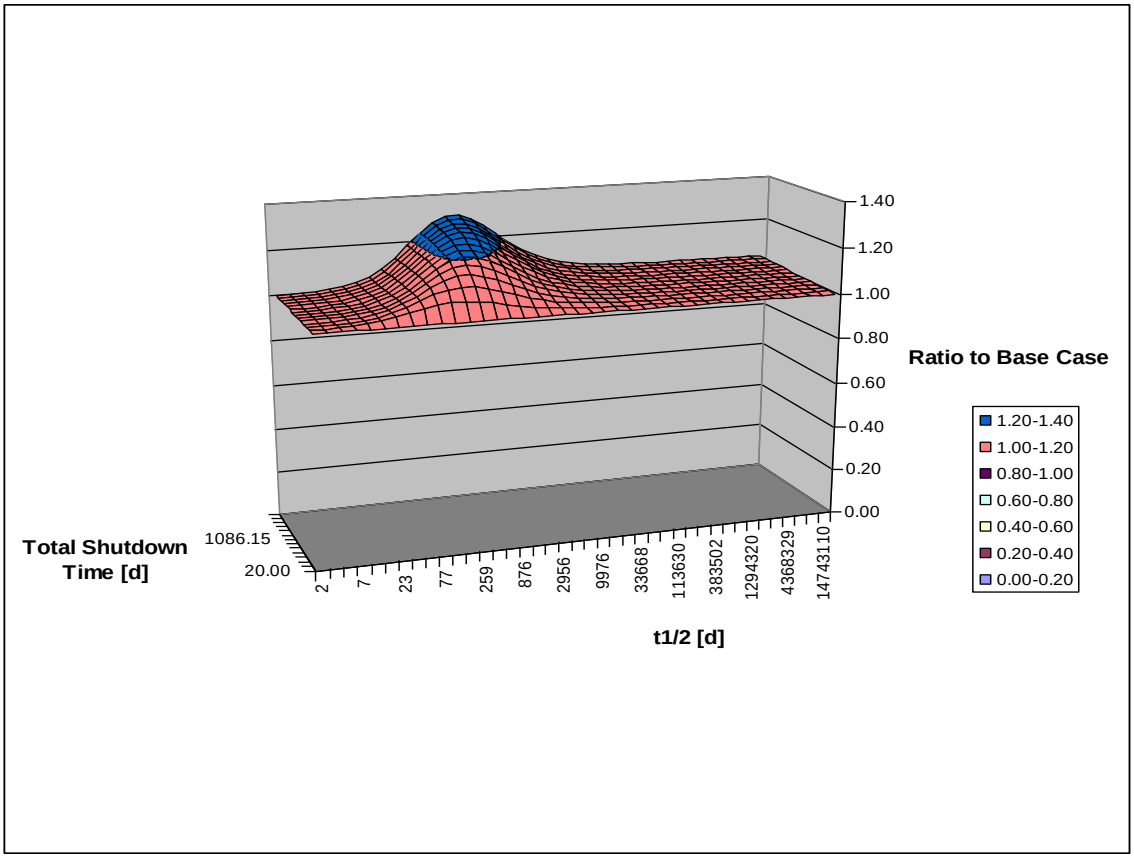

Figure 64. Stable Nuclide Concentration Ratio to Base Case of a Three Cycle Power History with Three Burn Cycles of Equal Length, a Constant Ps = 35 W/g for All Burn Cycles, and 20 days of Total Shutdown Time Divided Evenly Between Two Shutdowns Separating the Burn cycles, $\sigma_{a,R}$ = 1 b, and $\sigma_{a,S}$ = 100 b for Each Half-life of Radioactive Parent.

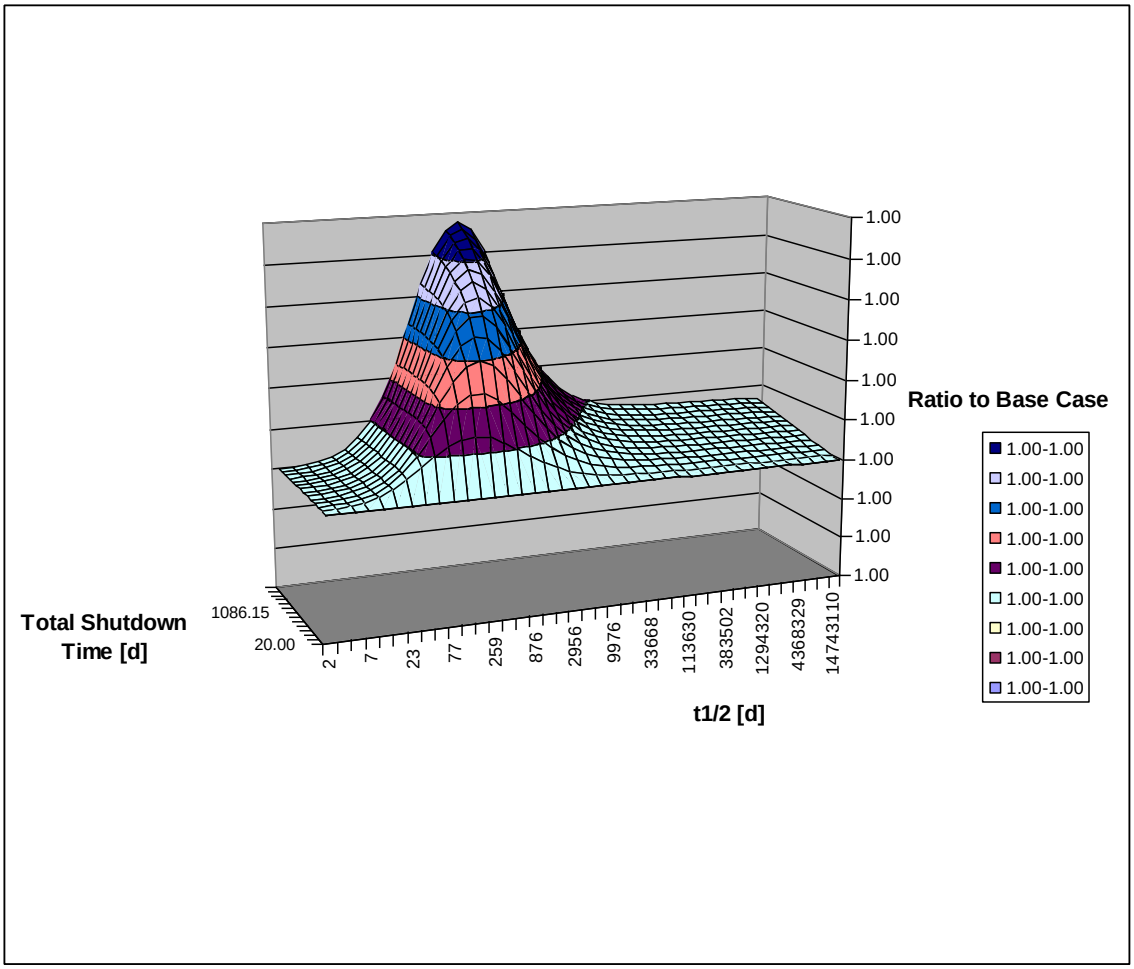

Figure 65. Stable Nuclide Concentration Ratio to Base Case of a Three Cycle Power History with Three Burn Cycles of Equal Length, a Constant Ps = 35 W/g for All Burn Cycles, and 20 days of Total Shutdown Time Divided Evenly Between Two Shutdowns Separating the Burn cycles, $\sigma_{a,R}$ = 1 b, and $\sigma_{a,S}$ = 1000 b for Each Half-life of Radioactive Parent.

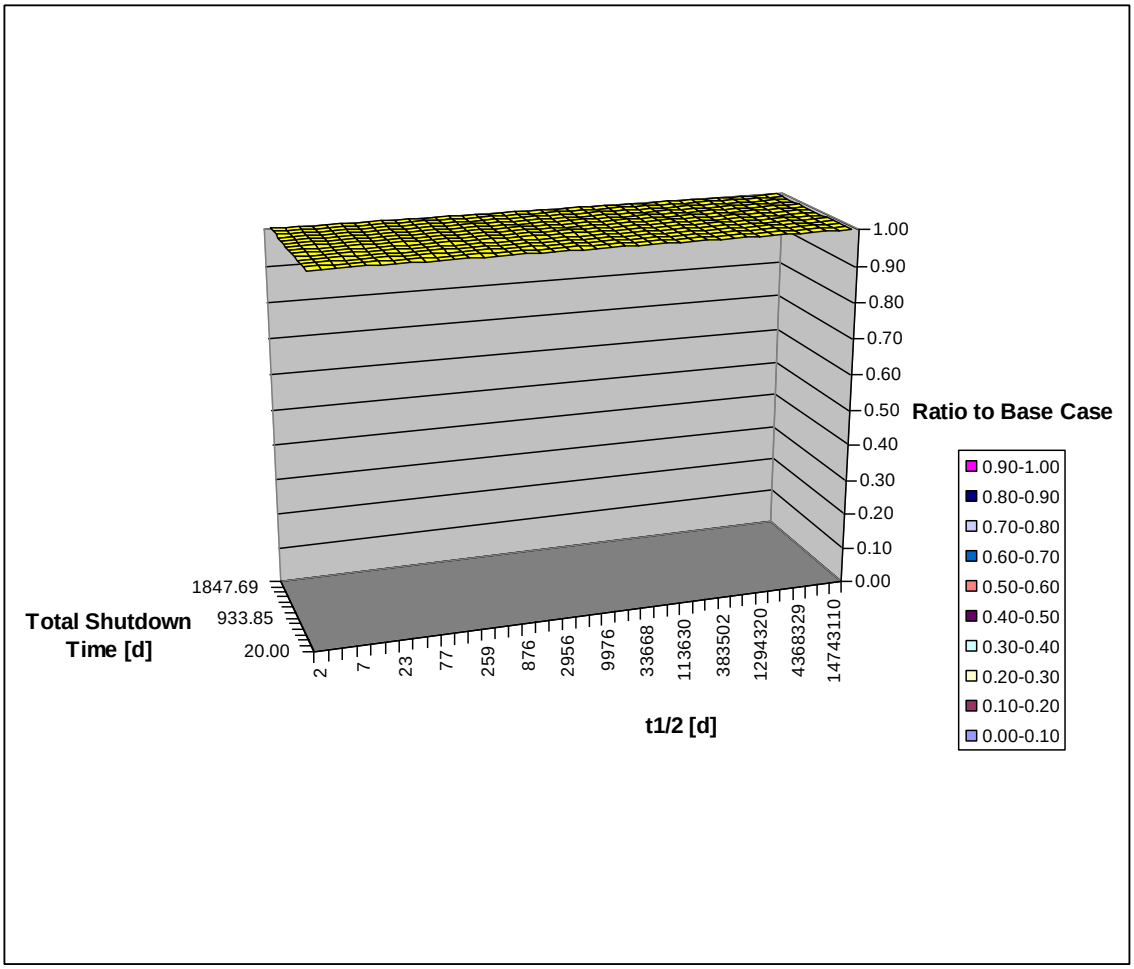

Figure 66. Stable Nuclide Concentration Ratio to Base Case of a Three Cycle Power History with Three Burn Cycles of Equal Length, a Constant Ps = 35 W/g for All Burn Cycles, and 20 days of Total Shutdown Time Divided Evenly Between Two Shutdowns Separating the Burn cycles, $\sigma_{a,R}$ = 1 b, and $\sigma_{a,S}$ = 10000 b for Each Half-life of Radioactive Parent.

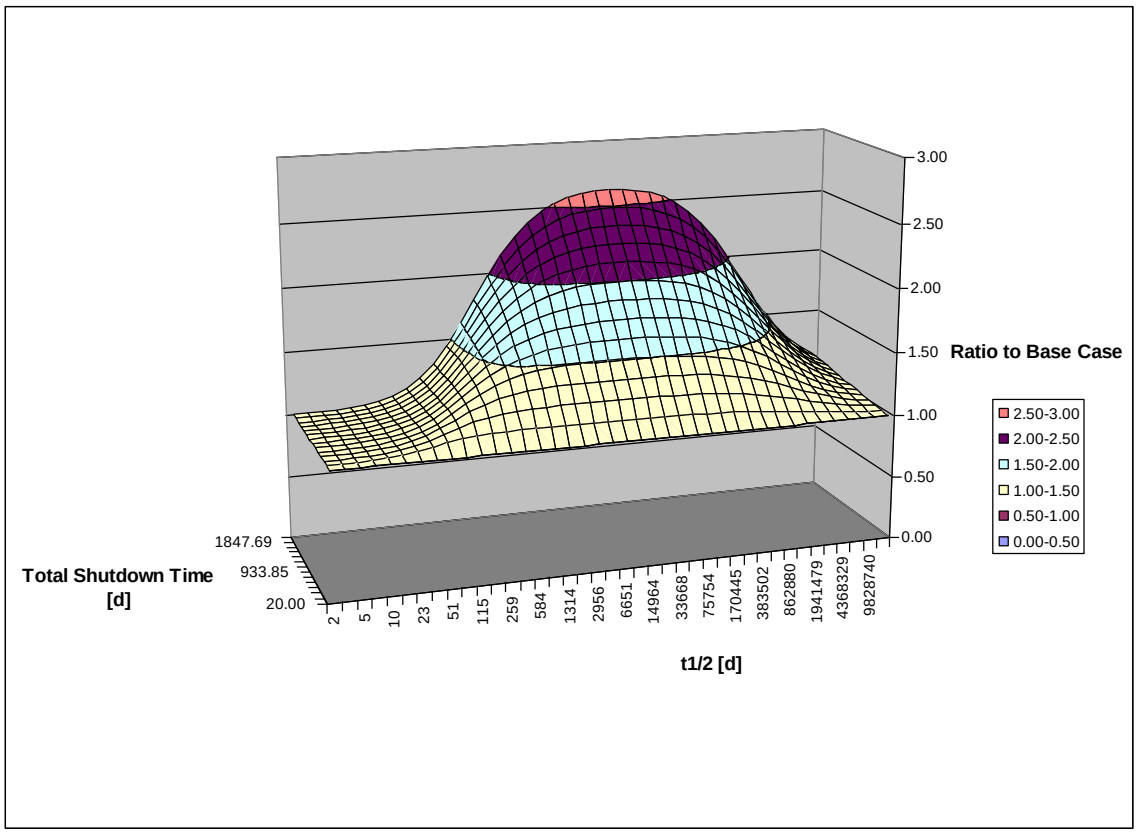

Figure 67. Stable Nuclide Concentration Ratio to Base Case of a Three Cycle Power History with Three Burn Cycles of Equal Length, a Constant Ps = 35 W/g for All Burn Cycles, and 20 days of Total Shutdown Time Divided Evenly Between Two Shutdowns Separating the Burn cycles, $\sigma_{a,R}$ = 100 b, and $\sigma_{a,S}$ = 1 b for Each Half-life of Radioactive Parent.

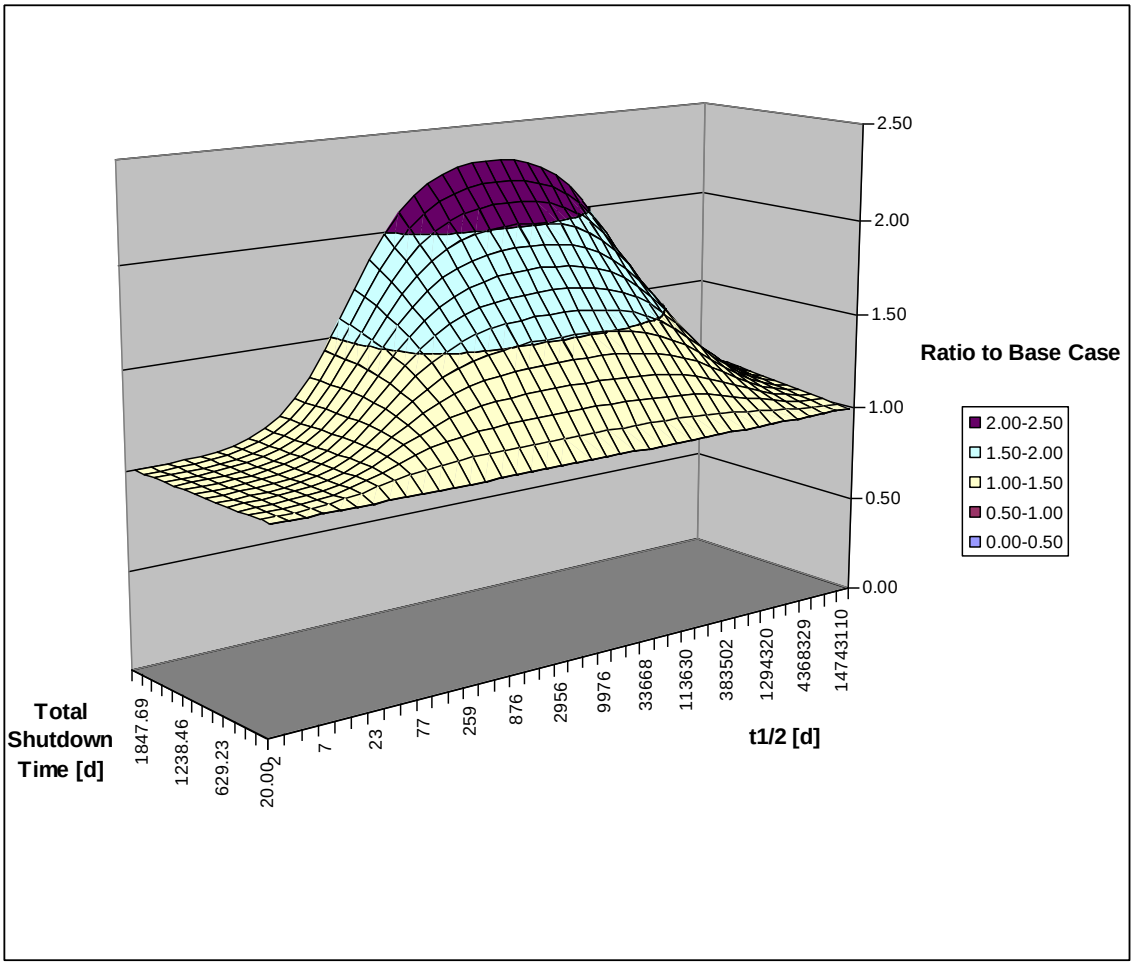

Figure 68. Stable Nuclide Concentration Ratio to Base Case of a Three Cycle Power History with Three Burn Cycles of Equal Length, a Constant Ps = 35 W/g for All Burn Cycles, and 20 days of Total Shutdown Time Divided Evenly Between Two Shutdowns Separating the Burn cycles, $\sigma_{a,R}$ = 100 b, and $\sigma_{a,S}$ = 100 b for Each Half-life of Radioactive Parent.

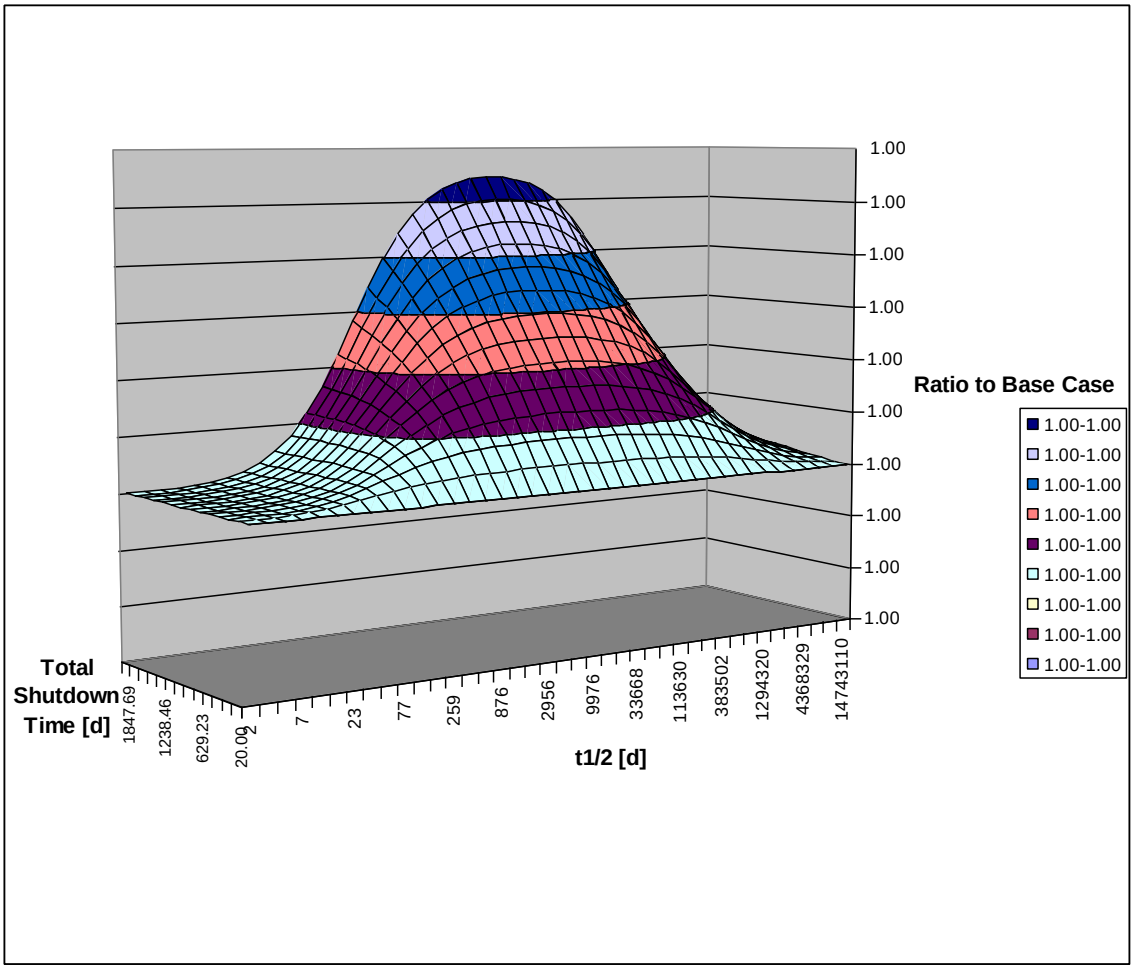

Figure 69. Stable Nuclide Concentration Ratio to Base Case of a Three Cycle Power History with Three Burn Cycles of Equal Length, a Constant Ps = 35 W/g for All Burn Cycles, and 20 days of Total Shutdown Time Divided Evenly Between Two Shutdowns Separating the Burn cycles, $\sigma_{a,R}$ = 100 b, and $\sigma_{a,S}$ = 1000 b for Each Half-life of Radioactive Parent.

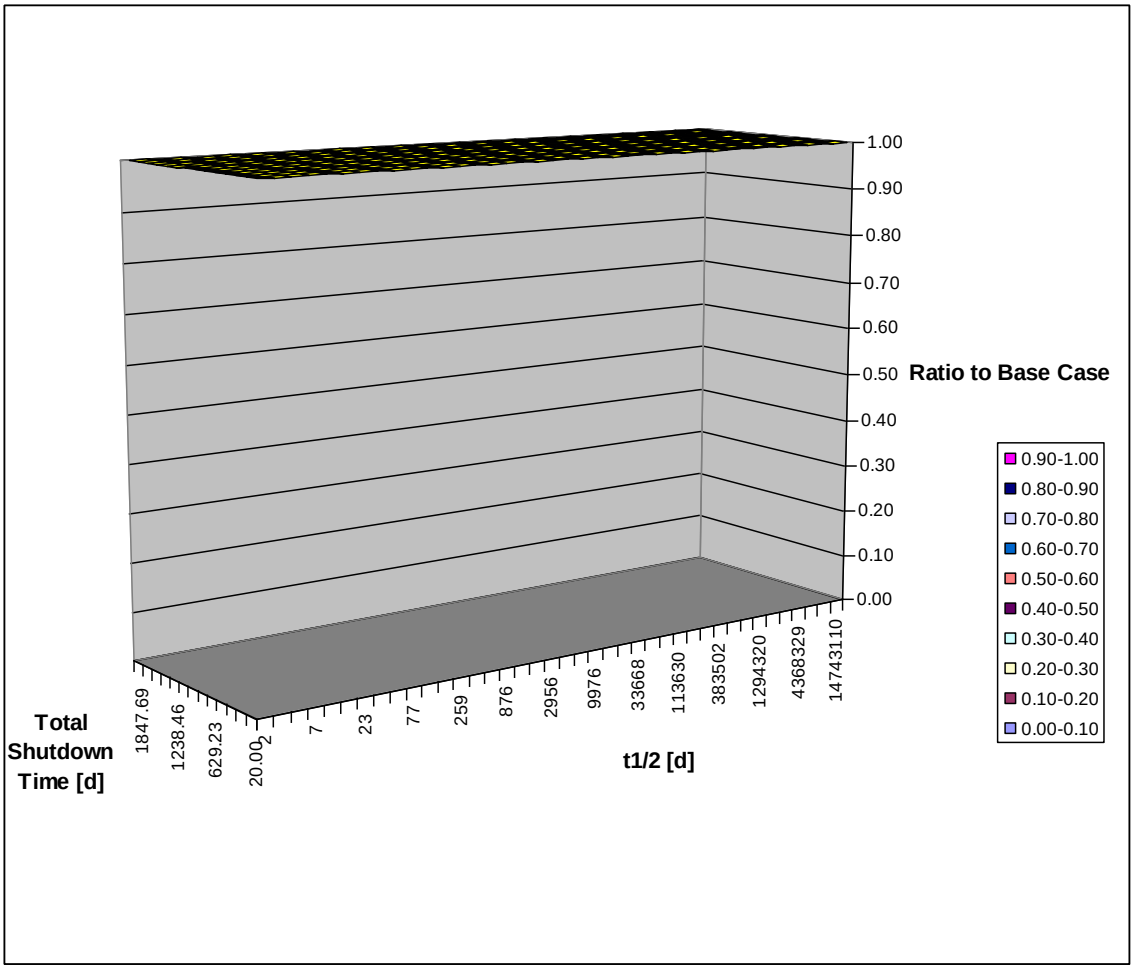

Figure 70. Stable Nuclide Concentration Ratio to Base Case of a Three Cycle Power History with Three Burn Cycles of Equal Length, a Constant Ps = 35 W/g for All Burn Cycles, and 20 days of Total Shutdown Time Divided Evenly Between Two Shutdowns Separating the Burn cycles, $\sigma_{a,R}$ = 100 b, and $\sigma_{a,S}$ = 10000 b for Each Half-life of Radioactive Parent.

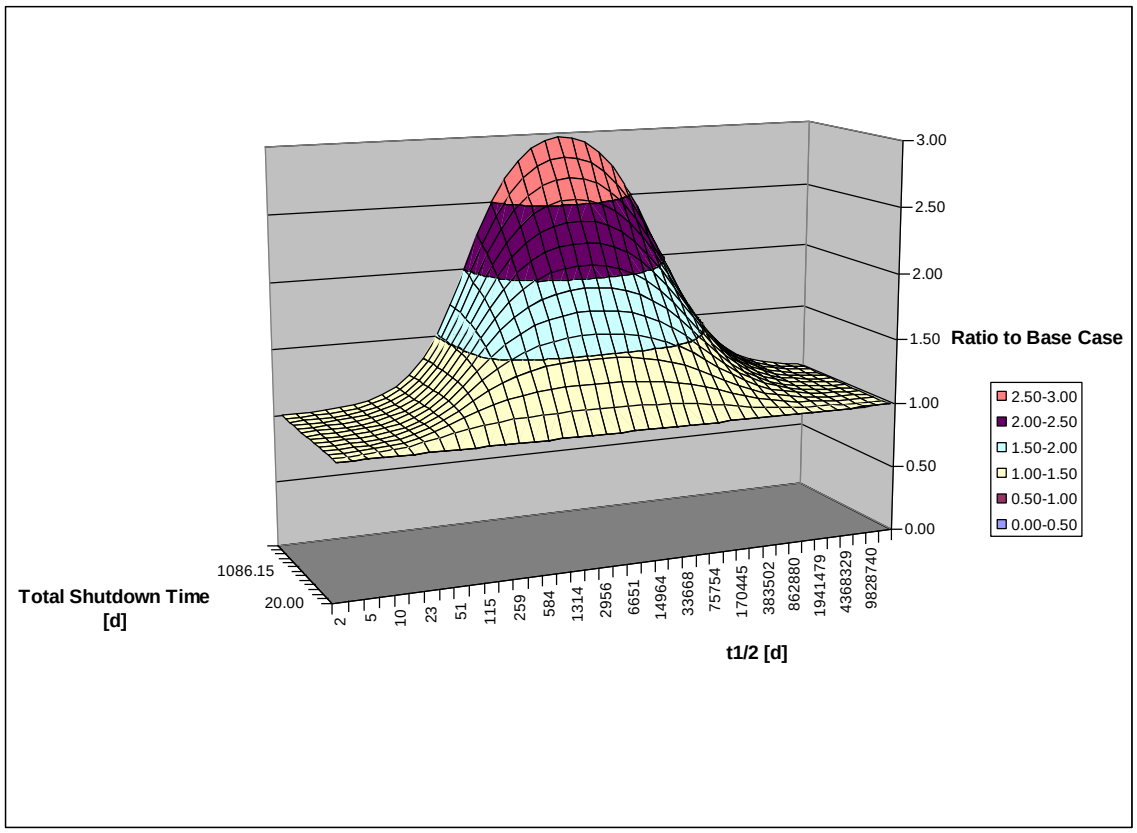

Figure 71. Stable Nuclide Concentration Ratio to Base Case of a Three Cycle Power History with Three Burn Cycles of Equal Length, a Constant Ps = 35 W/g for All Burn Cycles, and 20 days of Total Shutdown Time Divided Evenly Between Two Shutdowns Separating the Burn cycles, $\sigma_{a,R}$ = 1000 b, and $\sigma_{a,S}$ = 1 b for Each Half-life of Radioactive Parent.

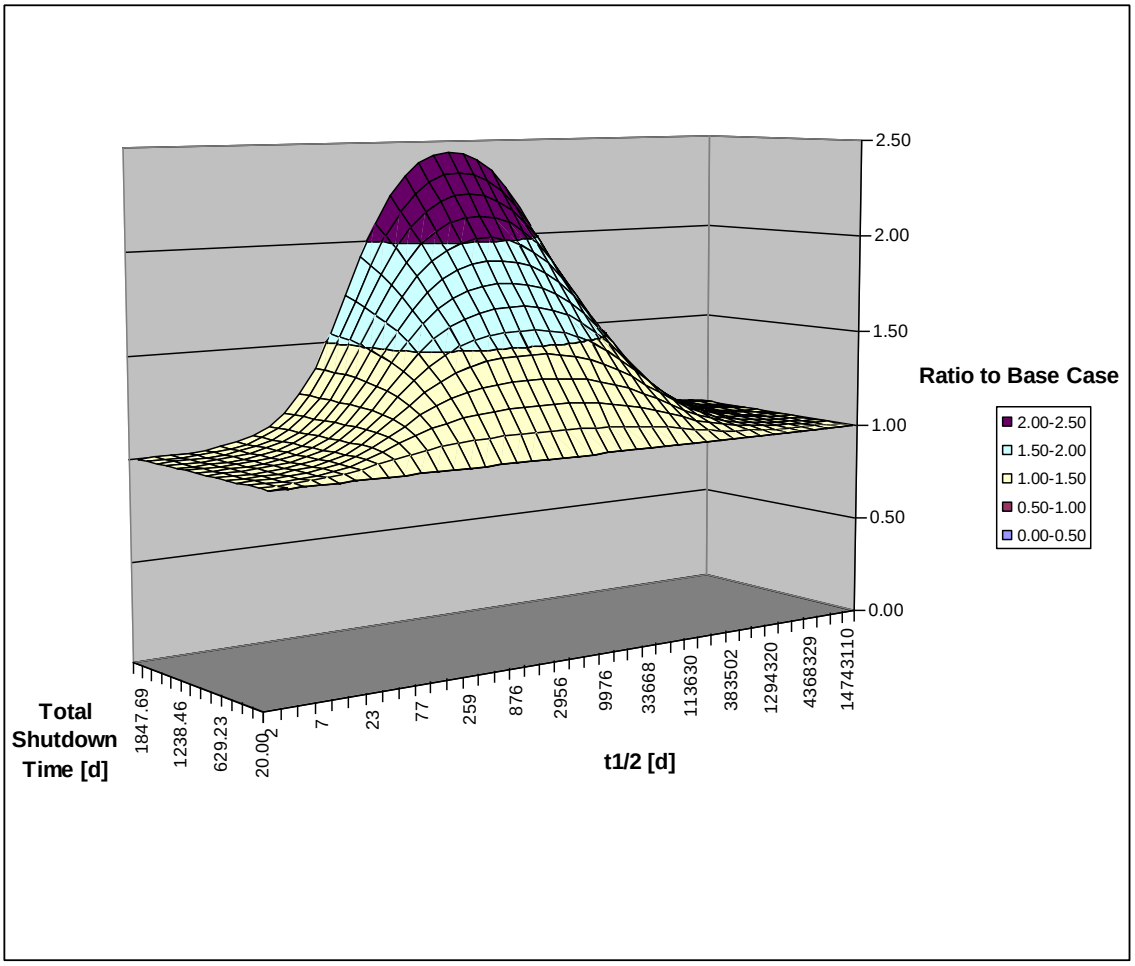

Figure 72. Stable Nuclide Concentration Ratio to Base Case of a Three Cycle Power History with Three Burn Cycles of Equal Length, a Constant Ps = 35 W/g for All Burn Cycles, and 20 days of Total Shutdown Time Divided Evenly Between Two Shutdowns Separating the Burn cycles, $\sigma_{a,R}$ = 1000 b, and $\sigma_{a,S}$ = 100 b for Each Half-life of Radioactive Parent.

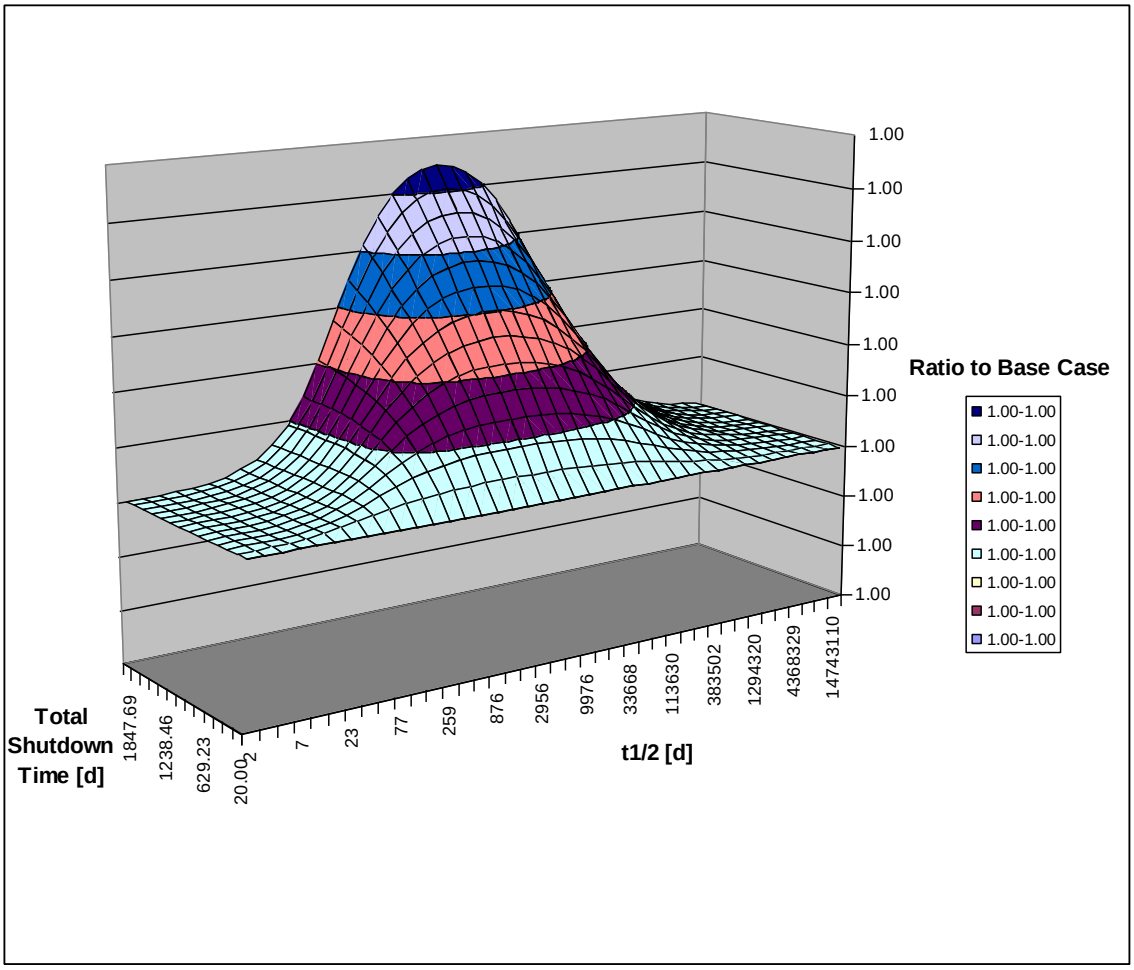

Figure 73. Stable Nuclide Concentration Ratio to Base Case of a Three Cycle Power History with Three Burn Cycles of Equal Length, a Constant Ps = 35 W/g for All Burn Cycles, and 20 days of Total Shutdown Time Divided Evenly Between Two Shutdowns Separating the Burn cycles, $\sigma_{a,R}$ = 1000 b, and $\sigma_{a,S}$ = 1000 b for Each Half-life of Radioactive Parent.

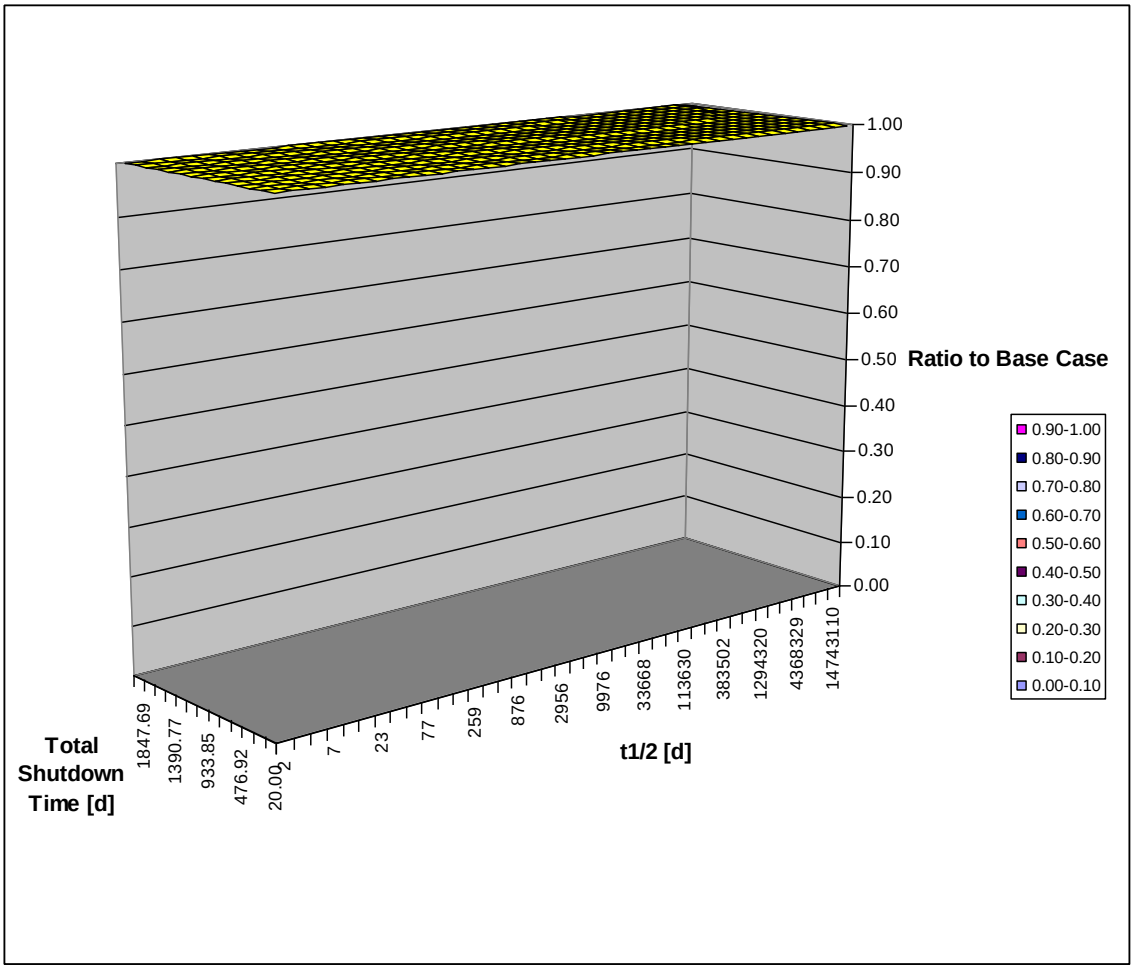

Figure 74. Stable Nuclide Concentration Ratio to Base Case of a Three Cycle Power History with Three Burn Cycles of Equal Length, a Constant Ps = 35 W/g for All Burn Cycles, and 20 days of Total Shutdown Time Divided Evenly Between Two Shutdowns Separating the Burn cycles, $\sigma_{a,R}$ = 1000 b, and $\sigma_{a,S}$ = 10000 b for Each Half-life of Radioactive Parent.

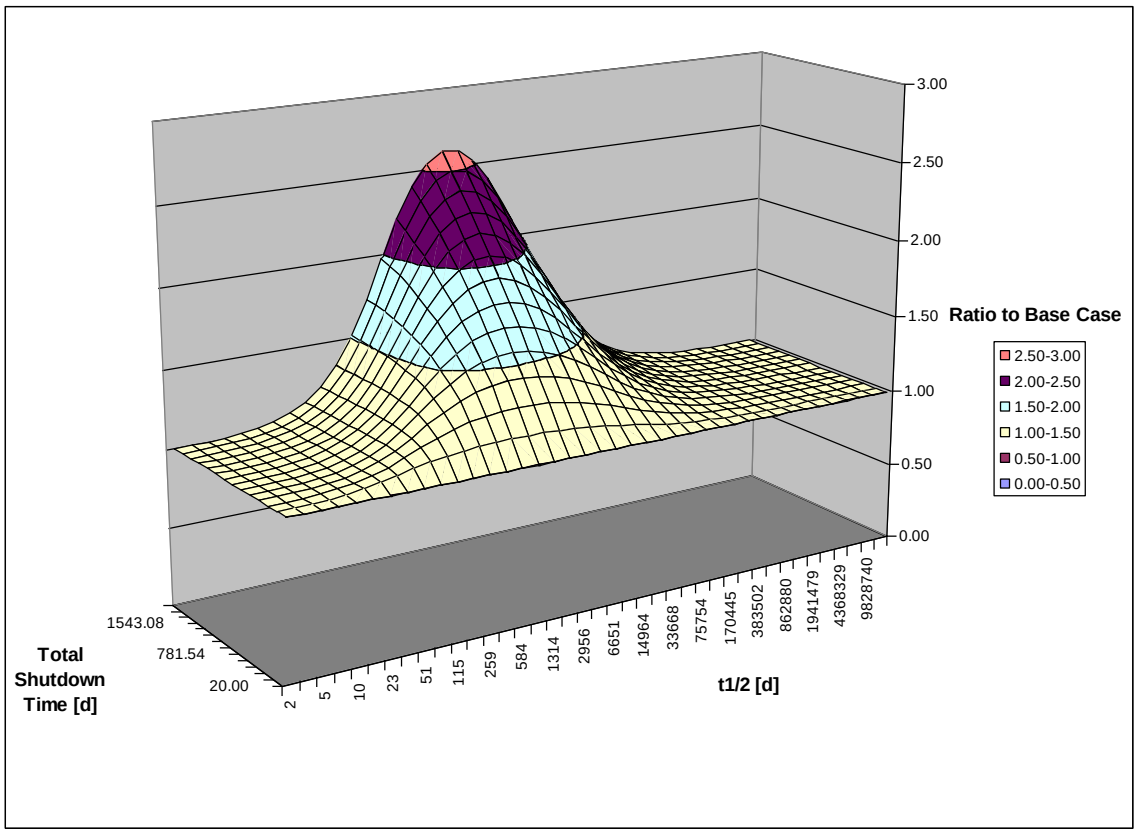

Figure 75. Stable Nuclide Concentration Ratio to Base Case of a Three Cycle Power History with Three Burn Cycles of Equal Length, a Constant Ps = 35 W/g for All Burn Cycles, and 20 days of Total Shutdown Time Divided Evenly Between Two Shutdowns Separating the Burn cycles, $\sigma_{a,R}$ = 10000 b, and $\sigma_{a,S}$ = 1 b for Each Half-life of Radioactive Parent.

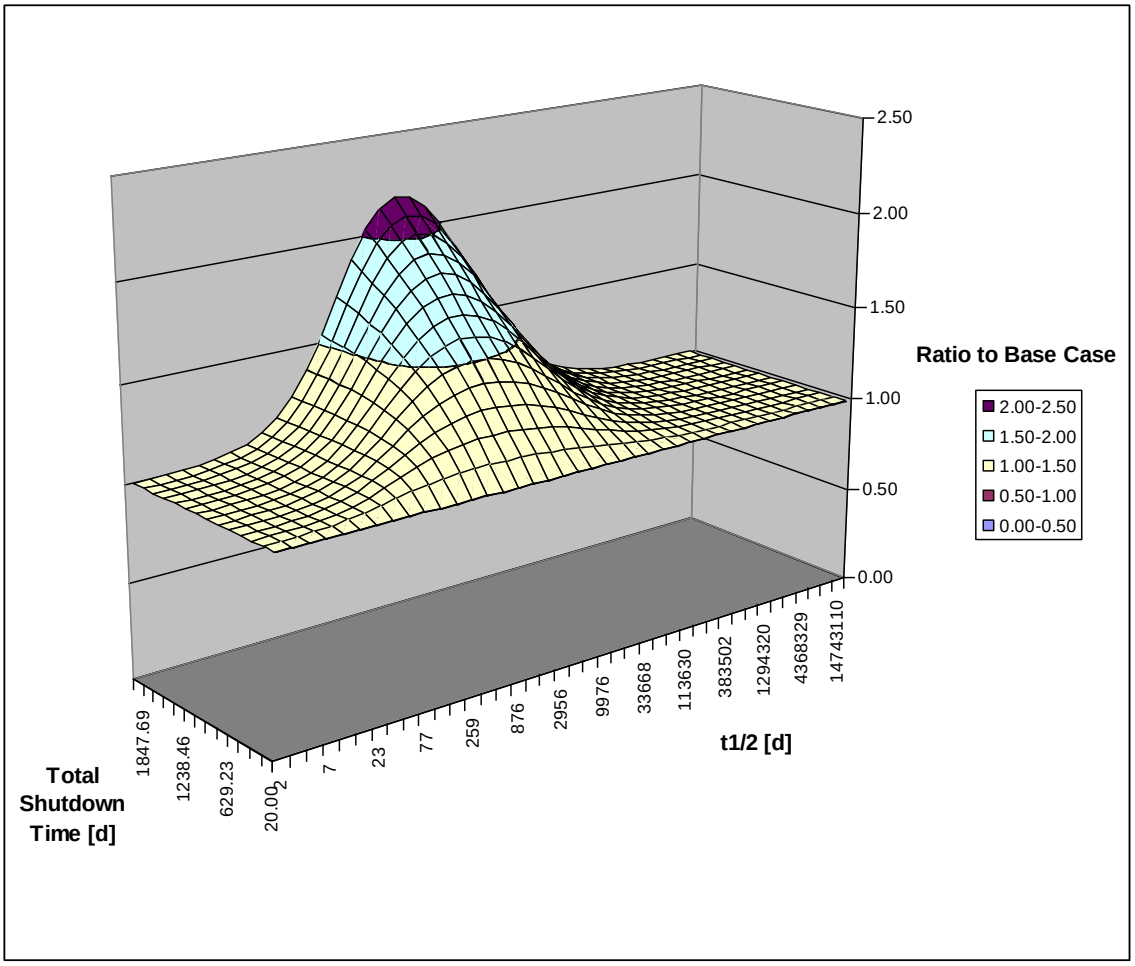

Figure 76. Stable Nuclide Concentration Ratio to Base Case of a Three Cycle Power History with Three Burn Cycles of Equal Length, a Constant Ps = 35 W/g for All Burn Cycles, and 20 days of Total Shutdown Time Divided Evenly Between Two Shutdowns Separating the Burn cycles, $\sigma_{a,R}$ = 10000 b, and $\sigma_{a,S}$ = 100 b for Each Half-life of Radioactive Parent.

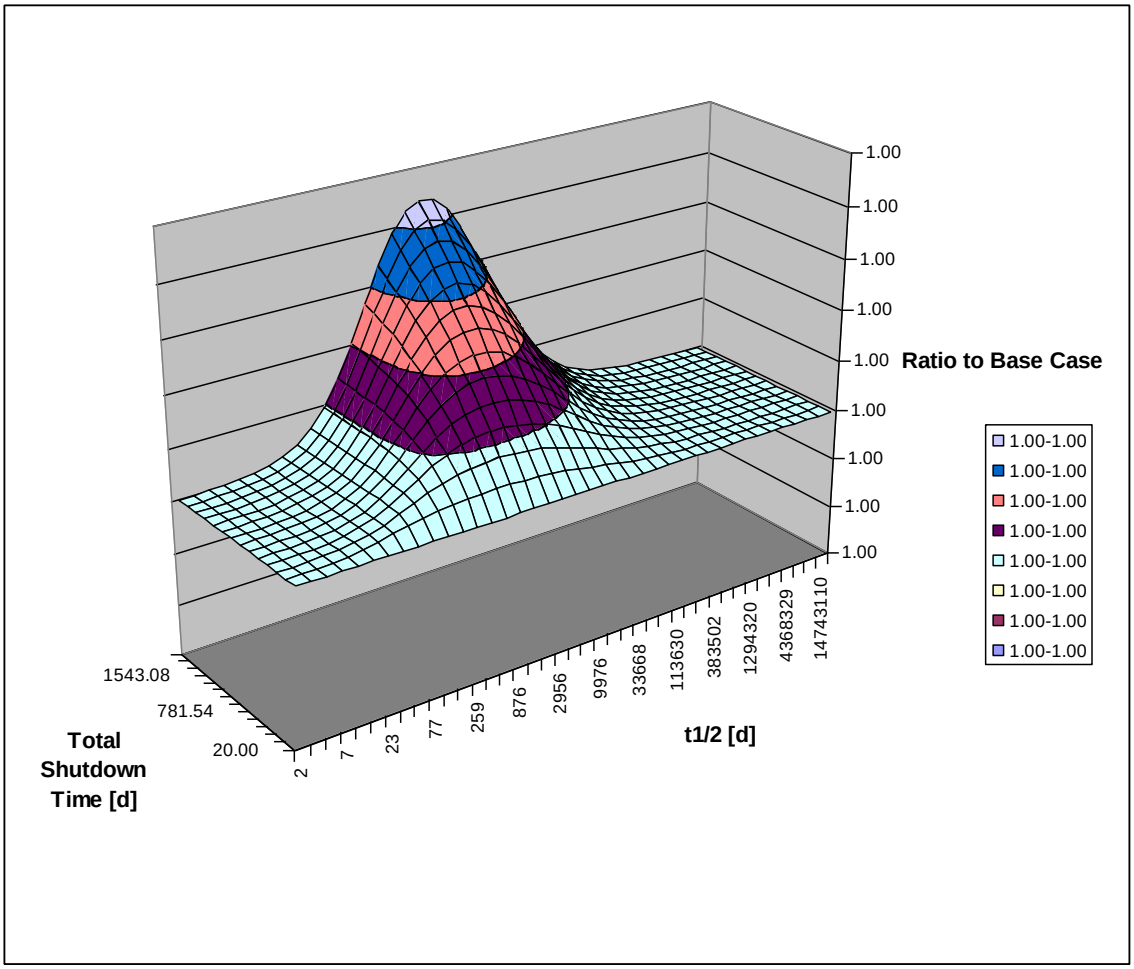

Figure 77. Stable Nuclide Concentration Ratio to Base Case of a Three Cycle Power History with Three Burn Cycles of Equal Length, a Constant Ps = 35 W/g for All Burn Cycles, and 20 days of Total Shutdown Time Divided Evenly Between Two Shutdowns Separating the Burn cycles, $\sigma_{a,R}$ = 10000 b, and $\sigma_{a,S}$ = 1000 b for Each Half-life of Radioactive Parent.

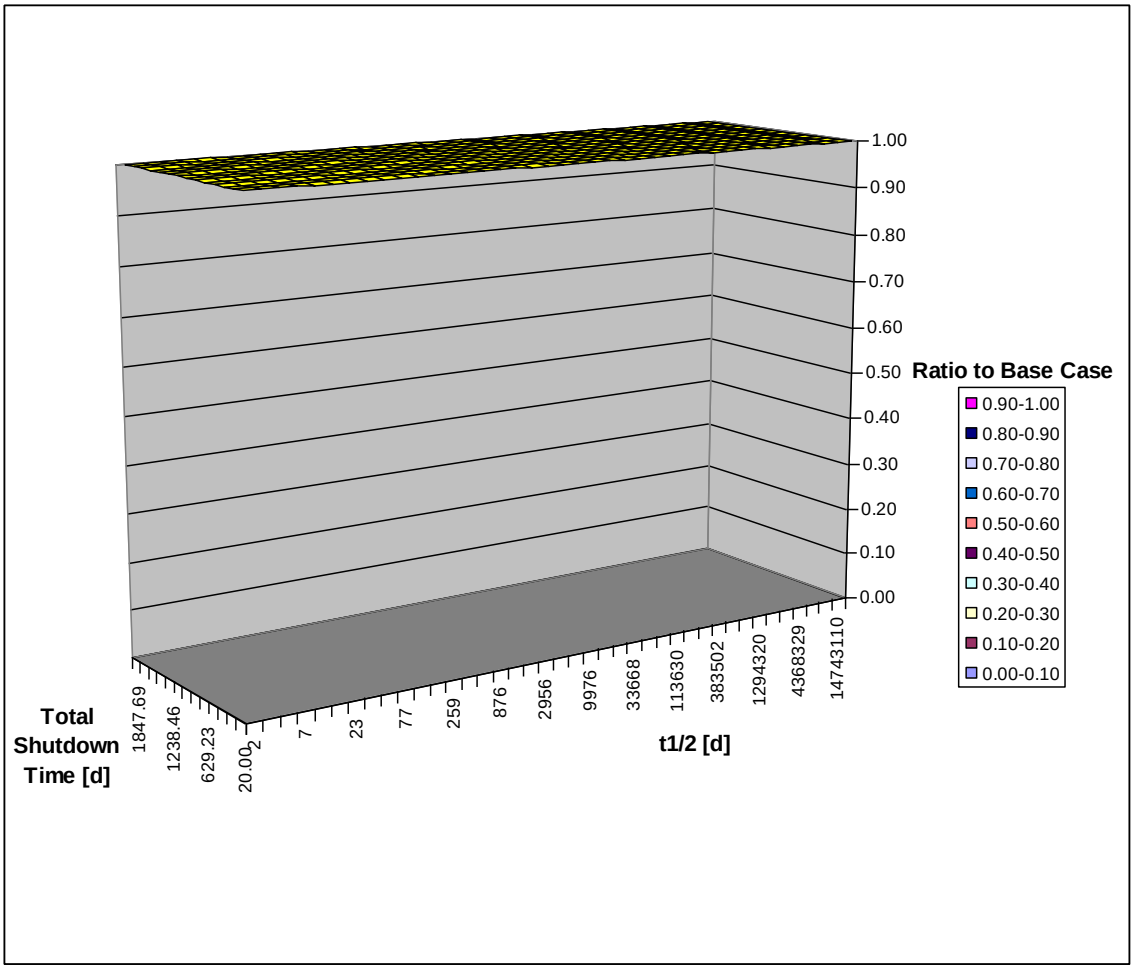

Figure 78. Stable Nuclide Concentration Ratio to Base Case of a Three Cycle Power History with Three Burn Cycles of Equal Length, a Constant Ps = 35 W/g for All Burn Cycles, and 20 days of Total Shutdown Time Divided Evenly Between Two Shutdowns Separating the Burn cycles, $\sigma_{a,R}$ = 10000 b, and $\sigma_{a,S}$ = 10000 b for Each Half-life of Radioactive Parent.

APPENDIX D

Table XIII

Monitor Ratios

	% Difference with Case 1a						
Ratio	Case 1b	Case 1c	Case 2	Case 3	Case 4	Case 5	Case 6
Zr-90/Zr-96	-92.87	48.33	-5.89	-50.89	-7.40	-2.22	-9.00
Ru-106/Ru-100	37.08	-34.96	2.37	18.85	-7.73	0.40	6.83
Pd-106/Pd-110	-25.57	18.71	-1.93	-15.74	1.64	-0.29	-5.67
Ag-110m/Ag-109	34.11	-31.79	1.39	10.43	-18.05	0.04	7.60
Sn-123/Sn-126	47.48	-73.51	2.06	11.65	-37.17	0.12	12.81
Sb-125/Sb-123	23.57	-16.99	1.57	13.40	-0.19	0.39	3.49
Te-125/Te-130	-70.23	46.87	-4.58	-39.95	0.55	-1.18	-9.30
Te-127m/Te-125	-69.79	243.79	-6.27	-35.62	43.74	-1.28	-21.70
Cs-134/Cs-135	48.93	-88.85	1.03	9.14	-11.89	0.29	3.31
Ba-134/Ba-138	-69.35	46.18	-3.67	-34.33	11.55	-0.45	-10.46
Cs-135/Cs-133	-56.48	40.08	-0.10	0.42	6.42	-0.18	-0.05
Ba-137/Ba-138	-94.81	48.93	-5.77	-52.01	-5.39	-1.95	-9.67
Ce-144/Ce-140	-47.58	60.85	-3.82	-25.90	10.03	-0.89	-9.28
Nd-144/Nd-148	-19.20	23.55	-1.55	-9.71	3.93	-0.43	-3.56
Sm-147/Sm-150	-89.41	51.68	-6.98	-45.83	-2.86	-1.72	-11.08
Eu-151/Eu-153	-89.86	47.82	-18.69	-18.27	40.44	0.17	-63.08
Gd-154/Gd-157	-96.73	48.74	-5.02	-51.42	5.46	-0.67	-12.98
Gd-155/Gd-157	-93.39	48.19	-9.93	-19.85	34.72	-0.12	-26.57
Absolute Maximum Difference	96.73	243.79	18.69	52.01	43.74	2.22	63.08

*Bolded Ratios are comprised of only stable nuclides

Table XIV

Double Monitor Ratios Containing Radioactive Parent and Stable Daughter Pair

	% Difference with Case 1a						
Ratio	Case 1b	Case 1c	Case 2	Case 3	Case 4	Case 5	Case 6
[Zr-90/Zr-96]/ [Sr-90/Sr-88]	-92.49	44.89	-6.04	-53.50	-14.39	-2.29	-8.02
[Pd-106/Pd-110]/ [Ru-106/Ru-100]	-98.93	39.47	-4.41	-42.37	8.59	-0.70	-13.43
[Cd-110/Cd-113]/ [Ag-110m/Ag-109]	-55.19	25.33	-2.00	-13.00	15.14	-0.05	-9.18
[Sb-123/Sb-125]/ [Sn-123/Sn-126]	-149.13	50.73	-3.73	-30.70	27.23	-0.52	-18.84
[Te-125/ Te-130] /[Sb-125 /Sb-123]	-122.72	54.59	-6.24	-61.61	0.74	-1.58	-13.24
[I-127/I-129]/ [Te-127m/Te-125]	223.17	-69.98	7.25	55.76	-29.20	1.13	27.36
[Cs-134/Cs-135]/ [Ba-134/Ba-138]	69.85	-250.89	4.53	32.36	-26.51	0.73	12.47
[Ba-137/Ba-138]/ [Cs-137/Cs-135]	-216.47	70.26	-6.08	-53.94	2.34	-2.21	-10.09
[Nd-144/Nd-148]/ [Ce-144/Ce-140]	-127.42	52.47	-5.58	-48.05	12.69	-1.33	-14.15
[Eu-151/Eu-153]/ [Sm-151/Sm-147]	-244.91	73.68	-26.09	-69.51	38.54	-1.58	-79.71
[Gd-154/Gd-157]/ [Eu154/Eu-151]	-283.09	73.58	-24.76	-79.84	44.30	-0.53	-85.28
[Gd-155/ Gd-157]/ [Eu-155/ Eu-151]	-276.92	73.32	-30.25	-41.90	61.81	0.05	-107.05
Absolute Maximum Difference	283.09	250.89	30.25	79.84	61.81	2.29	107.05

VITA

David J. Sweeney graduated from Northwestern University in June 2004 with a Bachelor of Science in Chemical Engineering. After graduation he remained at Texas A&M to pursue his Doctorate in Nuclear Engineering, expected graduation May 2010. Future contact can be made by email at sween67@tamu.edu or by mail forwarded through the Department of Nuclear Engineering, c/o Dr. William Charlton, Texas A&M University, College Station, TX 77843-3133.